LASER INDUCED FLUORESCENCE : STUDY OF V-V ENERGY TRANSFER IN CO_2–CF_2Cl_2 , CO_2–C_4H_4S AND CO_2–$(CD_3)_2$ CO MIXTURES

By

AMIT SIRCAR

DEPARTMENT OF PHYSICS

INDIAN INSTITUTE OF TECHNOLOGY KANPUR

DECEMBER, 1992

LASER INDUCED FLUORESCENCE : STUDY OF V-V ENERGY TRANSFER IN CO_2–CF_2Cl_2 , CO_2–C_4H_4S AND CO_2–$(CD_3)_2$ CO MIXTURES

A Thesis Submitted
in Partial Fulfilment of the Requirements
for the Degree of
DOCTOR OF PHILOSOPHY

By

AMIT SIRCAR

to the

DEPARTMENT OF PHYSICS
INDIAN INSTITUTE OF TECHNOLOGY KANPUR

DECEMBER, 1992

28/12/92
CP-119

CERTIFICATE

It is certified that the work contained in the thesis entitled **"LASER INDUCED FLUORESCENCE : V-V ENERGY TRANSFER STUDIES IN CO_2-CF_2Cl_2, CO_2-C_4H_4S AND CO_2-$(CD_3)_2CO$ MIXTURES"**, by Amit Sircar has been carried out under our supervision and that this work has not been submitted elsewhere for a degree.

Lalita Sarkar 28.12.92
(K. Lalita Sarkar)
Asst. Professor
Department of Physics
Indian Institute of Technology
Kanpur

Y.V.C. Rao 29/12/92
(Y.V.C. Rao)
Professor
Department of Chemical Engineering
Indian Institute of Technology
Kanpur

December, 1992

To

Chhotomama, Ma and Bapi

ACKNOWLEDGMENTS

I would like to express my sincere gratitude to Dr. K. Lalita Sarkar and Dr.Y.V.C. Rao for their able guidance and active participation throughout the course of this work. It was really a pleasant experience to have worked with them.

Dr.D.P. Rao's constant encouragement throughout the work is acknowledged. Dr. R.K. Thereja's suggestions and Dr. Bansi Lal's experience in the fabrication of CO_2 laser helped me in the initial stages. Dr. H.D. Bist and Dr. O.P. Katyal gave me valuable suggestions throughout my work. I am grateful to all of them.

But for Razee's help with his expertise in computational work, I would have spent lot of time in writing computer programs. I gratefully acknowledge his help.

Mr. K.M.S. Prasad contributed significantly in the success of this work. Mr. R.P. Yadav's day to day help and general maintenance of the lab needs special mention.

Many people in various workshops of our institute rendered valuable help to me. Some of the names are, Messrs. G.C. Dasgupta, A. Attrey and Samson from central workshop; Mr. V.K. Srivastava from precision shop; L.S. Rao and R.K. Sharma from Chemical Engineering workshop; S.D. Sharma, V.S. Yadav, V.K. Bajpai and Om Prakash from CELT workshop; Sharmaji, Ram Singh and Raghunath Singh from physics workshop. I thank all of them.

Maintenance cell of A.C.E.S. helped me by repairing my electronic equipment nicely and without any delay. I am thankful

to all the members of the maintenance cell.

Glass blowing shop contributed significantly towards my work. Messrs. B. Sairam and M.J. Bhaskaran cheerfully did all the glass blowing jobs even at odd hours. Special mention must be made about the expertise and experience of Mr. J.N. Sharma for sealing the leak in the InSb detector. This job was skillfully performed by Mr. B. Sairam. I am thankful to all of them.

I thank all the members of the liquid nitrogen plant and air conditioning unit. Mr Zaidi promptly repaired the air conditioners even beyond the office hours. General help extended by S. Kuldip Singh and Mr. P.N. Mishra is also acknowledged. Mr. N.V.G. Swamy assisted me in using our computer terminal room even at odd hours.

Dr. J. Narayan of A.C.E.S. helped me with his expert advices to repair the Au:Ge detector. Mr. J.P. Verma repaired the synchronous motor used for Q-switching the laser at a very crucial time. I acknowledge their help.

Any amount of thanks will be less for my friends Ramsharan, Razee, and Prasad, who devoted enormous time in typing the thesis.

During the entire course of my work, I got warm friendship and direct or indirect help from many of my friends. It is not possible to name all of them. But some of them are Ranjit, Govind, Reddy, Rama, Ravi, Bipin, Subba Rao, Divakar, Rajan, Alok Sharan, Prasad, Sathaiah, Khulbe, Razee, Rajput, Alika, Vinay, Amitabh, Alok Banerjee, Abhilasha, Anup, Ramsharan, Saifuddin, Sarabjit, Sanjay, D.N. Singh, P.K. Chaudhury "Dada", Karandikar and Dharam Pal. I thank all the friends.

Mr. G.C. Dasgupta, S. Jagir Singh and their families gave homely atmosphere to me. The affection and care I received from my Didi Ms. Reba Chakravarty, made my stay at I.I.T.K. very enjoyable. I express my gratitude to all of them. I thank Ranjit and his family for their warm friendship and company, which was a memorable experience.

My uncle Dr. C.R. Mitra introduced me to the exciting world of physics. He alongwith my other uncles and aunts remained constant source of encouragement throughout the course of the work.

Finally, I express my gratitude to my parents for their sacrifice, patience and encouragement during the present work.

Amit Sircar

CONTENTS

LIST OF FIGURES

Figure Page

LIST OF TABLES

SYNOPSIS

The energy transfer rates in gas molecules can be studied by the techniques of selective excitation, of a particular energy level, which creates a non-equilibrium distribution, and subsequent observation of the rate at which it relaxes. The thesis presents a study of the vibration-vibration energy transfer processes in mixtures of CO_2 with other gases [Dichlorodifluoromethane (CF_2Cl_2), Thiophene (C_4H_4S) or Acetone-d_6 $(CD_3)_2CO$] by Laser Induced Fluorescence (LIF) technique. A home built Q-switched CO_2 laser was used to selectively pump the molecules in $CO_2(10^\circ0)$ and $CO_2(02^\circ0)$ levels to $CO_2(00^\circ1)$ level. This creates a population in excess of the equilibrium value in $CO_2(00^\circ1)$ level. Since the intensity of the fluorescence signal from $CO_2(00^\circ1)$ level is proportional to the excess population in that level, the rate of relaxation of $CO_2(00^\circ1)$ level can be obtained by studying the time history of fluorescence.

The fluorescence from the vibrationally excited $CO_2(00^\circ1)$ level was monitored using an InSb detector. The time history of the fluorescence signal was recorded using signal averaging technique. The deactivation rate of $CO_2(00^\circ1)$ was studied in pure CO_2 as well as in CO_2-CF_2Cl_2; CO_2-C_4H_4S and CO_2-$(CD_3)_2CO$ gas mixtures at different temperatures in the range of 323-463 K. The experiments were performed with various compositions of the gas mixtures. The deactivation rates and the probabilities of energy

transfer from $CO_2(00^\circ 1)$ to its collision partners are reported. Some of the transition dipole moment matrix elements of the involved transitions were not available in the literature and they were estimated by comparing the experimental and the theoretically calculated probabilities.

The thesis contains seven chapters and three appendices. Chapter I presents a brief introduction to the energy transfer processes and the various techniques used to observe the energy transfer processes. The laser induced fluorescence technique and experimental set-up are described in Chapter II.

In Chapter III different theories of energy transfer based on short range and long range interaction between the colliding molecules are reviewed. The Schwartz, Slawsky and Herzfeld (SSH) theory and SSH-Tanczos breathing sphere model are presented in detail among the theories based on short range forces. Sharma and Brau (SB) theory and Tam's modification of SB-theory (SB-Tam theory) are discussed in detail among the theories which consider the long range forces to be responsible for energy transfer.

Experimental results are discussed and interpreted in Chapters IV through VI. In Chapter IV, the experimental results of CO_2-CF_2Cl_2 mixtures are discussed. The experimental energy transfer probabilities in CO_2-CF_2Cl_2 were found to be independent of temperature. SSH-Tanczos breathing sphere model and SB-Tam theory were used to interpret the experimental results. The SSH theory could not explain the observed energy transfer probabilities either quantitatively or its dependence on

temperature, whereas SB-Tam theory explained both the magnitude and the temperature dependence satisfactorily. The square of transition dipole moment matrix elements for two of the levels ($2\nu_8$ and $\nu_4+\nu_7$) in CF_2Cl_2, which are not available were estimated by matching the experimental data with the theoretically calculated values. They are in qualitative agreement with the reported data on relative intensity.

The experimental results of CO_2-C_4H_4S mixtures are discussed in Chapter V. The energy transfer probabilities in CO_2-C_4H_4S were found to be decreasing with temperature. Therefore the results were interpreted using SB-Tam theory. The sum of the square of the transition dipole moment matrix elements for ν_6 and ν_7 levels in C_4H_4S were estimated by matching the experimental data with the theoretically obtained values.

The experimental results for CO_2-$(CD_3)_2CO$ mixtures are discussed and interpreted in Chapter VI. The experimental probabilities of energy transfer showed a negative temperature dependence. The SB-Tam theory was used to explain the results. It was found that five levels in $(CD_3)_2CO$, viz. ν_4, ν_{21}, ν_{16}, ν_{17} and $\nu_6+\nu_{24}$ are responsible in deactivating $CO_2(00^\circ1)$ level. The transition dipole moments for none of these levels are available. With the present data, it was not possible to obtain the dipole moments for each of these levels. Therefore a model was considered in which only one level is assumed to be responsible for deactivating $CO_2(00^\circ1)$. Since it was reported that ν_{21} level is strong whereas the other four levels are of medium intensity,

ν_{21} level is considered. The transition dipole moment of ν_{21} level was estimated by matching the theoretical probabilities with the experimental values.

Conclusions and further scope of work is presented in Chapter VII. Three appendices are presented at the end of the thesis. The first one contains the procedure to calculate breathing sphere parameters using normal coordinate analysis. The second and third appendices are devoted to the procedure involved in numerical calculation of the integrals required in SB and SB-Tam theories.

CHAPTER I

INTRODUCTION

The energy transfer processes which occur during molecular collisions in gases and gas mixtures play a dominant role in chemical reactions, isotope separation through laser excitation and in the design of gas lasers. The importance of the knowledge of energy transfer rates in the design of gas laser systems can be realized from the impact they made on the CO_2 laser output power. From a level of 3 mW in pure CO_2, the power output has increased to a few kilowatts in mixtures of CO_2-N_2-He[1-6]. This power enhancement is closely related to the efficient vibration-vibration (V-V) energy transfer in CO_2-N_2 and the vibration-translation (V-T) energy transfer in CO_2-He. With the development of lasers, the laser initiated chemical reactions have been widely studied.[7-10] Once the reactants are selectively excited using a laser radiation, the energy gets redistributed among the translational and various internal modes of the molecule during collisions and a knowledge of the V-V and V-T energy transfer rates is required for a complete understanding of the reaction mechanism. The aim of the present work is to study the energy transfer rates from the $CO_2(00^\circ1)$ level to dichlorodifluoromethane (CF_2Cl_2), thiophene (C_4H_4S) and acetone-d_6 [$(CD_3)_2CO$].

Vibrational energy transfer processes may be divided into two broad categories, namely, radiative processes and collisional

processes. The former are characterized by the radiative lifetime of the excited state. The vibrationally excited states have long natural lifetimes. For molecules with electric dipole moments and reasonably strong IR bands, they are of the order of tens of milliseconds. For molecules such as N_2, with no dipole moment, the radiative lifetime exceeds many seconds. Since under normal experimental densities a great many collisions occur during the course of one radiative lifetime, it is generally true that collisional relaxation predominates over radiative relaxation.

Vibrational energy transfer is an example of inelastic molecular collisions. This phenomenon is different from, both elastic collisions and chemically reactive scattering. In elastic collisions, the internal states of the molecules remain unchanged before and after the collision event has taken place resulting in no transfer of energy. In chemical reactions, rearrangements of the chemical bonds take place resulting in a qualitative change from reactants to products. In the case of vibrational energy transfer, only the internal quantum states of a molecule change without any rearrangement of chemical bonds.

Shock tube and ultrasonic techniques have been widely used[11-15] to obtain V-T energy transfer rates in the gas phase by measuring the rate at which the vibrational heat capacity comes into equilibrium with translational degrees of freedom. In ultrasonic studies either the absorption of the power or the dispersion of the velocity is measured. On the other hand in shock tube the temperature decrease or the density increase behind

a shock front due to the feeding of the energy from translation to vibration is observed. These studies showed that V-V energy transfer is much faster than V-T energy transfer, but no precise rates for V-V processes were measured for a long time. Latter it was possible to obtain V-V transfer rates from shock tube experiments using infrared emission[16,17] and Laser Schlieren Techniques[18,19]. However, the measurement of V-V energy transfer rates using laser has the advantage that the initially excited level is precisely known. Consequently, from the time the first successful experiments on vibrational relaxation studies using laser were reported[20,22], variety of methods and the number of molecules and the types of energy transfer processes to which these methods may be applied continued to grow rapidly. Some of the methods currently being used for the measurement of the V-V energy transfer rates with lasers are the laser induced fluorescence (LIF), the IR double resonance, the thermal lensing and molecular beam techniques. The LIF technique is used in the present work and is discussed in Chapter II.

V-V energy transfer processes may be broadly classified into two types, near-resonant and non-resonant processes. In near resonant processes the amount of energy going into translation is very small whereas in non-resonant processes it is relatively large. V-V energy transfer processes are further classified as

(i) Intramolecular energy transfer processes where the excess energy is redistributed among the different vibrational degrees of freedom of the same molecule.

(ii) Intermolecular energy transfer processes where the energy is transferred into the vibrational modes of the collision partner.

Landau and Teller were the first to formulate[23] a classical theoretical model. According to the Ehrnfest's adiabatic principle, the duration of a collision has to be short compared to the period of vibration for efficient energy transfer to take place. Based on this principle, Landau and Teller derived an expression for the temperature dependence of the energy transfer probability assuming that the intermolecular potential can be represented by an exponential repulsive interaction. According to them, the probability of energy transfer $P \sim \exp(-T^{-1/3})$ which shows that high temperatures favor the probability of energy transfer. Later Schwartz, Slawsky and Herzfeld (SSH) obtained[24] an expression with the characteristic $T^{-1/3}$ dependence from quantum mechanical considerations but still retaining the exponential repulsive interaction. These models have successfully accounted for the magnitude and temperature dependence of the energy transfer rates in many systems[11-15].

The experimental observations for the transfer of energy from $CO_2(00^{\circ}1)$ to $N_2(v=1)$ in the range 300-1000 K showed[25] a negative temperature dependence for the first time where the energy transfer probabilities were found to vary as T^{-1}. The SSH theory could not account for either the large magnitude or the negative temperature dependence of energy transfer probability for CO_2-N_2 system. If long range forces play a dominant role for the energy

transfer, collisions with large values of impact parameter also contribute and the rates will be an order of magnitude greater than those observed for processes where only short range process cause the energy transfer. Sharma and Brau (SB) formulated[26] a semiclassical theory in which the long range forces, which are attractive in nature, cause the energy transfer for near-resonant processes. The first order perturbation calculations of Sharma and Brau[27] reproduced the magnitude and temperature dependence of the energy transfer probability in the range 300-1000 K for the system CO_2-N_2 assuming that energy transfer is due to the interaction of the transition dipole moment of CO_2 and the transition quadrupole moment of N_2. Subsequently many measurements of the energy transfer probabilities confirmed T^{-1} dependence[28] and SB theory was found to be applicable for near-resonant processes. Thus the study of energy transfer rates as a function of temperature should give an indication of the type of intermolecular forces that cause the energy transfer.

A brief description of the LIF technique and experimental set-up used in the present work is given in Chapter II. In Chapter III different theories of energy transfer based on short range and long range interaction between the colliding molecules are reviewed. The SSH and SSH-Tanczos theories for calculating energy transfer probabilities are presented in detail among the theories based on short range forces. SB theory and Tam's modification of SB theory (SB-Tam theory) are discussed in detail

among the theories which consider the long range forces to be responsible for energy transfer.

Experimental results are discussed in Chapter IV through VI. In Chapter IV, the experimental results for CO_2-CF_2Cl_2 mixtures are presented and discussed. Chapters V and VI present the experimental results and discussion for CO_2-C_4H_4S and CO_2-$(CD_3)_2CO$ mixtures, respectively.

The conclusions and further scope of the present work are given in Chapter VII. Three appendices are also presented. Appendix A contains the procedure to calculate breathing sphere parameters using normal coordinate analysis. Appendices B and C present the procedure involved in numerical calculation of the integrals required in SB and SB-Tam theories.

CHAPTER II
EXPERIMENTAL TECHNIQUE AND SET-UP

II.1 LASER INDUCED FLUORESCENCE (LIF) TECHNIQUE

Laser induced fluorescence from $(00^{\circ}1)$ level of CO_2 was monitored to measure the relaxation time of $CO_2(00^{\circ}1)$ level in the presence of dichlorodifluoromethane (CF_2Cl_2), thiophene (C_4H_4S) and acetone-d_6 ($(CD_3)_2CO$). The $CO_2(00^{\circ}1)$ level was excited by a Q-switched CO_2 laser. When a mixture of CO_2-M (M represents the collision partner) is excited by the CO_2 laser pulse, the molecules in the $CO_2(10^{\circ}0)$ and $CO_2(02^{\circ}0)$ levels are pumped to the $CO_2(00^{\circ}1)$ level creating a population in excess of that at equilibrium. $CO_2(00^{\circ}1)$ level is optically connected to the ground level. Therefore, after termination of the pump laser pulse, this excess population in $CO_2(00^{\circ}1)$ level reaches its equilibrium value and a fluorescence signal at 4.3μ is observed, the intensity of which decays with a time constant τ, known as relaxation time.

The decay of the excess population in the $CO_2(00^{\circ}1)$ level can proceed through the following three independent processes each having a characteristic time constant.

(i) Collisions with other molecules,

(ii) radiation decay

(iii) diffusion and subsequent deactivation by collisions with the walls of the container.

Thus the observed time constant is the sum of all the time constants of the above processes, that is,

$$\frac{1}{\tau} = \left(\frac{1}{\tau}\right)_{coll} + \left(\frac{1}{\tau}\right)_{rad} + \left(\frac{1}{\tau}\right)_{diff} \qquad (2.1)$$

Of the above three processes, the collisional deactivation rate $\left(\frac{1}{\tau}\right)_{coll}$ is directly proportional to the pressure as long as binary collisions are dominant. The rate of diffusion to the walls $\left(\frac{1}{\tau}\right)_{diff}$ varies inversely as the pressure. The radiative decay rate $\left(\frac{1}{\tau}\right)_{rad}$ is independent of the pressure. Under the condition, where the pressures are sufficiently high for the diffusion rate to be negligible, a plot of $\left(\frac{1}{\tau}\right)$ vs pressure should give a straight line whose slope $(P\tau)^{-1}_{coll}$ represents the collisional rate of deactivation.

The rate of collisional deactivation in gas mixtures CO_2-M, consists of the following two processes:

(i) the deactivation by collisions with other CO_2 molecules

(ii) the deactivation by collisions with the molecules of M.

Therefore, by studying the dependence of the $(P\tau)^{-1}_{coll}$ values on the composition of the gas mixture, one can obtain the deactivation rate due to collisions with M, which is a direct measure of the rate of energy transfer from $CO_2(00^\circ1)$ to M. Further, a study of the temperature dependence of these energy transfer rates provides information regarding the nature of intermolecular forces which cause the energy transfer. In case of the energy transfer rates which increase with temperature,

short-range forces are believed to be dominant[23,24], while in the case of systems showing negative temperature dependence long range forces are expected to play a dominant role[26,27] in causing the energy transfer.

The laser induced fluorescence (LIF) method has many advantages over the conventional methods of ultrasonic absorption and shock waves for the measurement of energy transfer rates in gases. In general any laser which operates on a vibrational transition, permits that transition to be excited in a gas sample when the sample absorbs the laser pulse. Hence the initial excited level of a gas is known in the LIF technique. The experimental methods using the shock tube or ultrasonic absorption are limited by the fact that excitation must go through the translational degrees of freedom. In these methods it is not possible to uniquely specify the initially excited level and the analysis of the results in many systems is considerably complicated. The large power densities and the narrow pulse widths of the laser radiation are exploited for the study of fast V-V energy transfer rates in gas mixtures. Most of the experimental data obtained from the shock tube and ultrasonic absorption methods till recently, were limited to the measurement of the rates of V-T energy transfer. However, during the last few years, V-V energy transfer data have also been obtained from shock tube experiments. The LIF measurements are generally performed from low to moderate temperature, the limiting temperature being approximately 900 K. To study the energy transfer values at high

temperature (up to 2000 K) usually a shock tube is preferred to the LIF method. The major limitation of the LIF technique was that only those molecules which absorb the laser radiation could be studied. But with the development of various tunable lasers, the number of molecules that can be studied with this technique has increased tremendously.

The data on energy transfer are frequently expressed in terms of rate constants k, cross sections σ and probabilities *P*. All these quantities are interrelated and the relations are given below. Experimentally measured rate constant which is thermally averaged is given by

$$k = \int v\sigma(v)f(v)dv \equiv \langle\sigma v\rangle \tag{2.2}$$

where,

v = relative velocity of the colliding molecules

f(v) = Maxwellian distribution function

$= 4\pi(\mu/2\pi k_B T)^{3/2} v^2 \exp(-\mu v^2/2k_B T)$

k_B = Boltzmann constant

μ = reduced mass of the two collision partners.

One may define cross section $\langle\langle\sigma\rangle\rangle$ per collision as

$$\langle\langle\sigma\rangle\rangle = \frac{k}{\langle v\rangle} = \frac{\langle\sigma v\rangle}{\langle v\rangle} \tag{2.3}$$

where,

$$\langle v\rangle = (8k_B T/\pi\mu)^{1/2} \tag{2.4}$$

n = number of molecules per cc per Torr.

This cross section is compared with the collision cross section πd^2, where d is the hard sphere diameter. The probability per collision $\langle\langle P \rangle\rangle$ is then given by

$$\langle\langle P \rangle\rangle = \frac{\langle\langle \sigma \rangle\rangle}{\pi d^2} \tag{2.5}$$

Here the double brackets are used for the above quantities as they do not represent the true averages as their names suggest. The true average cross section is given by

$$\langle \sigma \rangle = \int \sigma(v) f(v) dv$$

and Yardley[29] has shown that it differs from $\langle\langle \sigma \rangle\rangle$ by a factor of $\pi/4$ for dipole dipole interaction. Therefore,

$$\langle \sigma \rangle = \frac{\pi}{4} \langle\langle \sigma \rangle\rangle \tag{2.6}$$

Thus the experimental average probability is given by

$$\langle P \rangle = \frac{\langle \sigma \rangle}{\pi d^2} = \frac{\pi}{4} \frac{\langle\langle \sigma \rangle\rangle}{\pi d^2} \tag{2.7}$$

Using Eqns. (2.3) through (2.7), one can write

$$\langle P \rangle = 1.73 \times 10^{-2} d^{-2} (\mu T)^{1/2} k \tag{2.8}$$

where d = hard sphere collision diameter in Å

μ = collision reduced mass in amu

T = temperature in K

k = rate constant in $Torr^{-1}\mu s^{-1}$.

This probability <*P*> will be compared with the theoretically obtained probabilities while interpreting the data.

II.2 EXPERIMENTAL SET-UP

A Block diagram of the experimental set-up used for the measurement of relaxation time by LIF technique is shown in Fig. 2.1. The major components are,

(i) A Q-switched CO_2 laser

(ii) Gas handling system

(iii) Test Cell

(iv) IR detector

(v) Signal averaging and recording system.

A brief description of each is given below.

(i) Q-switched CO_2 laser

The laser was made of a discharge tube, 25 mm in diameter and 3 m long, which was cooled by water flowing in the surrounding jacket. One end of the tube was terminated by a stationary flat II-VI gold coated Si mirror fixed on a mirror mount and the other end was terminated by a II-VI ZnSe window at Brewster angle. The mirror mount for the stationary mirror was provided with micrometer adjustments for proper alignment of the mirror. This mirror had a central uncoated portion of 4 mm diameter through

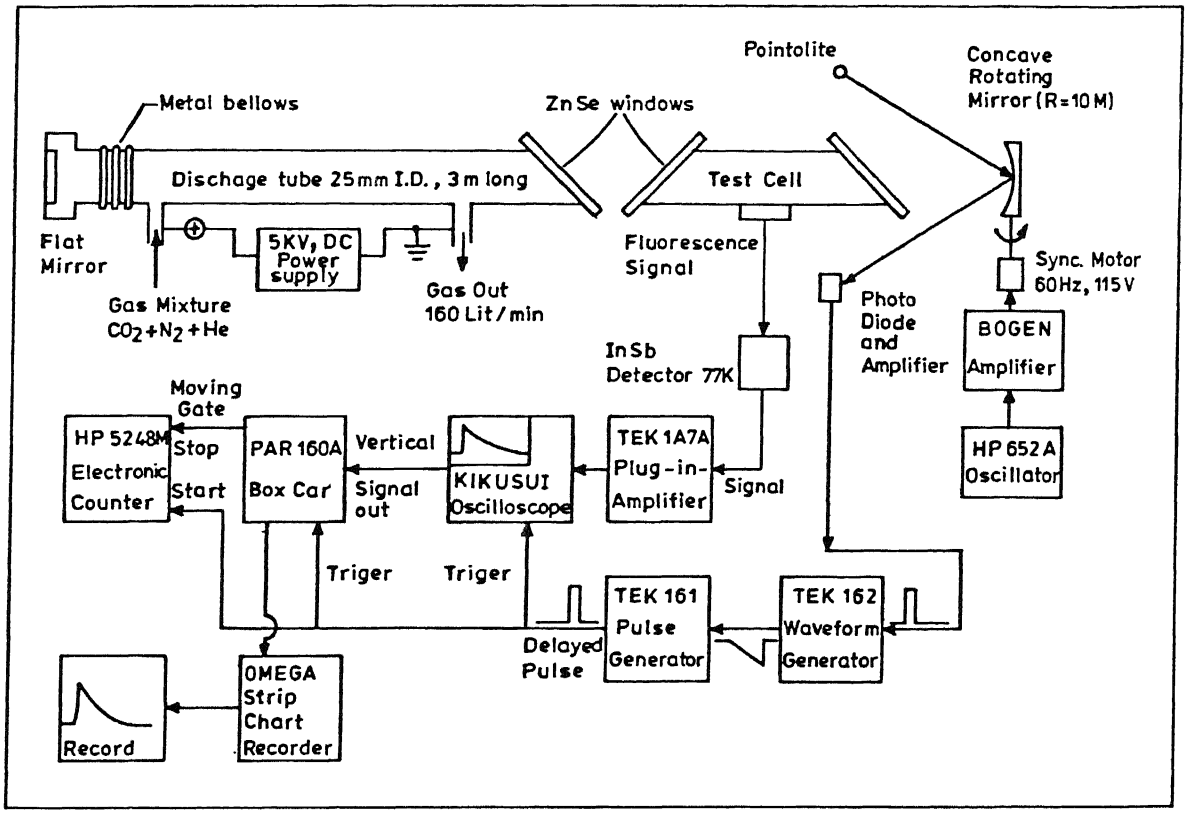

Fig. 2.1 Block diagram of the experimental set-up.

which the laser power was taken out. A rotating gold coated II-VI Si mirror with a 10 m radius of curvature, formed the other end of the cavity. The cavity length was 4.5 m and the cell containing the sample to be studied was placed inside the cavity. The rotating mirror was mounted on the shaft of an Amphenol synchronous motor which rotated with a speed of 3600 rpm. Whenever this Q-switching mirror gets aligned with the stationary mirror a laser pulse is given out. The repetition rate of the laser pulse was 60 Hz.

Longitudinal excitation was achieved by applying a DC potential between the two ends of the discharge tube. A gas mixture of CO_2, N_2 and He in the ratio 1:1:2 at a total pressure of $\approx$ 10 Torr was allowed to flow continuously in the discharge tube across which a DC potential of 13 kV was maintained. After passing through the discharge tube, the gas mixture was pumped out by a 160 liter/minute rotary pump. The composition of the gas mixture as well as the total pressure were varied to get the maximum power output from the laser. The optimum current in the discharge tube was found to be 30 mA. A gold coated germanium detector (SBRC Model 40742) was used to detect the laser pulses while a InSb detector (Judson Infra Red Corp.) was used to detect the fluorescence at 4.3μ.

(ii) Gas handling system

The mixture of test gases was prepared in glass bulbs of 1 liter volume at a total pressure of about 700 mm Hg. Pressure

measurements were made using two U-tube manometers. A mercury manometer was used for recording pressures greater than 25 Torr and a silicone oil manometer was used to measure pressures below 25 Torr. The gas handling system was pumped down to pressures less than 10^{-4} Torr by a silicone oil diffusion pump backed by a mechanical pump. Evacuation was continued for several hours before filling the bulbs.

The composition of the gas mixtures was determined from the partial pressures. One of the components (say component 1) of the gas mixtures was first filled in the glass bulbs at a pressure P_1 Torr. The other component was then added till the total pressure was P Torr. The mole fraction of component 1 in the gas mixture was calculated from the ratio P_1/P. The uncertainty in the measurement of pressures was 0.16 Torr when silicone oil manometer was used whereas it was 2 Torr in case of mercury manometer. The resulting error in the composition determination was less than 0.25%. The gas mixtures were left for at least 36 hours to ensure thorough mixing before withdrawing samples for fluorescence studies. The gases used were - CO_2 (Matheson, purity 99.8%), CF_2Cl_2 (Aldrich, purity 99+%), C_4H_4S (Merck, purity 99+%) and $(CD_3)_2CO$ (Sigma, purity 99.5%).

(iii) The Test Cell

The test cell was made of a 300 mm long glass tube with a T-joint. Two stainless steel tubes cut at Brewster angles were connected to the ends of the glass tube through teflon seals and

aluminum flanges. Two II-VI ZnSe windows were used to close the ends at Brewster angle. The central portion, perpendicular to the test cell axis, was sealed by a KRS window. Thus the fluorescence signal was detected from this window at right angle to the laser axis. A schematic diagram of the test cell is shown in Fig. 2.2. To facilitate evacuation and filling the cell with gas mixtures, a 6 mm glass tube with flexible metallic bellows through covar seals, a vacuum stop cock and a ball joint were attached to the test cell.

A 1000 W heating tape was wound on the test cell. A chromel-alumel thermocouple was attached to the test cell to measure the temperature. The temperature was controlled by a temperature controller whose accuracy was ±2 K.

(iv) Infrared detectors

The fluorescence signal at 4.3 μm from CO_2 was detected by a Judson Infrared Incorp. indiumantimonide (InSb) detector having maximum sensitivity at around 5 μm. The operating temperature of the detector was 77 K which was achieved with the help of liquid nitrogen. The time constant of the detector was reported to be less than 1 μs. The laser pulse was detected by a Santa Barbara Research Center Model 40742 (HS) gold doped germanium (Au:Ge) detector. The operating temperature for this detector also was 77 K.

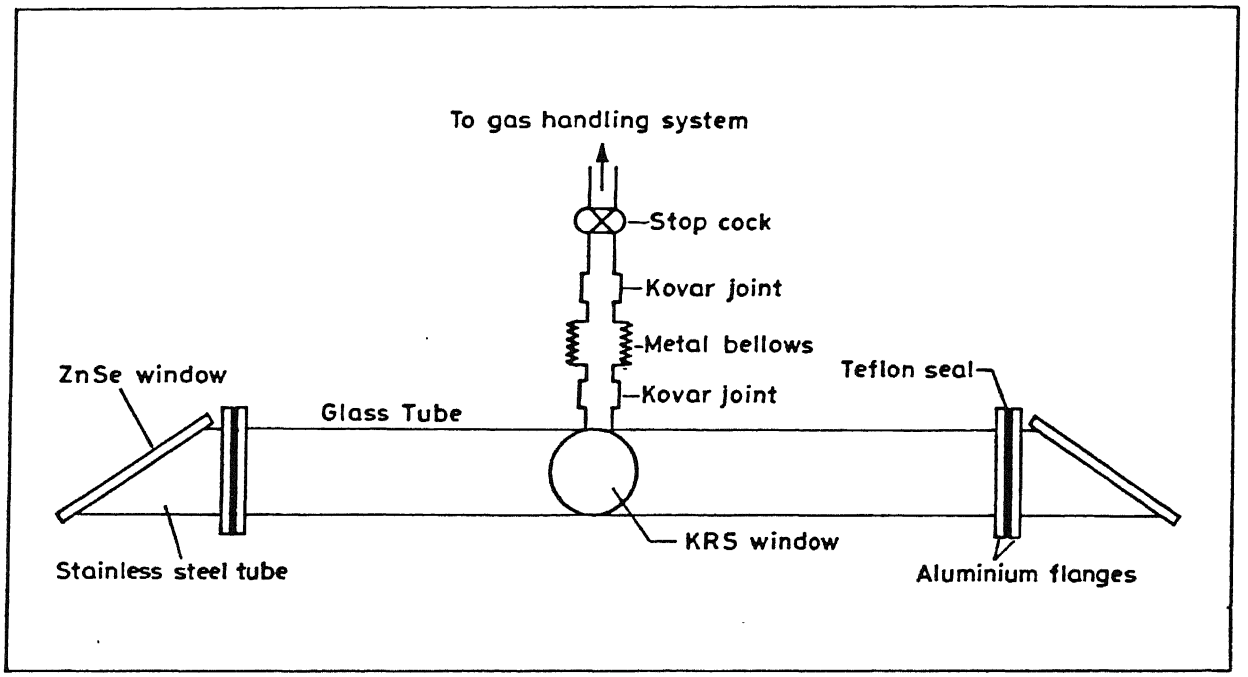

Fig. 2.2 Block diagram of the test cell.

(v) Signal Averaging and Recording System

The output from the InSb detector was fed to a Kikusui COS 160 oscilloscope for display, after amplifying it by a Tek 1A7A plug-in-unit. This plug-in-unit is a differential amplifier and the 3 db cut-off points were 1 Hz and 1 MHz in the low and high frequency range, respectively. After amplification typical signal intensities were of the order of 0.2 mV. The vertical signal output from the oscilloscope was fed to a PAR 160A boxcar integrator to improve the signal to noise ratio. A point source of light was used to provide incident ray of light onto the rotating mirror and the reflected light was collected by a photodiode. The pulses from the photodiode, after amplification, were fed to a Tek 162 waveform generator, which generates a sawtooth voltage. The sawtooth voltage is then given to a Tek 161 pulse generator which generates a square pulse with adjustable delay and Pulse width. The time delayed pulses (with respect to the onset of the pump laser pulse) were used to trigger the oscilloscope and boxcar integrator, and to start the HP5248M electronic counter. The boxcar integrator starts a gate, after being triggered by the delayed pulse from Tek 161 pulse generator, which scans the signal to be averaged. The gate width and the time base over which the gate has to scan the signal could be adjusted. Since the gate samples a very large number of signals at a point before moving to the next point on the intensity versus time curve, the random noise is eliminated and the signal is reproduced with an increased signal to noise ratio.

The HP5248M electronic counter was used to measure time. The delayed pulse from Tek 161 pulse generator started the counter whereas the moving gate from the boxcar was used to stop the counter.

The output of the boxcar integrator was fed to an Omega strip chart recorder which records the fluorescence intensity versus time trace. A typical plot of the recorded signal is shown in Fig. 2.3.

To test the performance of the equipment and associated electronics regarding the reproducibility of data, fluorescence measurements were performed with pure CO_2 and the results are presented in Chapter IV. The measured values were found to be in good agreement with those reported in the literature[28,30-32].

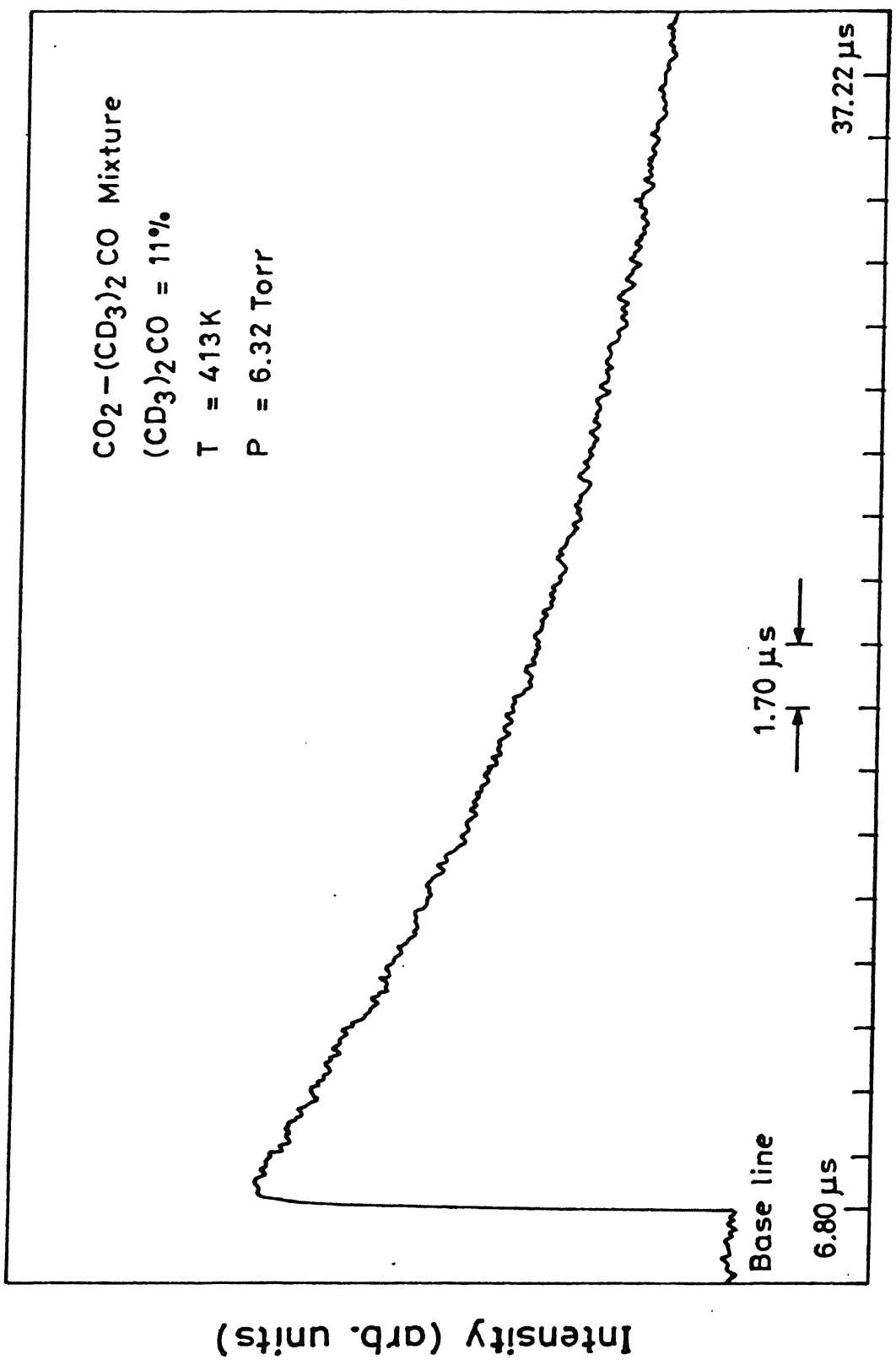

Fig. 2.3 A typical fluorescence signal.

CHAPTER III

THEORY

III.1 GENERAL

Energy transfer between the internal and the translational degrees of freedom of a molecule is caused by intermolecular forces during collisions. A transition between the internal states of molecule results in energy transfer from one internal degree of freedom to another internal degree of freedom. Various theories of vibrational energy transfer attempt to estimate the probability that a molecule undergoes a transition from one vibrational state to another during a molecular collision. A preliminary understanding of the nature of intermolecular interactions that cause the energy transfer can be obtained by applying Ehrenfest's adiabatic principle to molecular collisions. This principle states that if a changing external force acts on a periodic motion the process will be adiabatic, if the change of force is small during a period of the motion. In such processes the probability for energy transfer is very low. The criterion for a non-adiabatic process, which involves transfer of energy, is the duration of the collision is short compared to the period of oscillation. At moderate temperatures the time taken to traverse the range of the long-range forces which is approximately 5 Å in a molecular collision, is much longer than the period of a vibration. Therefore, the vibrations are assumed to be adiabatic with respect

to these forces. On the other hand, in a molecular collision the time taken to recoil from the short-range repulsive forces (range ≈0.2 Å) is of the order of the period of molecular vibration. The vibrations, therefore, are not strongly adiabatic with respect to these forces. Because of this, the vibrational transitions in collisions are believed to be caused by the short-range repulsive forces between the molecules. The theories of Landau and Teller[23], and of Schwartz, Slawsky and Herzfeld (SSH)[24] and Tanczos[33] and Rapp[34] which are based on this premise have been successful in explaining a wide variety of vibrational relaxation rates. These are discussed by Yardley[29]. All these theories predict that the probability of energy transfer increases with temperature. Since then many systems were studied in which the temperature dependence of energy transfer probability could not be explained by SSH theory and its modification. One of the first examples was the following near resonant vibrational energy transfer from CO_2 to N_2

$$CO_2(00^\circ 1) + N_2(v=0) \longrightarrow CO_2(00^\circ 0) + N_2(v=1) + \Delta E(=18\ cm^{-1}) \qquad (3.1)$$

The observed probability of energy transfer for the process (3.1) shows a negative temperature dependence[25] below 1000 K in contrast to the results predicted by SSH theory. This raises doubts about the applicability of SSH theory to such processes. In addition to this, SSH theory also underestimates the value of the energy transfer probability at room temperature for process (3.1) by a factor of four. This discrepancy in the magnitude of the energy

transfer probability was however could be eliminated in the Tanczos modification of SSH theory. Failure of these theories was attributed to the assumption that only short-range forces are responsible for vibrational energy transfer.

Mahan was the first to use the long range dipole-dipole interaction to calculate the probability for near-resonant vibration-vibration (V-V) energy transfer[35] which predicts that the probability is proportional to $T^{1/2}$. A detailed discussion of this theory can be found in ref. 29. Later Sharma and Brau[26] (SB) also obtained the probabilities for V-V transfer for long range interaction using a different approach. In particular, they have demonstrated that the negative temperature dependence of probability for process (3.1) is due to long range dipole-quadrupole interaction between CO_2 and N_2 which varies as r^{-4}. The magnitude as well as the temperature dependence of the probabilities for the process (3.1), obtained using the Tam's modification of SB theory, were in agreement with the experimental values. Since then SB theory has been applied to many systems with reasonable success[37-45] where long range forces are believed to cause the energy transfer. The SB theory was modified by Tam[50] to include the non-resonant processes. Tam showed that the head-on collisions play a dominant role in non-resonant energy transfer processes.

In the present work SB theory with Tam's modification is used to calculate the probability of energy transfer form CO_2 ($00^{\circ}1$) to dichlorodifluoromethane (CF_2Cl_2), acetone-d_6 [$(CD_3)_2CO$], and

thiophene (C_4H_4S). Estimates of the transition dipole moments for the involved transitions in these molecules were also made using this theory. SSH-Tanczos theory is also used to calculate energy transfer probability for CO_2-CF_2Cl_2 system. A brief review of the relevant theories is presented below.

III.2 LANDAU AND TELLER THEORY

Landau and Teller[15,23] contributed extensively to the physical understanding of the energy transfer processes. They were the first to derive an expression for the temperature dependence of the probability of energy transfer during a collision, by a purely classical treatment. If an atom A approaches a diatomic molecule BC along the molecular axis and makes a head-on collision with B, the collision makes the intermolecular distance to contract. In other words, the collision compresses the *spring* connecting B and C which is a molecular bond. For an efficient energy transfer A should be rebounded from B when B comes back to its equilibrium position. Otherwise there will be a second collision transferring the energy back to A from B. Consequently a little or no net kinetic energy is transferred from A to the vibrating mode of BC and the collision becomes adiabatic.

Thus, Landau and Teller concluded that the probability of energy transfer depends on (and increases with) the ratio of the period of vibration to the time of interaction. If ν is the frequency of oscillation, ℓ is the range of interaction force i.e. the distance travelled by A in the repulsive potential field of

BC, and v_0 is the relative velocity, the criterion for non-adiabatic collisions can be written as

$$\frac{(1/\nu)}{(\ell/v_0)} > 1 \quad \text{or} \quad \frac{\ell\nu}{v_0} < 1 \tag{3.2}$$

From this they concluded that only short range forces are effective in producing transitions. Since the repulsive intermolecular forces have shorter range than the attractive ones, only the former need to be considered.

They assumed the following repulsive exponential potential

$$V = Ce^{-\alpha x} \tag{3.3}$$

and obtained the probability P as

$$P \sim \exp\left[-\left(\frac{\Delta E}{kT}\right)^{1/3}\right] \tag{3.4}$$

Thus

$$\ln P \propto -T^{-1/3} \tag{3.5}$$

which means the probability P increases with increasing temperature T.

III.3 SCHWARTZ, SLAWSKY AND HERZFELD (SSH) THEORY

Schwartz, Slawsky and Herzfeld[24] extended the theory of V-V energy transfer in diatomic gases to chemically non-reacting gas mixtures and to gas molecules with several normal vibrational

modes. They considered the molecules to be rotationless and approach each other along a straight line. The motion can be described in terms of the distance between the centers of mass of the collision pair r, and the normal vibrational coordinates s_1, s_2, ...s_n. It was further assumed that the zero-order wave functions describing the collision are separable in these coordinates and the interaction potential between the molecules was approximated by a product functions of the coordinates. That is,

$$V = V_0 V_r(r) V_1(s_1) \ldots . V_n(s_n) \tag{3.6}$$

where V_0 is a constant with dimension of energy.

With these assumptions the probability that the system, made up of a pair of colliding molecules, originally of relative velocity v_0, initial vibrational states i_1, i_2, i_3, ... i_n and final vibrational states f_1, f_2, f_3, ... f_n. can be expressed, following the method of Zener[47], as follows

$$p^{i \longrightarrow f}(v_0) = \frac{16\pi^2 V_0^2}{v_0 v_f h^2} \left[V(i_1 \longrightarrow f_1) \ldots . V(i_n \longrightarrow f_n) R \right]^2 \tag{3.7}$$

where

$$R = \int_{-\infty}^{+\infty} F_0 F_F V_r dr \tag{3.8}$$

and F_0, F_F are the solutions of the Schrödinger wave equation (3.9) for the motion of a free particle in a potential field V_r.

$$\frac{d^2}{dr^2} F_F + \frac{8\pi^2\mu}{h^2}\left(\frac{\mu v_F^2}{2} - V_0 V_r\right)F_F = 0 \qquad (3.9)$$

where μ is the reduced mass of the molecules and

$$V(i_n \rightarrow f_n) = \int_{-\infty}^{+\infty} \psi_i^{(n)} V_n^{(s_n)} \psi_f^{(n)} ds_n \qquad (3.10)$$

where

$\psi_i^{(n)}$, $\psi_f^{(n)}$ = normalized oscillator wave function for the s_nth normal vibrational coordinate

v_0 = relative velocity of the molecules before collision

v_F = relative velocity after collision.

SSH assumed that the interaction between individual atoms of different molecules to be

$$V = Ce^{-\alpha\chi} \qquad (3.11)$$

where χ = distance between colliding atoms

$$= r + A_0 + A_1 s_1 + A_2 s_2 + \ldots + A_n s_n$$

The interaction potential V is of the form of Eqn. (3.6). In order to determine α, the first term of eqn (3.11)

$$V \cong V_0 e^{-\alpha r} \qquad (3.12)$$

is fitted to Lennard-Jones potential function

$$V = 4\varepsilon\left\{\left(\frac{r_0}{r}\right)^{12} - \left(\frac{r_0}{r}\right)^{6}\right\} \tag{3.13}$$

at the point $r = r_c$, r_c being the classical distance of closest approach of the two molecules approaching each other with a relative velocity v_0. This is achieved by matching the values of V and slopes $\frac{dV}{dr}$ of eqns. (3.12) and (3.13) and adding the condition that $V \longrightarrow \varepsilon$ as $r \longrightarrow \infty$. Then

$$\alpha = \frac{12}{r_0 D}\left[\frac{1}{2} + \frac{1}{2}(1 + D)^{1/2}\right]^{1/6}\left[1 + (1 + D)^{1/2} + D\right] \tag{3.14}$$

and

$$r_c = r_0\left[\frac{1}{2} + \frac{1}{2}(1 + D)^{1/2}\right]^{-1/6} \tag{3.15}$$

where $D = \dfrac{\frac{1}{2}\mu v_0^2 + \varepsilon}{\varepsilon}$

Now, for the potential of the form $V_r = e^{-\alpha r}$, $p^{i\longrightarrow f}$ is shown to be

$$p^{i\longrightarrow f} = V^2(i_1 \longrightarrow f_1) \ldots\ldots\ldots V^2(i_n \longrightarrow f_n)\frac{1}{16\pi^2}(\theta_0^2 - \theta_F^2)^2$$

$$\times \frac{(e^{\theta_0} - e^{-\theta_0})\,(e^{\theta_F} - e^{-\theta_F})}{(e^{\theta_0} + e^{-\theta_0} - e^{\theta_F} - e^{-\theta_F})^2} \tag{3.16}$$

where $\theta_0 = \dfrac{4\pi^2\mu v_0}{\alpha h}$

$$\theta_F = \frac{4\pi^2\mu v_F}{\alpha h}$$

Here v_0 and v_F are not independent but they are related by the fact that the total energy of the collision system is conserved in the collision i.e.,

$$\frac{\mu}{2}(v_0^2 - v_F^2) = \Delta E \qquad (3.17)$$

= total energy exchanged between vibration and translation during a collision.

The probability $p^{i\rightarrow f}$ given by eqn (3.16) is dependant on the initial velocity v_0. Therefore the probability has to be averaged over all initial velocities assuming Maxwellian velocity distribution. Thus the overall probability $p^{i\rightarrow f}$ is given by

$$p^{i\rightarrow f} = 2\left(\frac{\mu}{2kT}\right)^2 \int_0^\infty v_0^3 p^{i\rightarrow f}(v_0)\exp\left(\frac{-\mu v_0^2}{2kT}\right)dv_0 \qquad (3.18)$$

The integral in (3.18) cannot be evaluated in a closed form. Hence the following two limiting cases will be discussed.

(i) Non-resonant Energy Exchange

(ii) Resonant Energy Exchange

(i) Non-resonant Energy Exchange

The probability $p^{i\rightarrow f}(v_0)$ increases with increasing velocity v_0. On the other hand due to Boltzmann factor $\exp\left(\frac{-\mu v_0}{2kT}\right)$ the number of molecules with higher velocity decreases strongly with increasing v_0. Thus the integral in (3.18) is expected to go through a maximum value at certain value of $v_0 = v_0^*$, called the

most favorable velocity. Assuming

$$\exp\left(\frac{-4\pi^2\Delta E}{\alpha^* h\nu_0^*}\right) \ll 1 \tag{3.19}$$

$$\frac{\mu}{2}(v_0^*)^2 \gg \Delta E \tag{3.20}$$

$$\frac{\mu}{2}(v_F^*)^2 \gg \Delta E \tag{3.21}$$

SSH obtained the overall probability to be

$$p^{i\rightarrow f} = 0.394V^2(i_1\rightarrow f_1)....V^2(i_n\rightarrow f_n)\left[\frac{8\pi^3\mu\Delta E}{(\alpha^*)^2h^2}\right]^2\frac{\sigma^{3/2}e^{-\sigma}}{(1-e^{-2/3\sigma})} \tag{3.22}$$

where

$$\sigma = 3\left[\frac{2\pi^4(\Delta E)^2\mu}{(\alpha^*)^2h^2kT}\right]^{1/3} \pm \frac{\Delta E}{2kT} \tag{3.23}$$

α^* = value of α at $v = v_0^*$

$$v_0^* = \left[\frac{4\pi^2kT\Delta E}{\alpha^* h\mu}\right]^{1/3} \mp \frac{\Delta E}{2\mu}\left[\frac{4\pi^2kT\Delta E}{\alpha^* h\mu}\right]^{-1/3} + ... \tag{3.24}$$

In Eqn. (3.23) + or - sign corresponds to decrease or increase of the total vibrational energy respectively.

(ii) Resonant Energy Exchange

When $\Delta E = 0$, Eqn. (3.22) cannot be used to calculate the probability of energy transfer. But Eqn. (3.16) for $p^{i\rightarrow f}$ reduces to

$$p^{i\rightarrow f} = V^2(i_1\rightarrow f_1)....V^2(i_n\rightarrow f_n)\left[\frac{2\pi\mu v_0}{\alpha h}\right]^2 \qquad (3.25)$$

and Eqn. (3.18) can be integrated to yield

$$p^{i\rightarrow f} = V^2(i_1\rightarrow f_1)....V^2(i_n\rightarrow f_n)\left[\frac{8\pi^2\mu kT}{\alpha^2 h^2}\right] \qquad (3.26)$$

III.4 TANCZOS' BREATHING SPHERE MODEL

The SSH method for calculating the probability of energy transfer in gases was extended to polyatomic molecules by Tanczos[33]. In the breathing sphere approximation, Tanczos assumed that the motion of each of the surface atoms for all normal modes is directed radially, that is along the most effective direction for energy transfer. He used the theory to calculate vibrational relaxation times in methane and chloromethanes. Later Stretton[49] successfully applied the SSH-Tanczos theory to estimate the relaxation times in acetylenes, ethylenes, methane and methane derivatives.

A. Non-resonant Energy Exchange

To calculate the transition probability, Tanczos considered bimolecular collisions resulting in transition of (i) the simple kind, involving a change in a vibrational state of one of the colliding molecules and (ii) the complex kind, involving the simultaneous change of a vibrational state in each of the colliding molecules.

Following the lines of SSH[24] and Schwartz and Herzfeld[48] a repulsive exponential potential function was used for interaction potential and was fitted to the repulsive part of the Lennard-Jones potential. It was found that the probability that a pair of molecules a and b originally with vibrational states a_i and b_k will, after collision, arrive at vibrational states a_j and b_l is

$$P(a,b) = P_0(a)P_0(b)P_c|U_{ij}(a)|^2|U_{kl}(b)|^2\left(\frac{\pi}{3}\right)^{1/2}\left[\frac{8\pi^3\mu\Delta E}{(\alpha^*)^2h^2}\right]^2$$

$$\times X^{1/2}\exp\left[-\left(3X - \frac{\Delta E}{2kT} - \frac{\varepsilon}{kT}\right)\right] \qquad (3.27)$$

where

$$X = \frac{\mu(v_0^*)^2}{2kT} = \left[\frac{2\pi^4\mu(\Delta E)^2}{(\alpha^*)^2h^2kT}\right]^{1/3} \qquad (3.28)$$

and

$$\Delta E = h\nu_a(i - j) + h\nu_b(k - l) \qquad (3.29)$$

Except for numerical constants, Eqn. (3.27) is same as Eqn. (22), given by Schwartz and Herzfeld[48]. Here $P_0(a)$ and $P_0(b)$ represent the geometrical or steric factors of the molecules a and b respectively. In the present work, they are taken as $\frac{1}{3}$ for linear and $\frac{2}{3}$ for nonlinear molecules, following Stretton[49]. In Eqn. (3.27) $|U_{ij}(a)|^2$ denotes the vibrational matrix element of molecule a and is given by

$$|U_{ij}(a)|^2 = \prod_n |U_{ij}^n(a)|^2 \qquad (3.30)$$

where $|U^n_{ij}(a)|^2$ is the matrix element for the mode n for molecule a and is defined for 0, 1 and 2 quantum jumps by Stretton[49] as

$$|U^n_{ii}|^2 = 1 \tag{3.31}$$

$$|U^n_{(i+1)-i}|^2 = |U^n_{i-(i+1)}|^2 = \alpha^2 \langle A^2_n \rangle \frac{(i+1)}{2\gamma} \tag{3.32}$$

$$|U^n_{(i+2)-i}|^2 = |U^n_{i-(i+2)}|^2 = \alpha^4 \langle A^4_n \rangle \frac{(i+1)(i+2)}{16\gamma^2} \tag{3.33}$$

where,

$$\gamma = \frac{4\pi^2 \nu}{h} \tag{3.34}$$

Here, $\langle A_n \rangle$ represents the average cartesian displacement of the surface atoms of the molecule for unit change of the normal coordinate. The averaging is carried out according to the *breathing sphere* model, i.e., the full displacements of the surface atoms are taken and the appropriate powers averaged. This assumes that the displacements are always normal to the surface and corresponds to the molecule having a favorable orientation of collision. This was achieved by introducing steric factors P_0 for each vibration undergoing a change in its quantum state. $\langle A^2_n \rangle$ is the average of the squares of cartesian displacements of surface atoms for unit change of the normal coordinate and is called the breathing sphere parameter. The procedure to calculate $\langle A^2_n \rangle$ using normal coordinate analysis is given in Appendix A.

B. Resonant Energy Exchange

The vibrational transition probability under resonance conditions, ($\Delta E = 0$), becomes

$$P(a,b) = P_0(a)P_0(b)|U_{ij}(a)|^2|U_{ij}(b)|^2 \frac{64\pi^2\mu kT}{\alpha^2 h^2} \exp(\varepsilon/kT) \qquad (3.35)$$

The value of α is chosen such that it is consistent with the average relative translational energy X.

III.5 Sharma-Brau (SB) Theory

Sharma and Brau were among the first to recognize the importance of long-range interactions in near-resonant V-V energy transfer. They developed a theory of vibrational energy transfer caused by long-range forces along the lines of Gray and Van Kranendonk's theory[51] of pressure broadening. Sharma and Brau, in their theory, considered binary collisions and adopted semi classical or impact parameter approximation. It was assumed that the time between collisions is much greater than the duration of collisions and any correlations between the collisions were ignored. The translational motion was treated classically while the rotational and vibrational motions were handled quantum mechanically. The justification for treating, translational motion classically is discussed in detail by Sharma and Brau[27]. The probability of vibrational energy transfer is calculated using first Born approximation which is true if (i) the kinetic energy

of the relative motion is much greater than the potential energy. (ii) the probability of vibrational energy transfer is small.

According to first-order perturbation theory, the probability P that a transition occurs during a collision from the initial vibration-rotation state $|i\rangle = |n_1 j_1 m_1 n_2 j_2 m_2\rangle$ to the final state $\langle f| = \langle n_1' j_1' m_1' n_2' j_2' m_2'|$ is given by

$$P = \frac{1}{\hbar^2}\left|\int_{-\infty}^{+\infty} e^{i\omega t}\langle f|V(t)|i\rangle dt\right|^2 \qquad (3.36)$$

where subscripts 1 and 2 denote molecules 1 and 2 respectively and V(t) is the intermolecular potential which is a function of time. In the present work molecule 1 is CO_2 and molecule 2 is CF_2Cl_2, $(CD_3)_2CO$ and C_4H_4S, n_i, j_i and m_i represent the vibrational, rotational and magnetic quantum numbers, respectively for molecule i.

$$\hbar\omega = E(n_1', j_1') + E(n_2', j_2') - E(n_1, j_1) - E(n_2, j_2) \qquad (3.37)$$

where $E(n_i, j_i)$ is the vibration-rotation energy of molecule i. $\hbar\omega$ represents the energy transferred to translation that is the net change in vibrational energy during the collision. Neglecting any magnetic interaction, V may be written as

$$V(t) = \sum_{\alpha,\beta} \frac{e_\alpha e_\beta}{r_{\alpha\beta}(t)} \qquad (3.38)$$

where e_α(or e_β) is the charge on particle (electron or nucleus) α(or β) in the molecule 1 (or 2), $r_{\alpha\beta}$ is the distance between the particles α and β and the sum is taken over all combinations of α and β. Since the long-range forces extend to larger distances than the charge distribution, V(t) may be expressed in terms of the multipole expansion for axially symmetric non-overlapping charge distributions

$$V(t) = 4\pi \sum_{\ell_1\ \ell_2\ m} Q^{(1)}_{\ell_1} Q^{(2)}_{\ell_2} \varepsilon_{\ell_1\ell_2}[R(t)].T_{\ell_1+\ell_2,m}(\hat{\Omega}_1,\ \hat{\Omega}_2) Y^{m\,*}_{\ell_1+\ell_2}(\hat{\Omega}) \tag{3.39}$$

where,

$$m = \ell_1 + \ell_2,\ \ldots\ldots,\ -(\ell_1 + \ell_2)$$

and $Q^{(i)}_{\ell_i}$ is the $\ell_i{}^{th}$ multiple moment of molecule i defined by

$$Q^{(i)}_{\ell_1} = \sum_\alpha e_\alpha r_\alpha^\ell P_\ell(\hat{\Omega}_\alpha.\hat{\Omega}_i) \tag{3.40}$$

$$\varepsilon_{\ell_1\ell_2}(R) = \frac{(-1)^{\ell_2}}{(2\ell_1+2\ell_2+1)} \cdot \left[\frac{4\pi(2\ell_1+2\ell_2+1)}{(2\ell_1+1)!(2\ell_2+1)!}\right]^{1/2} \frac{1}{R^{\ell_1+\ell_2+1}} \tag{3.41}$$

where $\mathbf{r} = r_\alpha\hat{\Omega}_\alpha$ is the radius vector from the center-of-mass (CM) of molecule i to particle α, $\hat{\Omega}_i$ denotes the orientation of the internuclear axis of molecule i, and $\mathbf{R} = R\hat{\Omega}$ is the vector from the CM of molecule 1 to CM of molecule 2. The function $T_{\ell m}(\hat{\Omega}_{m_1},\hat{\Omega}_{m_2})$

is defined by the expression

$$T_{\ell m} = \sum_{m_1 m_2} C(\ell_1 \ell_2 \ell; m_1 m_2) Y_{\ell_1}^{m_1}(\hat{\Omega}_1) Y_{\ell_2}^{m_2}(\hat{\Omega}_2) \tag{3.42}$$

where $C(\ell_1 \ell_2 \ell; m_1 m_2)$ is a Clebsch-Gordon coefficient, the axis of quantization being along $\hat{\Omega}$.

Having specified the potential V(R), it is necessary to know the trajectory R(t) during the collision to evaluate P. It was assumed that for the values of impact parameter b≥d, where d is the hard sphere collision diameter, the relative translational motion continues in a straight line. This assumption implies that the energy transferred to or from the internal degrees of freedom be much less than the energy of relative translational motion.

The probability of energy transfer caused by the interaction of ℓ_1^{th} multipole of molecule 1 with the ℓ_2^{th} multipole of molecule 2 can be obtained by integrating Eqn. (3.36) over the trajectory, averaging over the initial magnetic quantum numbers and summing over the final ones following Gray and Van Kranendonk[51] and is given below

$$P_{\ell_1 \ell_2}(b \geq d) = \frac{4(2\ell)!}{(2\ell_1+1)!(2\ell_2+1)!} G_\ell(\omega, \tau)$$

$$\times \frac{|\langle n_1' | Q_{\ell_1}^{(1)} | n_1 \rangle|^2 |\langle n_2' | Q_{\ell_2}^{(2)} | n_2 \rangle|^2}{\hbar^2 v^2 b^{2\ell}} C^2(j_1 \ell_1 j_1'; 00) C^2(j_2 \ell_2 j_2'; 00) \tag{3.43}$$

where b = impact parameter

d = hard sphere collision diameter

$\ell = \ell_1 + \ell_2$

v = the relative velocity of the colliding molecules

$\tau = \frac{b}{v}$ is approximately the duration of a collision

$C(j\ell j';00)$ = Clebsch-Gordon coefficient

$\langle n'|Q_\ell^{(i)}|n\rangle$ = matrix element of the ℓ^{th} multipole moment (for molecule i) between the initial vibrational state n and the final vibrational state n′ and

$$G_\ell(\omega,\tau) = \sum_{\mu=-\ell}^{+\ell} \frac{(\omega\tau)^{2\ell}\, K_\mu^2(\omega\tau)}{(\ell+\mu)!\,(\ell-\mu)!} \tag{3.44}$$

where K_μ is the modified Bessel function of order μ.

The total probability of energy transfer is obtained by summing over ℓ_1 , ℓ_2

$$\bar{P}(b\geq d) = \sum_{\ell_1\ell_2} P_{\ell_1\ell_2}(b\geq d)$$

$$= \sum_{\ell_1\ell_2} D_\ell b^{-2\ell} v^{-2} G_\ell(\omega b/v) \tag{3.45}$$

where

$$D_\ell = \frac{4(2\ell)!}{\hbar^2(2\ell_1+1)!\,(2\ell_2+1)!}\, |\langle n_1'|Q_{\ell_1}^{(1)}|n_1\rangle|^2 |\langle n_2'|Q_{\ell_2}^{(2)}|n_2\rangle|^2$$

$$\times C^2(j_1\ell_1 j_1';00)\; C^2(j_2\ell_2 j_2';00) \tag{3.46}$$

Sharma and Brau gave the following expression for b = 0

$$\bar{P}(b=0) = \sum_{\ell_1 \ell_2} P_{\ell_1 \ell_2}(b=0) = \sum_{\ell_1 \ell_2} D_\ell d^{-2\ell} v^{-2} J_\ell^2(\omega d/v) \qquad (3.47)$$

where

$$J_\ell(x) = \int_0^\infty \frac{\cos(xs)}{(1+s)^{-(\ell+1)}}\, ds \qquad (3.48)$$

For values of impact parameter between 0 and d, they used the following parabolic interpolation formula

$$P_{\ell_1 \ell_2}(0<b<d) = P_{\ell_1 \ell_2}(0) + \frac{b^2}{d^2}\left[P_{\ell_1 \ell_2}(d) - P_{\ell_1 \ell_2}(0)\right] \qquad (3.49)$$

$$\bar{P}(0<b<d) = \sum_{\ell_1 \ell_2} P_{\ell_1 \ell_2}(0<b<d)$$

$$= \bar{P}(b=0) + \frac{b^2}{d^2}\left[\bar{P}(b=d) - \bar{P}(b=0)\right] \qquad (3.50)$$

The above expressions for $\bar{P}$ are averaged over velocities and then impact parameter to obtain the transition probability $\langle\bar{P}\rangle$. The averaging over the velocities is done using the Maxwell-Boltzmann distribution as follows

$$\langle P(b,\omega,T)\rangle_v = \frac{\int_0^\infty \bar{P}(b,\omega,v)v^3\exp\left(-\frac{Mv^2}{2kT}\right)dv}{\int_0^\infty v^3\exp\left(-\frac{Mv^2}{2kT}\right)dv}$$

$$= 2\left(\frac{M}{2kT}\right)^2\int_0^\infty \bar{P}(b,\omega,v)v^3\exp\left(-\frac{Mv^2}{2kT}\right)dv \qquad (3.51)$$

where M is the reduced mass of the colliding pair. To facilitate the integration over velocities in closed form, the functions $G_\ell(x)$ and $J_\ell(x)$ were least-square fitted to the following forms

$$G_\ell(x) = e^{-2x}\left(A_\ell+B_\ell x+C_\ell x^2+D_\ell x^3+E_\ell x^4\right) \qquad (3.52)$$

and

$$J_\ell^2(x) = e^{-x/2}\left(a_\ell+b_\ell x+c_\ell x^2+d_\ell x^3\right) \qquad (3.53)$$

The constants in Eqns. (3.52) and (3.53) for various values of ℓ were tabulated[27]. Using Eqn. (3.52), Eqn. (3.45) can be written as

$$\langle P_{\ell_1\ell_2}(b\geq d)\rangle_v = D_\ell b^{-2l}\langle v^{-2}G_\ell(\omega b/v)\rangle_v$$

$$= 2\alpha^2 D_\ell b^{-2\ell}\int_0^\infty ve^{-2\beta/v}\left(A_\ell+B_\ell(\omega b/v)+C_\ell(\omega b/v)^2+D_\ell(\omega b/v)^3+\ \ldots\right)e^{-\alpha v^2}dv \qquad (3.54)$$

where $\alpha = \frac{M}{2kT}$ and $\beta = \omega b$.

The details of evaluation of the integrals in Eqn. (3.54) are described in Appendix B and the final result is given by

$$\langle P_{\ell_1\ell_2}(b\geq d)\rangle_v = 2\alpha D_\ell b^{-2\ell}\Big(A_\ell f_1(2x)+B_\ell x f_0(2x)+C_\ell x^2 f_{-1}(2x)$$

$$+ D_\ell x^3 f_{-2}(2x)+E_\ell x^4 f_{-3}(2x)\Big)$$

$$= 2\alpha D_\ell b^{-2\ell} I_\ell(b,\omega,T) \qquad (3.55)$$

where $x = \omega b\sqrt{\alpha}$. Here $f_n(x)$ is the integral

$$f_n(x) = \int_0^\infty \exp\left[-\left(\frac{x}{u}\right)+u^2\right]u^n du \qquad (3.56)$$

A rapidly converging expression for $f_1(x)$ is given by[52]

$$2f_1(x) = \sum_{k=0}^{\infty}(a_k \ln x + b_k)x^k \qquad (3.57)$$

where a_k and b_k are constants. For large values of x, the asymptotic expression given below is used

$$f_n(x) = \sqrt{\frac{\pi}{3}}\, 3^{-n/2} v^{n/2} e^{-V}\left(a_0 + \frac{a_1}{V} + \frac{a_2}{V^2} + \ldots. + \frac{a_k}{V^k} + \ldots\right) \qquad (3.58)$$

where $V = 3\left(\frac{x}{2}\right)^{2/3}$. For the evaluation of $f_1(x)$ by polynomial approximation the constants a_k and b_k up to k = 20 were used and in the asymptotic approximation a_k and b_k up to k = 10 were used in the present work. For values of x less than 3 the polynomial approximation was used and for x greater than 3 the asymptotic approximation was used for the evaluation of $f_1(x)$. The relations

for obtaining the various constants a_k and b_k are also given in Appendix B.

Substituting Eqn. (3.53) into Eqn. (3.47) and averaging over the velocities yielded a similar expression

$$\langle P_{\ell_1\ell_2}(b=0)\rangle_v = D_\ell d^{-2\ell}\langle v^{-2}J_\ell^2(\omega d/v)\rangle_v$$

$$= 2\alpha D_\ell d^{-2\ell}\left(a_\ell f_1(x/2)+b_\ell x f_0(x/2)+c_\ell x^2 f_{-1}(x/2)+d_\ell x^3 f_{-2}(x/2)\right)$$

$$= 2\alpha D_\ell d^{-2\ell} I_\ell(0,\omega,T) \qquad (3.59)$$

where $x = \omega d\sqrt{\alpha}$.

The function $I_\ell(b,\omega,T)$ is the Fourier transform of the interaction potential and its value drops off rapidly for values of $x>1$. As will be seen later in this section, the probability of the energy transfer is directly proportional to the functions $I_\ell(b,\omega,T)$ and $I_\ell(0,\omega,T)$. Hence the strength of these Fourier transforms will give an indication of the magnitude of the probability. A plot of $I_\ell(b,\omega,T)$ and $I_\ell(0,\omega,T)$ is shown in Fig. 3.1 as a function of absolute value of energy transferred from internal degrees of freedom to translation in a CO_2-CF_2Cl_2 collision at b = 4.58 Å and T = 323 K. In this system dipole-dipole interaction is the dominant interaction. Therefore, $\ell_1=\ell_2=1$. It can be observed that the value $I_2(b,\omega,T)$ remains constant up to $\nu \simeq 7$ cm^{-1} (this value of ν corresponds to x = 1) after which it falls off rapidly. $I_2(0,\omega,T)$ is seen to fall off less rapidly than $I_2(b,\omega,T)$ which means that at higher values of

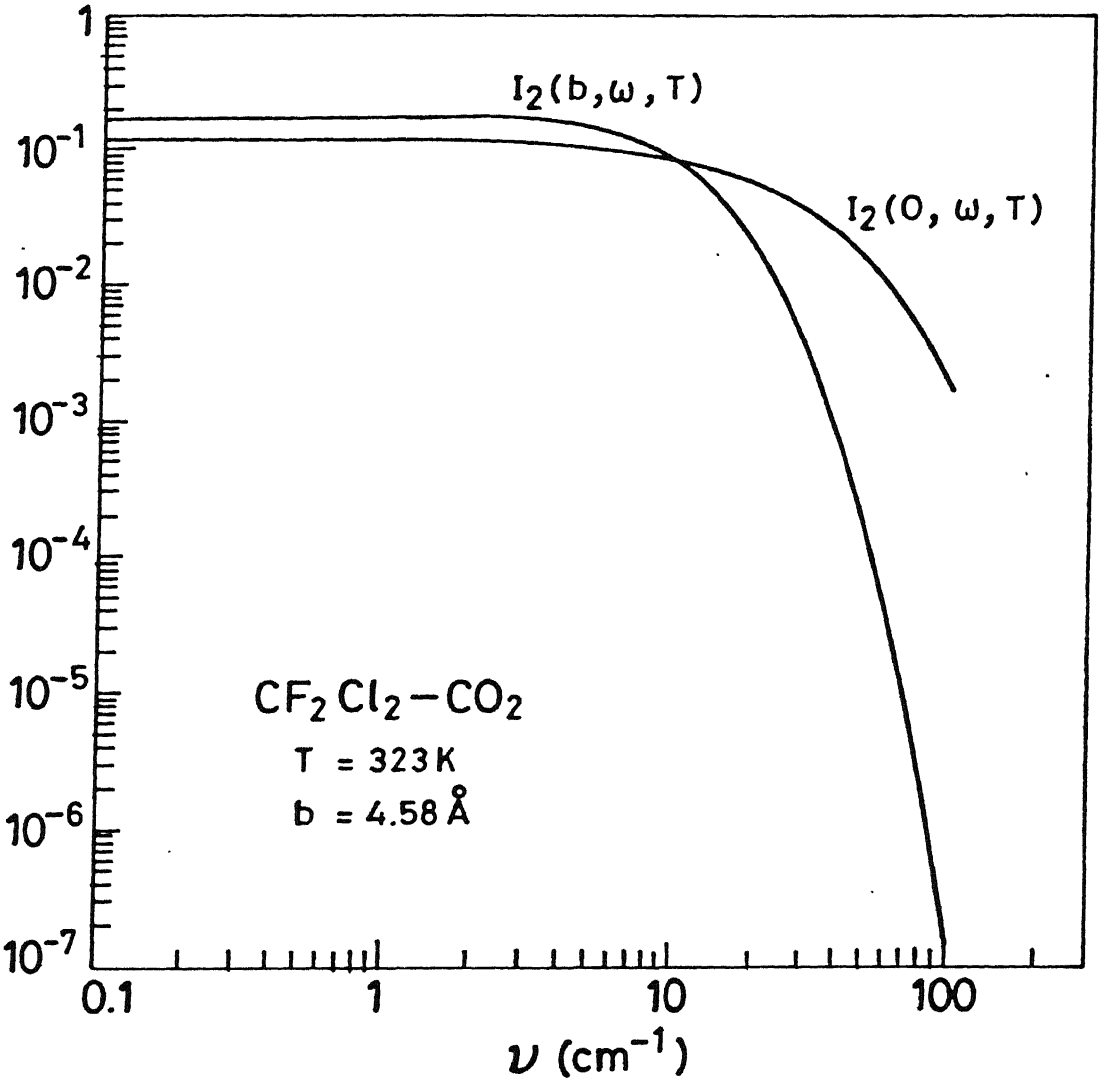

Fig. 3.1 Plot of $I_2(b,\omega,T)$ and $I_2(0,\omega,T)$ versus ν

v, the contribution from b=0 collisions is greater compared with b=d collisions. This is true not only for dipole-dipole interaction but also for other multipole interactions like dipole-quadrupole etc. and is not particular to the present system of CO_2-CF_2Cl_2 only.

The averaging of the probability over the impact parameter b is performed by

$$\langle\langle P_{\ell_1\ell_2}\rangle_v\rangle_b = 2\pi\int_0^\infty \frac{\langle P_{\ell_1\ell_2}\rangle_v}{\pi d^2}\, b\, db$$

$$= \left(\frac{2}{d^2}\right)\left[\int_0^d \langle P_{\ell_1\ell_2}\rangle_v\, b\, db + \int_d^\infty \langle P_{\ell_1\ell_2}\rangle_v\, b\, db\right] \qquad (3.60)$$

Using the interpolation formula given by Eqn. (3.49) for evaluating the integral in the above equation in the range 0<b<d, we get

$$\langle\langle P_{\ell_1\ell_2}\rangle_v\rangle_b = \frac{2}{d^2}\left[\int_0^d \left\{\langle P_{\ell_1\ell_2}(0)\rangle_v + \frac{b^2}{d^2}\left(\langle P_{\ell_1\ell_2}(d)\rangle_v - \langle P_{\ell_1\ell_2}(0)\rangle_v\right)\right\} b\, db\right.$$

$$\left. + \int_d^\infty \langle P_{\ell_1\ell_2}(b>d)\rangle_v\, b\, db\right] \qquad (3.61)$$

$$= \frac{1}{2}\left[\langle P_{\ell_1\ell_2}(0)\rangle_v + \frac{1}{2}\langle P_{\ell_1\ell_2}(d)\rangle_v\left(1 + \frac{2}{\ell-1}\right)\right] \qquad (3.62)$$

In obtaining Eqn. (3.62) the assumption made by Sharma and Brau was that $I_\ell(b,\omega,T)$ is independent of b and they used the

equality $I_\ell(b,\omega,T)=I_\ell(d,\omega,T)$ for b>d. This assumption was later shown to be unsatisfactory by Tam[53]. Tam's procedure did not require this assumption and is described in the next section.

For the specific case of dipole-dipole interaction, denoting the probability by P, Eqn. (3.62) becomes

$$\langle\langle P\rangle_v\rangle_b = \frac{1}{2}\left[\langle P(0)\rangle_v + 3\langle P(d)\rangle_v\right] \tag{3.63}$$

Using Eqns. (3.55) and (3.59) and rearranging Eqn. (3.63), we get

$$\langle\langle P\rangle_v\rangle_b=\frac{1}{2}\left[2\alpha D_2 I_2(0,\omega,T)/d^4\right]+\frac{1}{2}\left[2\alpha D_2 I_2(d,\omega,T)/d^4\right]+\frac{\alpha D_2}{d^4}\left[2I_2(d,\omega,T)\right] \tag{3.64}$$

Since the experiments are performed when the rotational motion of the gas is in equilibrium, Eqn. (3.63) should be weighted over initial rotational states by Maxwell-Boltzmann distribution as given below

$$\langle\langle \bar{P}\rangle_v\rangle_b=\frac{1}{2}\sum_{j_1,j_1'}\sum_{j_2,j_2'}\left[\langle P_{\ell_1\ell_2}(0)\rangle_v+\frac{1}{2}\langle P_{\ell_1\ell_2}(d)\rangle_v\left(1+\frac{2}{\ell-1}\right)\right]n_{j_1}^{(1)}n_{j_2}^{(2)} \tag{3.65}$$

where $n_j^{(i)}$ is the probability that the molecule i is in the rotational level j. The allowed transitions for j_1 and j_2 in case of dipole-dipole interaction are given by the optical selection rule Δj_1, $\Delta j_2 = \pm 1$.

III.6 Tam's Modification to the SB Theory (SB-Tam theory)

The assumption made by Sharma and Brau that $I_\ell(b,\omega,T)$ is independent of b for b>d was shown to be unsatisfactory by Tam[53] by comparing the values of $I_\ell(b,\omega,T)$ for two different values of b. It was shown that $I_\ell(b,\omega,T)$ decreases with increasing value of b for a given T and ω. This is to be expected since I_ℓ is a function of the product ωb and increasing the values of either of the two parameters will have the same effect of reducing the value of I_ℓ. Thus the theory of SB overestimates the probabilities when $\omega \neq 0$. In Tam's procedure[50], the integration over impact parameter b preceded the integration over velocity v. This reversal of the order of integration, did not give an analytical expression for the probability but required numerical evaluation of an integral. This procedure gave a better estimate of the probability and the details are given below.

The integration over the impact parameter is done as follows

$$\langle P_{\ell_1\ell_2}(b)\rangle_b = 2\pi\int_0^\infty \frac{P_{\ell_1\ell_2}(b)}{\pi d^2}\, b\, db \tag{3.66}$$

Here also the parabolic interpolation given by Eqn. (3.49), for the range 0<b<d, was used which results in

$$\langle P_{\ell_1\ell_2}(b)\rangle_b = \frac{2}{d^2}\int_0^d \left\{P_{\ell_1\ell_2}(b=0)+\frac{b^2}{d^2}\left(P_{\ell_1\ell_2}(b=d)-P_{\ell_1\ell_2}(b=0)\right)\right\} b\, db$$

$$+\frac{2}{d^2}\int_d^\infty P_{\ell_1\ell_2}(b\geq d)\, b\, db \tag{3.67}$$

Using the expression given in Eqn. (3.45), the Eqn. (3.49) results in

$$\langle P_{\ell_1\ell_2}(b)\rangle_b = \frac{1}{2}\left[P_{\ell_1\ell_2}(b=0)+P_{\ell_1\ell_2}(b=d)\right]+2D_\ell d^2 v^{-2} F_\ell(\omega d/v) \qquad (3.68)$$

where $$F_\ell(\omega d/v) = \int_d^\infty \frac{G_\ell(\omega b/v)}{b^{2\ell-1}}\, db \qquad (3.69)$$

Replacing $G_\ell(\omega b/v)$ by the polynomial expression given by Eqn. (3.52) this becomes

$$F_\ell(\omega d/v)=\int_d^\infty e^{-2\omega b/v}\left[A_\ell+B_\ell(\omega b/v)+C_\ell(\omega b/v)^2+D_\ell(\omega b/v)^3+E_\ell(\omega b/v)^4\right]\frac{db}{b^{2\ell-1}} \qquad (3.70)$$

Evaluation of the integrals in Eqn. (3.70) is given in Appendix C for the case of dipole-dipole interaction ($\ell_1=1$, $\ell_2=1$). The averaging over velocity v is done as in the previous case, resulting in

$$\langle\langle P_{\ell_1\ell_2}(b)\rangle_b\rangle_v = \frac{1}{2}\left[\langle P_{\ell_1\ell_2}(0)\rangle_v+\langle P_{\ell_1\ell_2}(d)\rangle_v\right]+2D_\ell d^{-2}\langle v^{-2}F_\ell(\omega d/v)\rangle_v \qquad (3.71)$$

From now onwards, only dipole-dipole interaction ($\ell_1=\ell_2=1$) which is of interest in the present work will be considered. Hence ℓ will be replaced by 2.

Using Eqns. (3.47), (3.51) and (3.53) the velocity averaged probability for b=0 is given by

$$\langle P(0)\rangle_v = D_2 \frac{2\alpha^2}{d^4} \int_0^\infty \left\{ e^{-\omega d/2v} \left[a_2 + b_2(\omega d/v) + c_2(\omega d/v)^2 + d_2(\omega d/v)^3 \right] \frac{e^{-\alpha v^2}}{v} \right\} dv \tag{3.72}$$

The evaluation of such integrals has already been done in Appendix B and the final result is

$$\langle P(0)\rangle_v = 2\alpha D_2 d^{-4} I_2(0,\omega,T) \tag{3.73}$$

Proceeding along the similar line for b=d, we get

$$\langle P(d)\rangle_v = 2\alpha\, D_2 d^{-4} I_2(d,\omega,T) \tag{3.74}$$

For the evaluation of $\langle v^{-2} F_2(\omega d/v)\rangle_v$, the expression given for $F_2(\omega d/v)$ in Appendix C was used and the integration over v results in

$$\langle v^{-2} F_2(\omega d/v)\rangle_v = \frac{2\alpha}{d^2} \left[\frac{1}{2} A_2 f_1(2x) + (B_2 - A_2) x f_0(2x) + \frac{1}{4}(2D_2 + E_2) x^2 f_{-1}(2x) \right.$$

$$\left. + \frac{1}{2} E_2 x^3 f_{-2}(2x) + (2A_2 - 2B_2 + C_2) x^2 \int_0^\infty \frac{1}{v} E_1(2\omega d/v) e^{-\alpha v^2} dv \right] \tag{3.75}$$

where $x = \omega d\sqrt{\alpha}$ and

$$E_1(2\omega d/v) = \int_{2\omega d/v}^\infty \frac{1}{y} e^{-y} dy$$

is the exponential integral.

In Eqn. (3.75) the integration over v, involving the exponential integral has to be evaluated numerically. Gaussian quadrature technique with 24 gauss-points was used in the present work to evaluate the integral and the polynomial and rational approximation given by Abramowitz and Stegun[54] was used for $E_1(2\omega d/v)$. When the upper limit of the integration was increased beyond 7.3, there was no further increase in the value of the integral. The probability of energy transfer is given by

$$\langle\langle P(b)\rangle_b\rangle_v = \frac{1}{2}\left[\frac{2\alpha\ D_2 I_2(0,\omega,T)}{d^4}\right]+\frac{1}{2}\left[\frac{2\alpha\ D_2 I_2(d,\omega,T)}{d^4}\right]$$

$$+\ (\alpha D_2/d^4)\left[\langle v^{-2}F_2(\omega d/v)\rangle_v \frac{2d^2}{\alpha}\right] \qquad (3.76)$$

Comparing Eqn. (3.76) with Eqn. (3.64), it can be seen that the first two terms are the same and the difference exists in the last term where the coefficient of $(\alpha D_2/d^4)$ is different. The values of $2I_2(d,\omega,T)$ and $2\alpha^{-1}s^2\langle d^{-2}F_2(\omega d/v)\rangle_v$ are plotted in Fig. 3.2 as a function of ν.

It can be seen from Fig. 3.2 that both the expressions give the same value when ν is very small ($\simeq 5cm^{-1}$) which can be expected because $I_2(b,\omega,T)$ can be assumed to be independent of b only in a small region around ν=0. In the same plot the dependence of $I_2(0,\omega,T)$ on ν is also shown. It can be seen that at large values of ν, the contribution of head-on collisions (zero impact parameter) is an order of magnitude greater than either $I_2(d,\omega,T)$ or $\alpha^{-1}d^2\langle v^{-2}F_2(\omega d/v)\rangle_v$. At large values of ν, both SB theory and

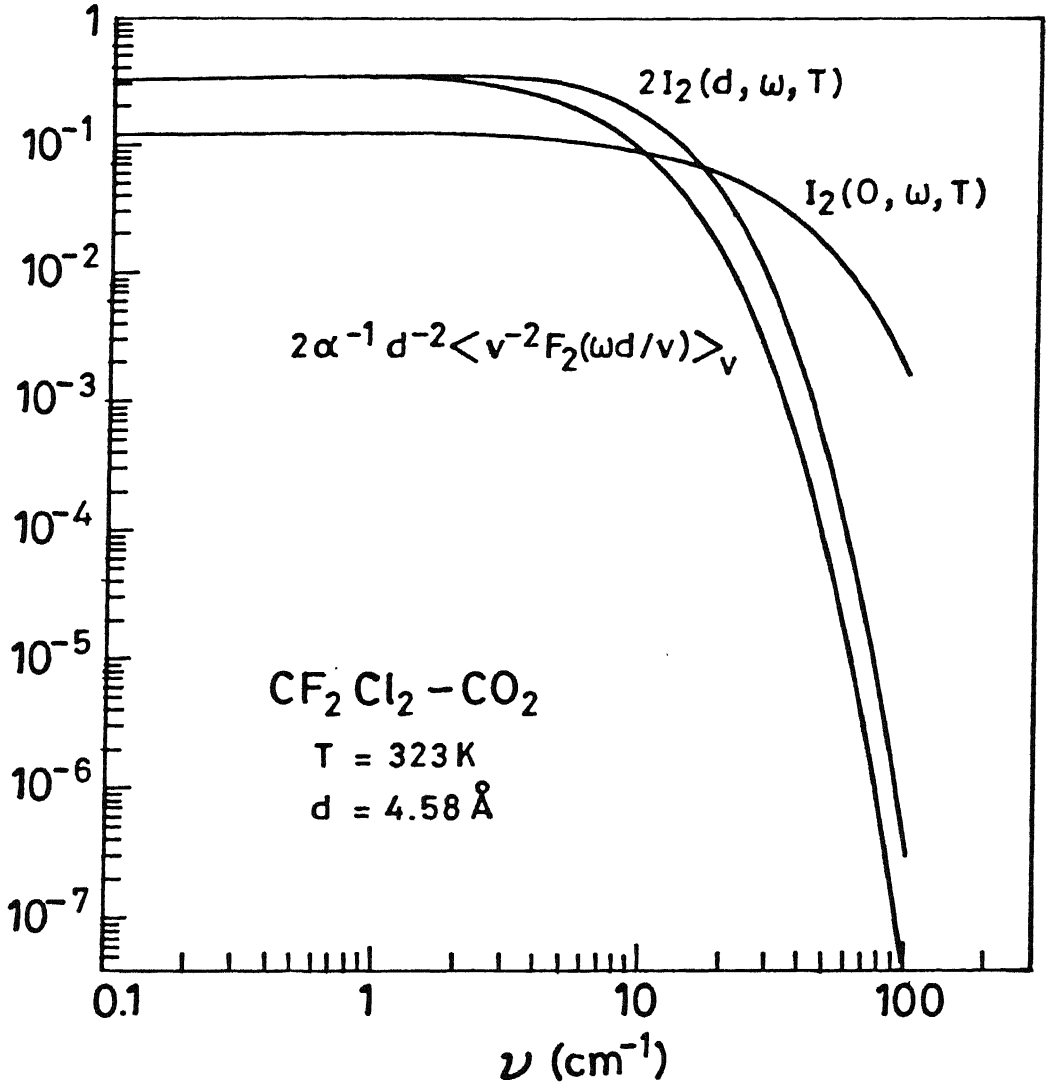

Fig. 3.2 Plot of $I_2(0, \omega, T)$, $2I_2(d, \omega, T)$ and $2\alpha^{-1} d^{-2} \langle v^{-2} F_2(\omega d/v) \rangle_v$ versus ν

Tam's modified theory will give identical values for the probability since only the first term of Eqns. (3.64) and (3.76) make a contribution.

In order to obtain the probability that can be compared with the experimental results, Eqn. (3.76) has to be averaged over initial rotational states using Maxwell-Boltzmann distribution as was done in the case of SB theory i.e.

$$\langle\langle\bar{P}\rangle_b\rangle_v = \sum_{j_1,j_1'}\sum_{j_2,j_2'}\left[\frac{1}{2}\left\{\frac{2\alpha D_2 I_2(0,\omega,T)}{d^4}\right\}+\frac{1}{2}\left\{\frac{2\alpha D_2 I_2(d,\omega,T)}{d^4}\right\}\right.$$

$$\left. + (\alpha D_2/d^4)\left[\langle v^{-2}F_2(\omega d/v)\rangle_v \frac{2d^2}{\alpha}\right] n_{j_1}^{(1)} n_{j_2}^{(2)}\right. \qquad (3.77)$$

As before, $n_j^{(i)}$ is the probability that the molecule i is in the rotational level j. The selection rule for j is $\Delta j=\pm 1$ for dipole-dipole interaction. The relation for the calculation of n_j are given by

$$n_j = \frac{g_j e^{-Bj(j+1)\frac{hc}{kT}}}{\sum_{j=0}^{\infty}\sum_{K=-j}^{+j} g_j e^{-Bj(j+1)\frac{hc}{kT}}} \qquad \text{(for diatomic and linear polyatomic molecules)}$$

$$n_{jK} = \frac{g_{jK} e^{-[Bj(j+1)+(A-B)K^2]\frac{hc}{kT}}}{\sum_{j=0}^{\infty}\sum_{K=-j}^{+j} g_{jK} e^{-[Bj(j+1)+(A-B)K^2]\frac{hc}{kT}}} \qquad \text{(for symmetric and prolate symmetric top molecules)}$$

and

$$n_{jK} = \frac{g_{jK} e^{-[Bj(j+1)+(C-B)K^2]\frac{hc}{kT}}}{\sum_{j=0}^{\infty} \sum_{K=-j}^{+j} g_{jK} e^{-[Bj(j+1)+(C-B)K^2]\frac{hc}{kT}}} \qquad \text{(for oblate symmetric top molecules)}$$

where A, B are the rotational constants in cm^{-1}. For $CO_2(00^\circ1)$ level, since the even rotational levels are absent (g_j=0 for even j) only odd rotational levels are considered (g_j=2j+1 for odd j) in the calculation. For the symmetric top, prolate symmetric top and oblate symmetric top molecules the g_{jK}=(2j+1). The sums over the rotational states according to Eqn. (3.78) were evaluated on Convex C-220 minisuper computer. The results of the calculation for CO_2-CF_2Cl_2, CO_2-C_4H_4S and $CO_2(CD_3)_2CO$ are presented in Chapters IV, V and VI respectively.

CHAPTER IV

EXPERIMENTAL RESULTS AND DISCUSSION : CO_2-CF_2Cl_2 SYSTEM

IV.1 General Remarks

The deactivation rates of $CO_2(00^\circ1)$ in mixtures of CO_2-CF_2Cl_2 have been measured in the temperature range 323-463 K. The rates were measured at four different temperatures viz. 323 K, 363 K, 413 K and 463 K, for four different compositions of CO_2 and CF_2Cl_2 mixtures. The compositions (by volume) studied were 3.0%, 7.7%, 10.1% and 13.9% CF_2Cl_2. The mixture compositions were estimated from the partial pressures of CO_2 and CF_2Cl_2. The measurement of partial pressures of the gases were performed with the help of a silicone oil and a mercury manometer. The uncertainty in the measurement of partial pressure was 0.16 Torr when silicone oil manometer was used, whereas it was 2 Torr for mercury manometer. The uncertainty in the composition was estimated in terms of the uncertainties in pressure measurements. The experiments were carried out on lean mixtures of CF_2Cl_2 to ensure that the measured relaxation times were at least four to five times greater than the time constant of the detector and associated electronics. Hence the maximum percentage of CF_2Cl_2 in the mixture was limited to 13.9%. The collisional deactivation rate of $CO_2(00^\circ1)$ due to

collisions with CF_2Cl_2 alone was obtained by extrapolating the measured rate to 100% CF_2Cl_2.

The experimental probabilities for the deactivation of $CO_2(00^\circ1)$ were found to be almost temperature independent in the range 323 K to 463 K. The energy transfer probabilities were calculated using SSH-Tanczos theory as well as SB-Tam theory. The SSH-Tanczos theory could not explain the magnitude or the temperature dependence of the energy transfer probabilities. However the SB-Tam theory successfully explained both the magnitude and the temperature dependence of the experimental probabilities. The experimental results and analysis are presented below in detail.

IV.2 Experimental Results

Pure CO_2 :

Experiments were performed in pure CO_2 to observe deactivation rate of $CO_2(00^\circ1)$ level in collisions with CO_2 at all the four temperatures, viz. 323 K, 363 K, 413 K and 463 K. The data are presented in Table 4.1 and are found to be in good agreement with the literature values[28,30-32].

Table 4.1 : Experimental Values of $(P\tau)^{-1}$ for Pure CO_2 at Different Temperatures.

T (K)	$(P\tau)^{-1}$ ($Torr^{-1}ms^{-1}$)
323	0.32±0.05
363	0.40±0.04
413	0.50±0.05
463	0.54±0.05

CO_2-CF_2Cl_2 :

The fluorescence from $CO_2(00^\circ1)$ level in this system exhibited a single exponential decay with a time constant τ for all the compositions of the mixtures studied. A typical fluorescence signal for a 10.1% CF_2Cl_2 mixture at 4.00 Torr and 413 K is shown in Fig. 4.1. A semilogarithmic plot of the intensity as a function of time was found to be a straight line and is shown in Fig. 4.2. A least squares fit of the intensity to the relation $I = I_0\exp(-t/\tau)$ yielded $\tau^{-1} = (31.25\pm3.47)\ ms^{-1}$.

The experiments were conducted at various pressures in the range 4-18 Torr and at each pressure the value of τ^{-1} was obtained. Since the deactivation rate due to radiation, $(\tau^{-1})_{rad}$ of $CO_2(00^\circ1)$ is reported[55] to be 0.4 ms^{-1} and the measured values of τ^{-1} are in the range 11-180 ms^{-1}, $(\tau^{-1})_{rad}$ can be neglected in comparison to τ^{-1}. It can be seen from Eqn. (2.1) that as long as the radiative and diffusional contributions to the deactivation rate are negligible, the observed τ^{-1} represents only the collisional deactivation rate of $CO_2(00^\circ1)$. In the pressure range where binary collisions are dominant, the collisional deactivation rate is proportional to the pressure P. Fig. 4.3 shows a plot of τ^{-1} vs P for 10.1% of CF_2Cl_2 at 413 K. The linearity of the plot throughout the pressure range indicates that the diffusion effects to deplete the molecules in $CO_2(00^\circ1)$ are negligible even at the

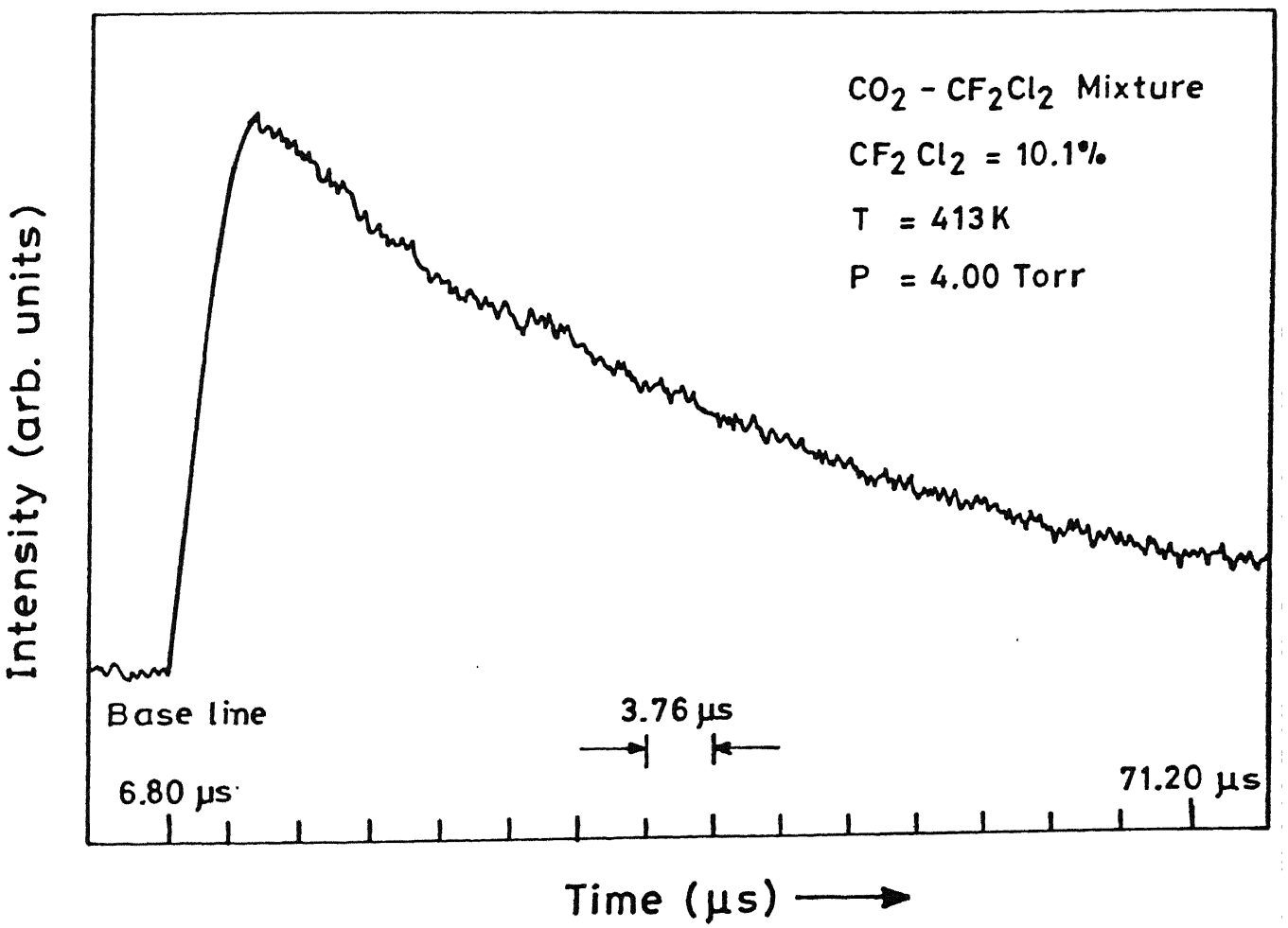

Fig. 4.1 Typical fluorescence signal.

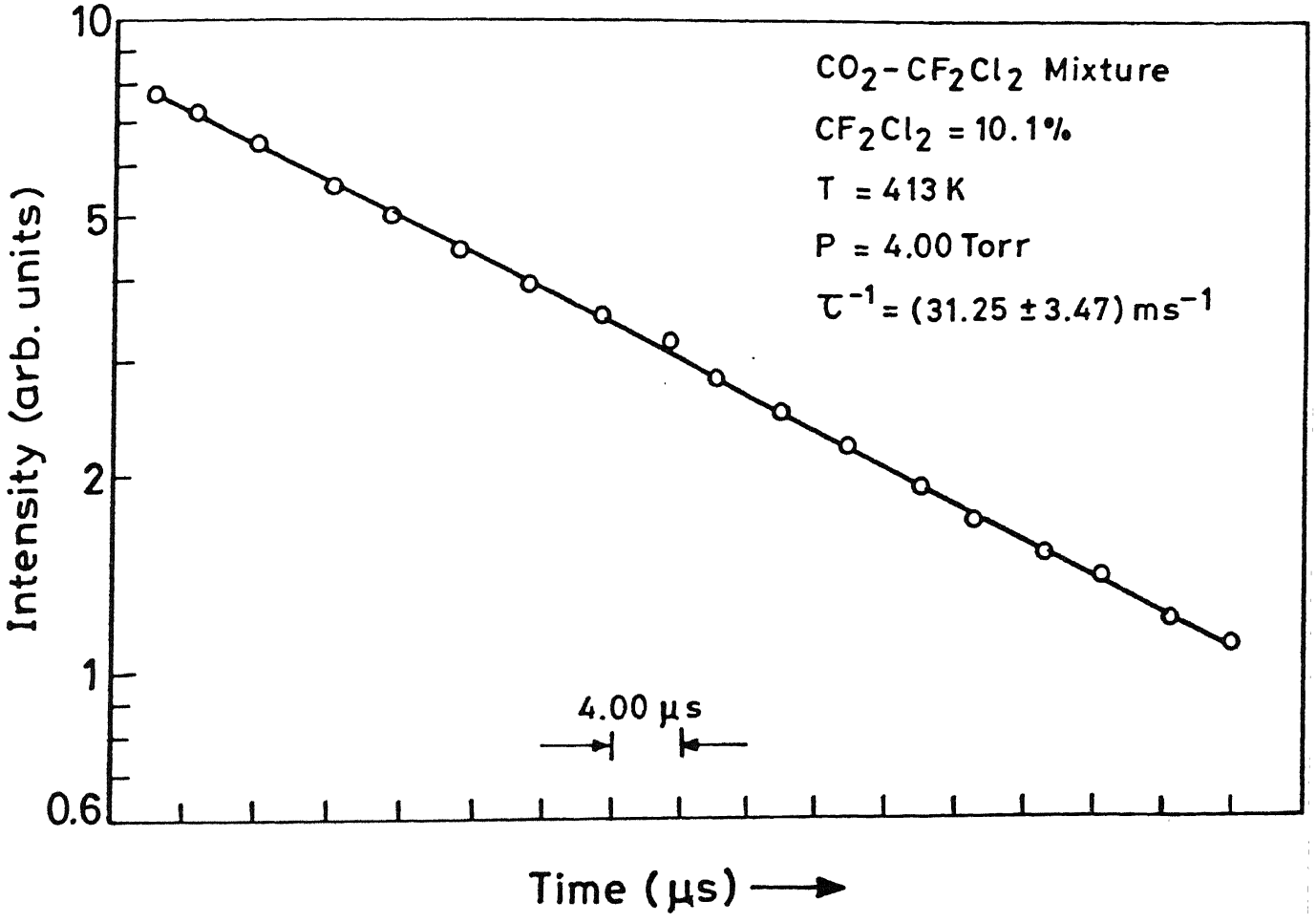

Fig. 4.2 Semilogarithmic plot of fluorescence intensity vs time.

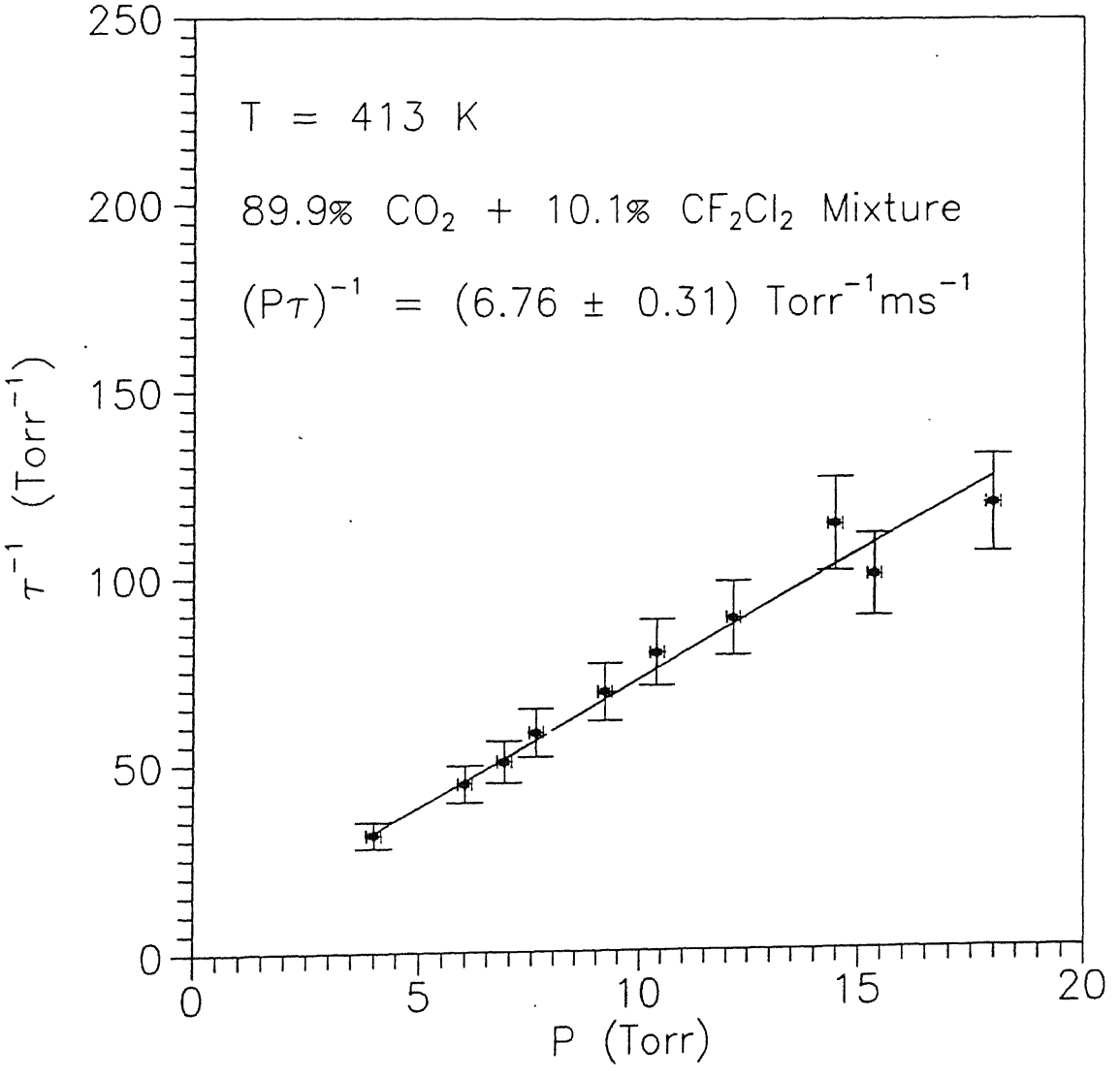

Fig. 4.3 Plot of τ^{-1} vs pressure.

lowest pressure studied. The experimental data of τ^{-1} versus P were fitted to a straight line by a least squares technique, developed by Reed[56], which takes into account the errors in both the parameters. This gave $(P\tau)^{-1} = (6.76\pm0.31)$ $Torr^{-1}ms^{-1}$, where the error corresponds to the standard deviation. The experiments were performed at four different temperatures and the results are presented in Table 4.2.

In a mixture of CO_2 and CF_2Cl_2 the deactivation of $CO_2(00^\circ1)$ can occur through collisions between CO_2 and CO_2 as well as through collisions between CO_2 and CF_2Cl_2. As the concentration of CF_2Cl_2 in the mixture increases, the collisions between CO_2 and CF_2Cl_2 increase. Thus the deactivation rate of $CO_2(00^\circ1)$ increases with increasing CF_2Cl_2 concentration if CF_2Cl_2 is more efficient than CO_2 in deactivating $CO_2(00^\circ1)$ and vice versa. To observe the effect of composition on the deactivation rate of $CO_2(00^\circ1)$, the relaxation times were measured for four different mixtures of CO_2 and CF_2Cl_2. The measured relaxation times at different temperatures and pressures for 3.0%, 7.7% and 13.9% CF_2Cl_2 mixtures are presented in Tables 4.3, 4.4 and 4.5, respectively.

Table 4.2 Experimental Values of τ^{-1} versus P at Different Temperatures for 10.1% CF_2Cl_2 mixture

T = 323 K		T = 363 K		T = 413 K		T = 463 K	
P (Torr)	τ^{-1} (ms^{-1})	P (Torr)	τ^{-1} (ms^{-1})	P (Torr)	τ^{-1} (ms^{-1})	P (Torr)	τ^{-1} (ms^{-1})
4.40	35.71	4.32	40.98	4.00	31.25	4.48	31.25
5.04	50.00	4.80	53.19	6.00	44.64	5.92	39.06
6.16	54.95	6.64	54.95	6.88	50.51	6.88	48.54
6.72	62.50	6.80	59.52	7.60	58.14	7.60	55.56
7.68	69.44	7.92	64.10	9.20	68.97	10.08	64.94
8.40	64.94	9.12	80.00	10.40	79.37	10.40	66.67
10.08	81.30	9.92	73.53	12.16	88.50	11.68	67.57
10.80	67.57	11.36	79.37	14.48	113.60	13.04	92.59
12.96	89.29	11.76	89.29	15.36	100.00	14.88	94.34
12.96	100.00	12.08	106.40	18.00	119.00	16.32	102.00
15.52	172.40						
17.28	135.10						
$(P\tau)^{-1}$ = (7.02±0.91) $Torr^{-1}ms^{-1}$		$(P\tau)^{-1}$ = (6.18±0.69) $Torr^{-1}ms^{-1}$		$(P\tau)^{-1}$ = (6.76±0.31) $Torr^{-1}ms^{-1}$		$(P\tau)^{-1}$ = (6.02±0.35) $Torr^{-1}ms^{-1}$	

Table 4.3 Experimental Values of τ^{-1} versus P at Different Temperatures for 3.0% CF_2Cl_2 mixture

T = 323 K		T = 363 K		T = 413 K		T = 463 K	
P (Torr)	τ^{-1} (ms^{-1})	P (Torr)	τ^{-1} (ms^{-1})	P (Torr)	τ^{-1} (ms^{-1})	P (Torr)	τ^{-1} (ms^{-1})
4.16	12.25	4.80	13.59	4.16	11.36	5.04	13.23
5.04	15.29	7.20	18.32	5.04	13.16	6.40	15.87
7.28	21.28	8.40	15.72	6.96	16.67	6.80	18.69
8.88	19.84	9.12	20.58	8.56	18.38	7.68	20.58
11.06	28.99	10.48	22.47	10.40	27.40	9.04	18.52
11.36	24.69	12.08	25.97	10.64	24.10	10.00	21.74
12.64	28.57	12.08	26.67	11.60	27.03	10.56	24.15
14.96	27.40	13.68	33.90	12.48	25.97	12.24	26.67
16.40	38.46	15.12	32.79	13.36	23.26	14.00	26.67
18.40	41.67	18.00	36.36	15.92	31.75	16.96	32.26
		18.00	37.74	18.24	39.22	17.68	29.85
				18.24	41.67	18.08	30.30
						18.08	32.79
$(P\tau)^{-1}$ = (1.80±0.18) $Torr^{-1}ms^{-1}$		$(P\tau)^{-1}$ = (1.87±0.17) $Torr^{-1}ms^{-1}$		$(P\tau)^{-1}$ = (1.84±0.15) $Torr^{-1}ms^{-1}$		$(P\tau)^{-1}$ = (1.38±0.11) $Torr^{-1}ms^{-1}$	

Table 4.4 Experimental Values of τ^{-1} versus P at Different Temperatures for 7.7% CF_2Cl_2 mixture

T = 323 K		T = 363 K		T = 413 K		T = 463 K	
P (Torr)	τ^{-1} (ms^{-1})	P (Torr)	τ^{-1} (ms^{-1})	P (Torr)	τ^{-1} (ms^{-1})	P (Torr)	τ^{-1} (ms^{-1})
4.40	28.09	5.04	31.65	5.12	29.07	4.88	26.32
5.28	35.21	6.40	37.88	6.08	32.89	5.20	27.78
6.72	37.31	8.40	43.86	7.84	46.30	6.56	33.90
8.48	64.10	10.08	56.82	9.12	52.08	7.68	32.89
9.20	56.82	11.52	54.35	10.56	56.82	9.04	45.45
11.04	64.10	12.72	69.44	11.92	55.56	10.56	53.19
12.16	67.57	13.60	80.65	12.40	55.56	11.12	53.19
12.96	65.79	14.40	79.37	13.36	63.29	12.08	69.44
15.04	86.21	16.56	92.59	14.40	68.49	13.68	60.98
16.08	90.91			15.60	78.13	16.00	67.57
$(P\tau)^{-1}$ = (5.19±0.45) $Torr^{-1}ms^{-1}$		$(P\tau)^{-1}$ = (5.00±0.40) $Torr^{-1}ms^{-1}$		$(P\tau)^{-1}$ = (4.23±0.32) $Torr^{-1}ms^{-1}$		$(P\tau)^{-1}$ = (4.24±0.40) $Torr^{-1}ms^{-1}$	

Table 4.5 Experimental Values of τ^{-1} versus P at Different Temperatures for 13.9% CF_2Cl_2 mixture

T = 323 K		T = 363 K		T = 413 K		T = 463 K	
P (Torr)	τ^{-1} (ms^{-1})	P (Torr)	τ^{-1} (ms^{-1})	P (Torr)	τ^{-1} (ms^{-1})	P (Torr)	τ^{-1} (ms^{-1})
4.08	43.86	3.92	37.88	4.48	51.55	4.32	50.00
5.60	69.44	4.88	53.76	6.24	56.82	5.04	54.35
6.64	69.93	6.88	65.79	6.32	67.57	6.16	58.48
7.04	79.37	8.24	84.75	7.92	75.19	8.24	94.34
7.84	96.15	9.60	94.34	9.92	119.00	9.12	92.59
9.44	94.34	11.20	114.90	11.04	120.50	11.60	117.60
10.24	108.70	13.04	112.40	13.60	135.10	13.36	137.00
11.20	126.60	14.48	138.90	13.76	126.60	13.76	133.30
12.96	147.10	15.76	172.40	15.44	181.80	15.84	181.80
14.88	156.30	17.44	151.50	15.60	147.10	16.96	158.70
$(P\tau)^{-1}$ = (10.71±0.66) $Torr^{-1}ms^{-1}$		$(P\tau)^{-1}$ = (9.25±0.55) $Torr^{-1}ms^{-1}$		$(P\tau)^{-1}$ = (9.86±0.90) $Torr^{-1}ms^{-1}$		$(P\tau)^{-1}$ = (9.70±0.58) $Torr^{-1}ms^{-1}$	

Figs 4.4a, 4.4b, 4.4c, and 4.4d show the dependence of $(P\tau^{-1})$ on the mole fraction of CF_2Cl_2, $X_{CF_2Cl_2}$, at various temperatures. The linearity of the plots suggest that the deactivation rate of the mixture can be expressed as

$$(P\tau)^{-1} = (P\tau)^{-1}_{CO_2-CO_2}(1 - X_{CF_2Cl_2}) + (P\tau)^{-1}_{CO_2-CF_2Cl_2}X_{CF_2Cl_2}$$

or $$k = k_{CO_2-CO_2}(1 - X_{CF_2Cl_2}) + k_{CO_2-CF_2Cl_2}X_{CF_2Cl_2}$$

where $k_{CO_2-CO_2}$ represents the rate constant for the deactivation of $CO_2(00^\circ1)$ in collisions with CO_2 molecules only, and $k_{CO_2-CF_2Cl_2}$ represents the rate constant for the deactivation of CO_2 in collisions with CF_2Cl_2 only. In principle the rate constant $k_{CO_2-CF_2Cl_2}$ can then be obtained by extrapolating the $(P\tau)^{-1}$ values to $X_{CF_2Cl_2} = 1$. A least squares analysis of $(P\tau)^{-1}$ vs $X_{CF_2Cl_2}$ data taking into account errors in both the parameters was performed to obtain the values of $k_{CO_2-CF_2Cl_2}$ at all the temperatures studied and the data are presented in Table 4.6. The rate constants, $k_{CO_2-CF_2Cl_2}$, are then converted into probabilities through the relation (2.8) and the results are presented in Table 4.7.

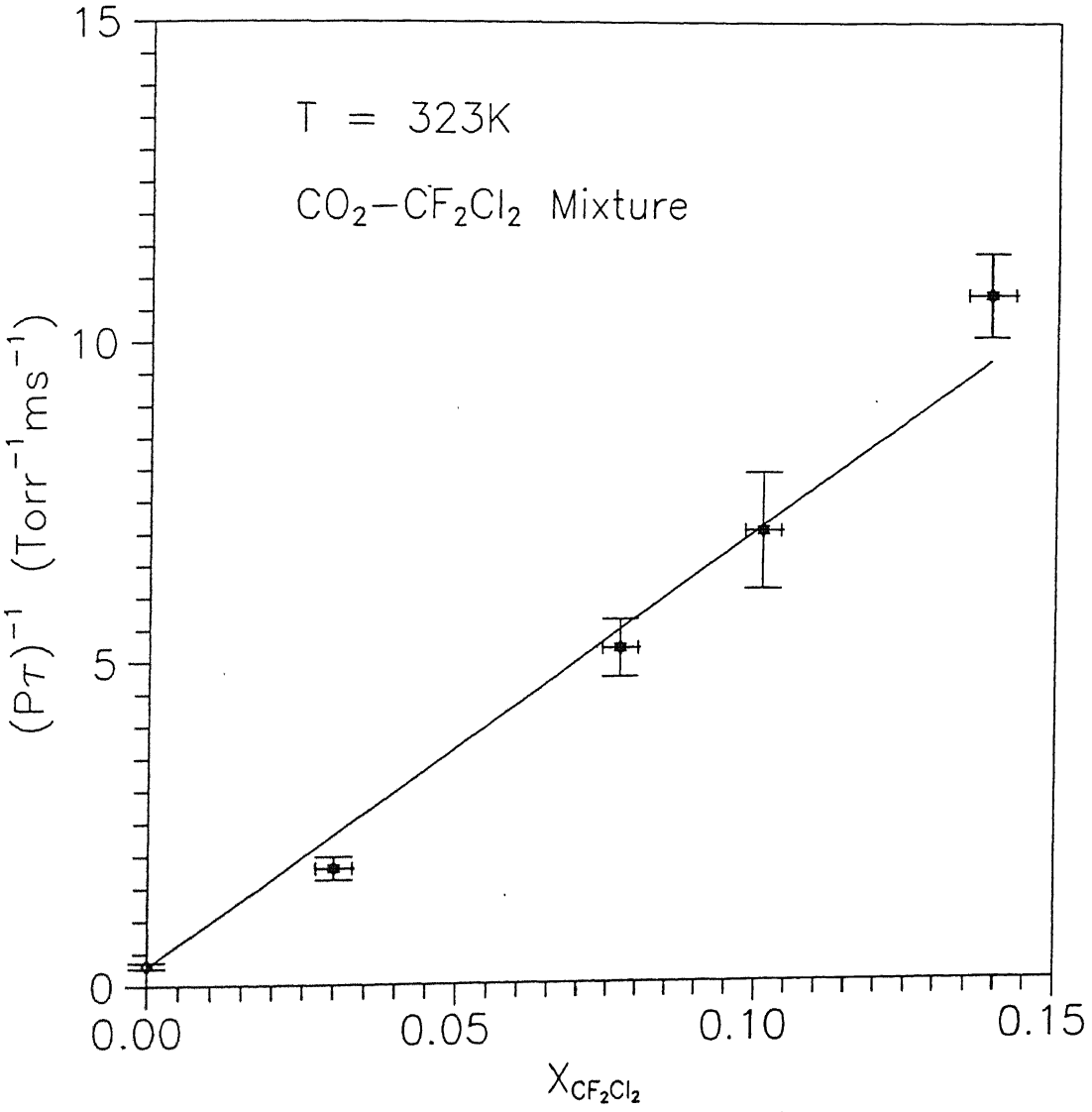

Fig. 4.4a Composition dependence of $(P\tau)^{-1}$ at 323 K.

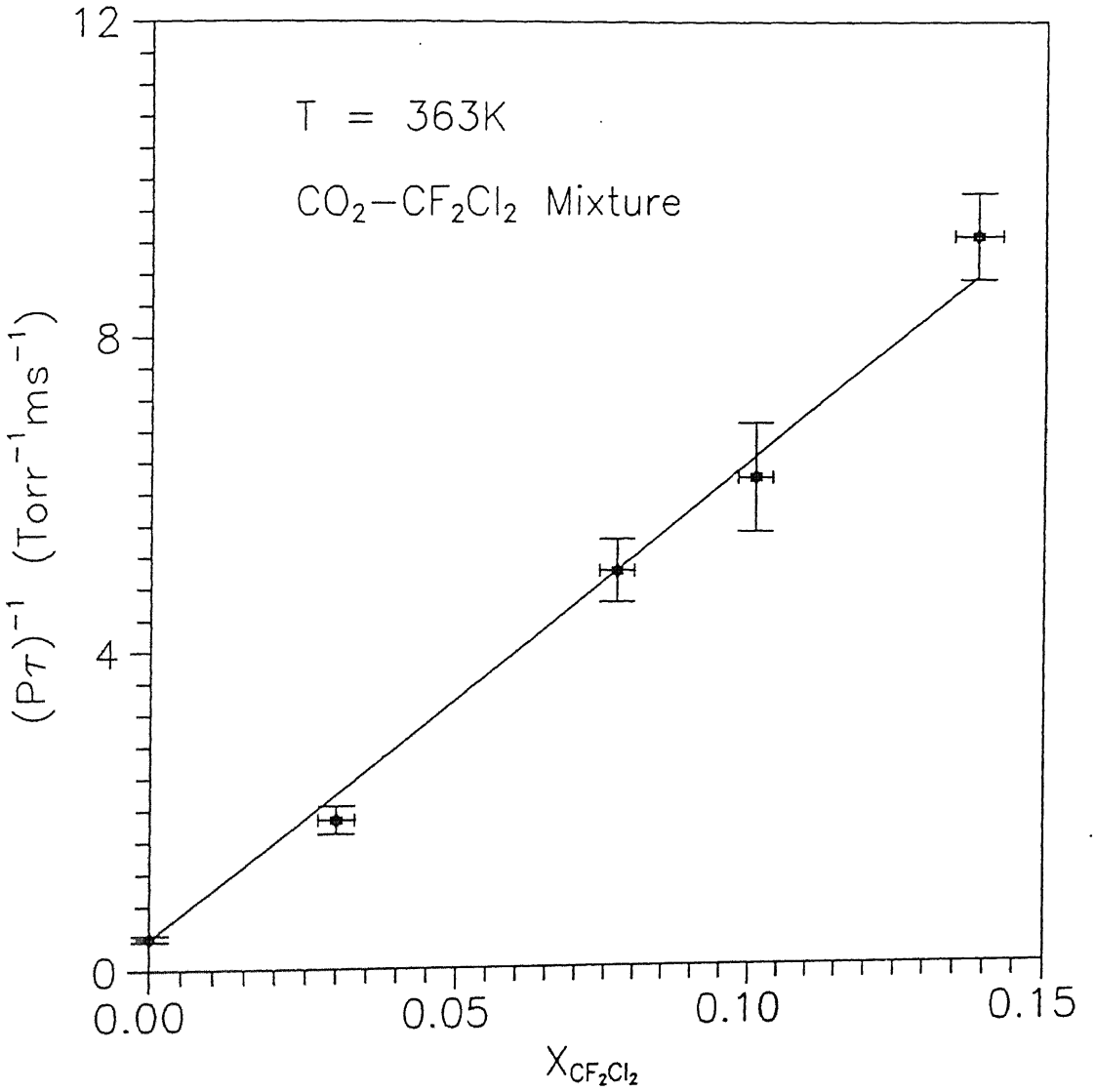

Fig. 4.4b Composition dependence of $(P\tau)^{-1}$ at 363 K.

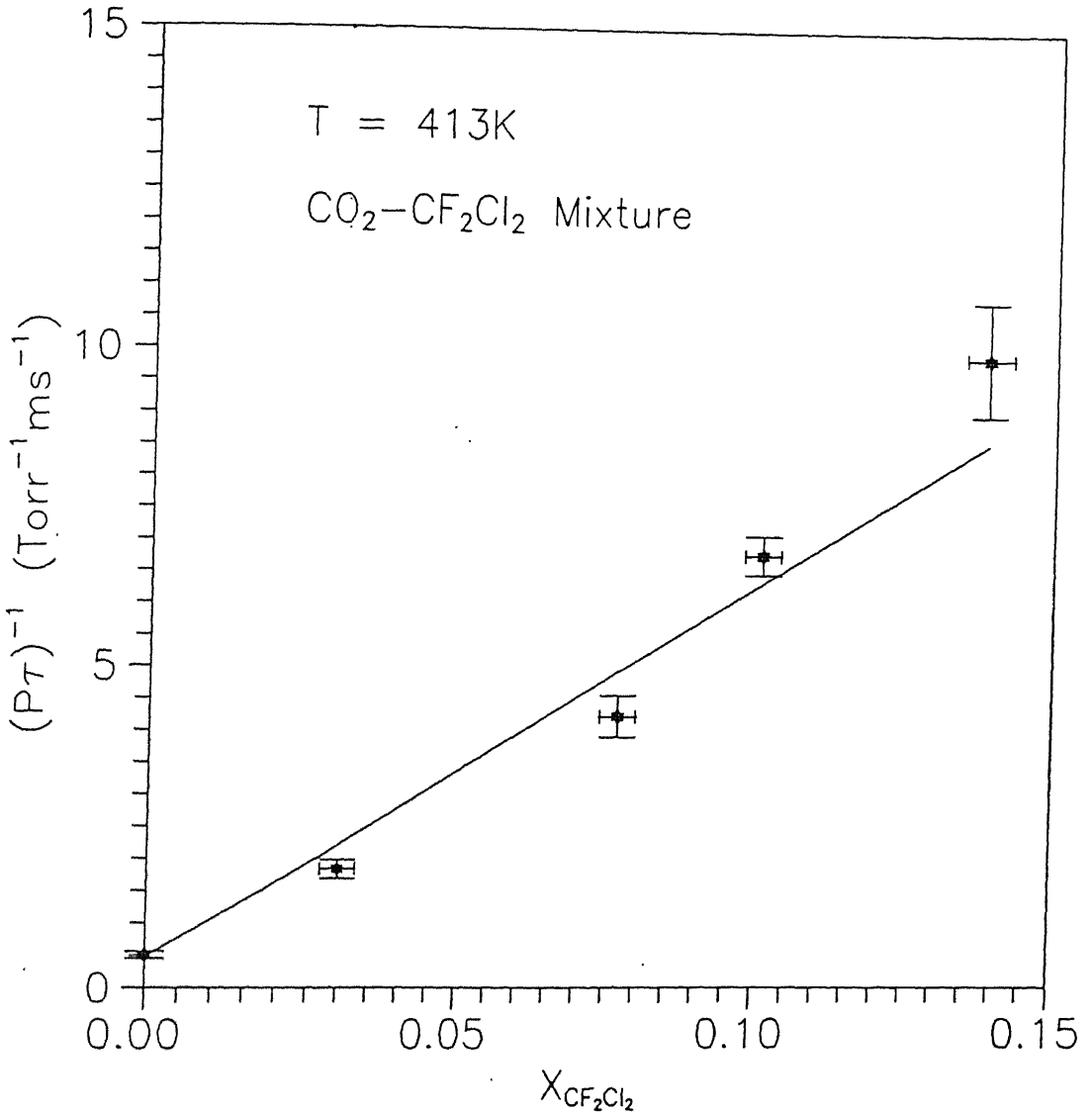

Fig. 4.4c Composition dependence of $(P\tau)^{-1}$ at 413 K.

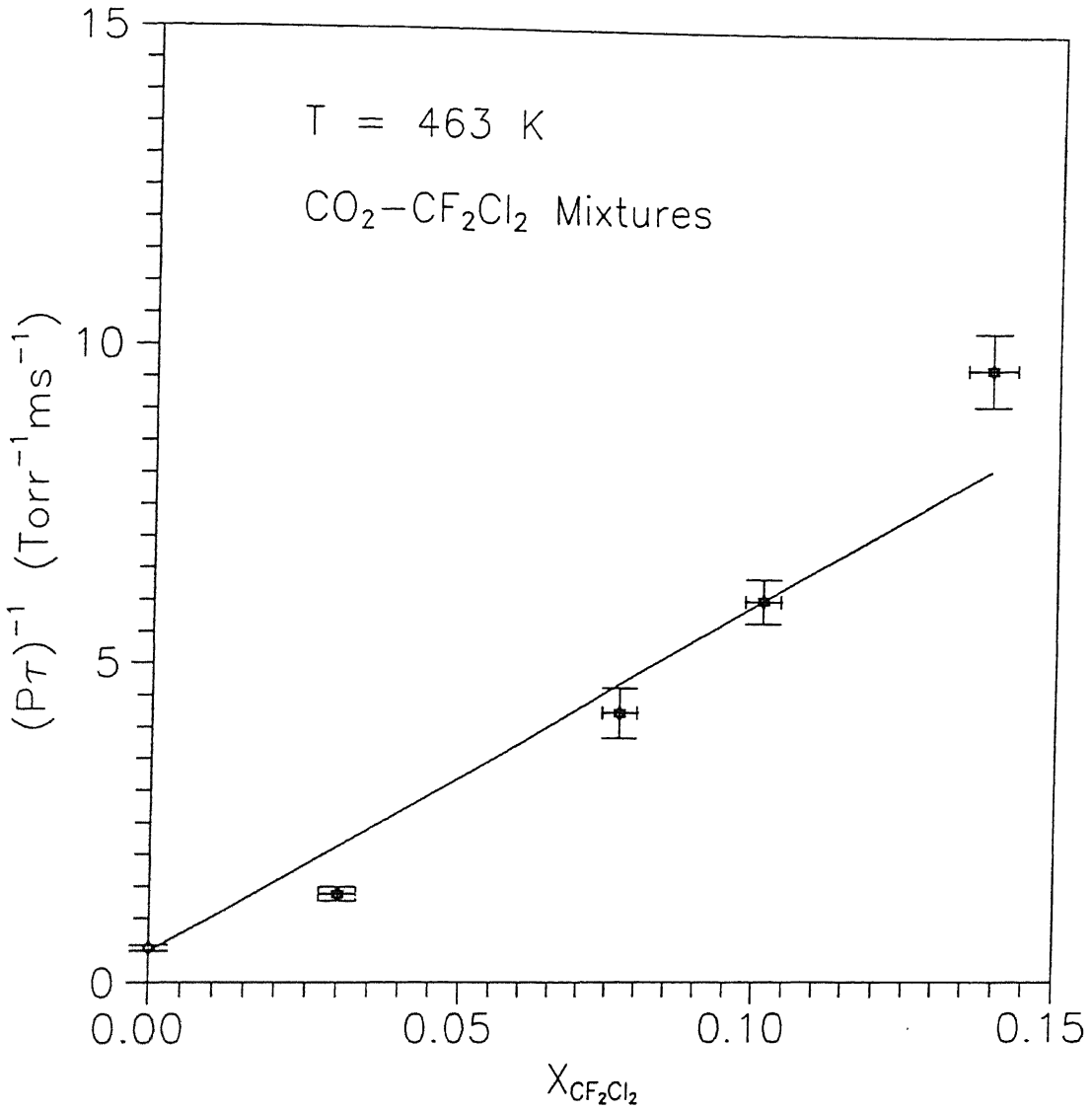

Fig. 4.4d Composition dependence of $(P\tau)^{-1}$ at 463 K.

Table 4.6 Dependence of $(P\tau)^{-1}$ on Composition at Different Temperatures.

$X_{CF_2Cl_2}$	$(P\tau)^{-1}$ $(Torr^{-1}ms^{-1})$			
	T = 323 K	T = 363 K	T = 413 K	T = 463 K
0	0.32	0.40	0.50	0.54
0.030	1.80	1.87	1.84	1.38
0.077	5.19	5.00	4.23	4.24
0.101	7.02	6.18	6.76	6.02
0.139	10.71	9.25	9.86	9.70

Table 4.7 Rate Constants and Probabilities for Energy Transfer From $CO_2(00^\circ1)$ to CF_2Cl_2

T (K)	$k_{CO_2-CF_2Cl_2}$ $(Torr^{-1}ms^{-1})$	Probability $(\times10^3)$
323	67.71±5.07	5.87±0.44
363	60.42±2.75	5.56±0.25
413	58.25±4.81	5.71±0.47
463	55.21±7.04	5.73±0.73

These experimental probabilities are used to identify the energy transfer processes in CO_2-CF_2Cl_2 mixtures. The broad guidelines for selection of deactivation processes are given below.

IV.3 Criteria for Selection of Processes

If the collision partner is a monatomic gas like He which does not have any internal degrees of freedom, the deactivation rate of CO_2 ($00^\circ1$) can be easily attributed to the vibrational - translational (V-T) energy transfer rate. If it is a diatomic molecule with only one vibrational degree of freedom, the energy transfer rate can be easily identified as either vibration to translation (V-T) rate or vibration to vibration (V-V) rate depending upon the magnitude of the energy transfer probability. However, if the collision is with a polyatomic molecule having a large number of vibrational modes (3N-5 for linear or 3N-6 for nonlinear molecules), several V-V processes are likely to occur and hence it is difficult to identify the exact vibrational levels to which the energy is transferred from CO_2 ($00^\circ1$). This problem is usually compounded by the presence of overtones, combination and difference bands. The experimentally observed rate is the net result of the various competing processes. In general the following criteria can be adopted in selecting the energy transfer probabilities which are likely to be responsible for the deactivation of CO_2 ($00^\circ1$).

(i) Energy Defect

Usually, the relaxation processes with V-V energy exchange are more efficient than V-T energy exchange, since much of the energy is received by the vibrational modes of the collision partner. The probability of energy transfer is maximum if the amount of energy which goes into the translation is very small. This can be seen from Fig. 3.1 where the Fourier transform of the interaction potential is plotted as a function of the amount of energy that goes into translation for CO_2-CF_2Cl_2 system at 323 K. The value of $I_2(b,\omega,T)$ is constant upto $\nu \simeq 7$ cm^{-1} and later on decreases with increase in ν. The value falls by an order of magnitude when $\nu \simeq 30$ cm^{-1} and three orders of magnitude when $\nu \simeq 70$ cm^{-1}. Thus the probability is small for the processes where the amount of energy goes into the translation is large and hence the processes with large ΔE can be neglected.

(ii) Magnitude of the Transition Dipole Moments

The probability of energy transfer between two molecules is directly proportional to the product of the squares of the transition dipole moments of the molecules. Therefore the transition having small transition dipole moments can be neglected.

(iii) Energy Level Population

Since the number of molecules in the excited vibrational levels is usually small, it is enough to consider ground state

molecules of the collision partner for the deactivation of $CO_2(00^\circ1)$.

(iv) Quantum Number Changes

The probability of a transition for the ground state to the fundamental is orders of magnitude greater than that of a transition from the ground state to overtone level where the quantum number change is greater than one. Therefore processes involving fundamentals should be preferred to those involving overtones when the energy defect is almost equal in both the cases.

IV.4 Interpretation of Experimental Results

A partial energy level diagram of CO_2 and CF_2Cl_2 molecules is shown in Fig 4.5. CO_2 is a linear symmetric molecule with four vibrational modes out of which the symmetric stretch mode $(10^\circ0)$ is IR inactive. The doubly degenerate bending mode $(01^\circ0)$ and the asymmetric stretch mode $(00^\circ1)$ have strong IR absorption bands. The CF_2Cl_2 molecule has nine fundamental modes of vibration out of which eight are reported to be IR active and $\nu_5(318\ cm^{-1})$ is reported to be IR inactive[57,58]. It can be seen from Fig. 4.5 that there is only one energy level $2\nu_8(2325\ cm^{-1})$ close to the $CO_2(00^\circ1)$ level $(2349\ cm^{-1})$. There are three fundamental levels $\nu_1(1101\ cm^{-1})$, $\nu_6(922\ cm^{-1})$ and $\nu_8(1159\ cm^{-1})$ and two combination bands $\nu_3+\nu_4(1101\ cm^{-1})$ and $\nu_4+\nu_7(882\ cm^{-1})$ close to either 961

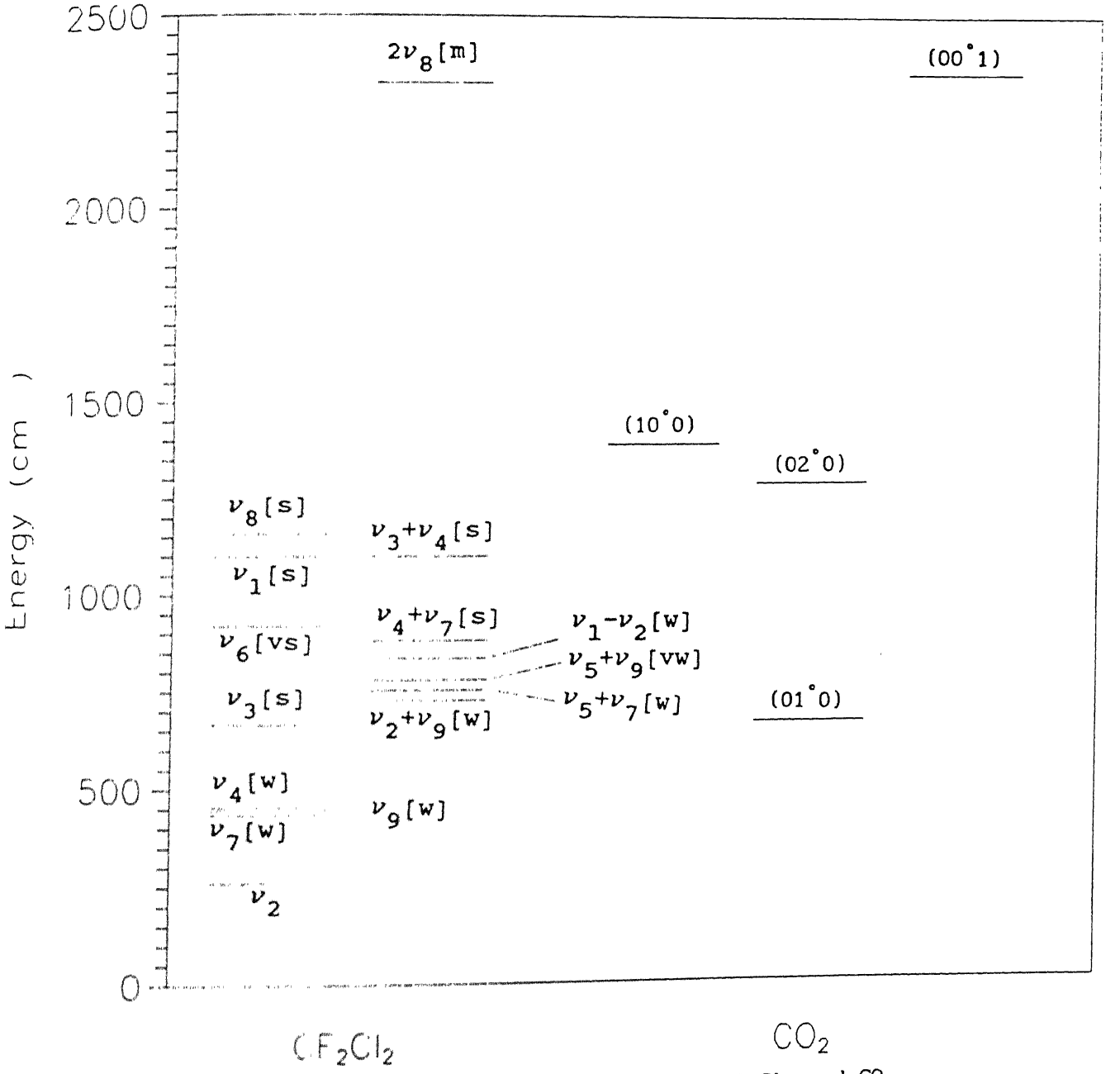

Fig. 4.5 Partial energy level diagram for CF_2Cl_2 and CO_2.

cm^{-1} or 1064 cm^{-1} corresponding to $(00^{\circ}1\text{-}10^{\circ}0)$ or $(00^{\circ}1\text{-}02^{\circ}0)$ transition in CO_2.

IV.4.1 Interpretation based on SSH-Tanczos Theory

In view of the criteria and discussion presented in Sections IV.3 and IV.4, the possible energy transfer pathways for the deactivation of $CO_2(00^{\circ}1)$ in collisions with CF_2Cl_2 are

Pathway I

$$CO_2(00^{\circ}1) + CF_2Cl_2(0) \longrightarrow CO_2(0) + CF_2Cl_2(2\nu_8) + 24\ cm^{-1} \quad (4.1)$$

$$CF_2Cl_2(2\nu_8) + CF_2Cl_2(0) \longrightarrow CF_2Cl_2(\nu_8) + CF_2Cl_2(\nu_8) + 7\ cm^{-1} \quad (4.2)$$

$$CF_2Cl_2(\nu_8) + M \longrightarrow CF_2Cl_2(\nu_3+\nu_4) + M + 58\ cm^{-1} \quad (4.3)$$

$$CF_2Cl_2(\nu_3+\nu_4) + CF_2Cl_2(0) \longrightarrow CF_2Cl_2(\nu_3) + CF_2Cl_2(\nu_4) - 21\ cm^{-1} \quad (4.4)$$

where M can be either $CF_2Cl_2(0)$ or $CO_2(0)$.

The vibrational relaxation times in pure CF_2Cl_2 have been reported to be approximately 5 μs at 1 Torr[59] which corresponds to 200 $Torr^{-1}ms^{-1}$. This value is much larger than the experimentally measured deactivation rate of $CO_2(00^{\circ}1)$ by CF_2Cl_2 which is in the range 55.21 $Torr^{-1}ms^{-1}$ to 67.7 $Torr^{-1}ms^{-1}$. This shows that the rate of equilibration of the vibrational levels in CF_2Cl_2 is much faster than the rate at which the energy flows from $CO_2(00^{\circ}1)$ to CF_2Cl_2. In view of this observation it appears to be reasonable

to assume that the processes (4.2) to (4.4) are in equilibrium. In view of the close energy levels between ν_4 (455 cm^{-1}) and ground state in CF_2Cl_2, there is no possibility for the build-up of population in the level ν_4. Thus the rate determining step will be the process (4.1) only.

Pathway II

$$CO_2(00^\circ1) + CF_2Cl_2(0) \longrightarrow CO_2(10^\circ0) + CF_2Cl_2(\nu_8) - 198\ cm^{-1} \quad (4.5a)$$

$$CO_2(00^\circ1) + CF_2Cl_2(0) \longrightarrow CO_2(02^\circ0) + CF_2Cl_2(\nu_8) - 95\ cm^{-1} \quad (4.5b)$$

The subsequent deactivation of $CF_2Cl_2(\nu_8)$ will be similar to that of pathway I. Therefore in this scheme, the rate determining step will be processes (4.5).

Pathway III

$$CO_2(00^\circ1) + CF_2Cl_2(0) \longrightarrow CO_2(10^\circ0) + CF_2Cl_2(\nu_1) - 140\ cm^{-1} \quad (4.6a)$$

$$CO_2(00^\circ1) + CF_2Cl_2(0) \longrightarrow CO_2(02^\circ0) + CF_2Cl_2(\nu_1) - 37\ cm^{-1} \quad (4.6b)$$

$$CF_2Cl_2(\nu_1) + M \longrightarrow CF_2Cl_2(\nu_3+\nu_4) + M + 0\ cm^{-1} \quad (4.7)$$

$$CF_2Cl_2(\nu_3+\nu_4) + CF_2Cl_2(0) \longrightarrow CF_2Cl_2(\nu_3) + CF_2Cl_2(\nu_4) - 21\ cm^{-1} \quad (4.4)$$

The energy from $CF_2Cl_2(\nu_3/\nu_4)$ will be subsequently relaxed by the mechanism discussed under pathway I. If deactivation rate of $CO_2(00^\circ1)$ is determined according to this mechanism then the rate determining step will be processes (4.6).

Pathway IV

$$CO_2(00^\circ1) + CF_2Cl_2(0) \longrightarrow CO_2(10^\circ0) + CF_2Cl_2(\nu_6) + 39\ cm^{-1} \quad (4.8a)$$

$$CO_2(00^\circ1) + CF_2Cl_2(0) \longrightarrow CO_2(02^\circ0) + CF_2Cl_2(\nu_6) + 142\ cm^{-1} \quad (4.8b)$$

$$CF_2Cl_2(\nu_6) + M \longrightarrow CF_2Cl_2(\nu_4+\nu_7) + M + 40\ cm^{-1} \quad (4.9)$$

$$CF_2Cl_2(\nu_4+\nu_7) + CF_2Cl_2(0) \longrightarrow CF_2Cl_2(\nu_4) + CF_2Cl_2(\nu_7) - 10\ cm^{-1} \quad (4.10)$$

If the $CO_2(00^\circ1)$ relaxes according to this mechanism, the rate determining steps will by processes (4.8) since the subsequent processes are expected to have large energy transfer probabilities.

In addition to the above pathways, there is still another possibility in which the energy flows from $CO_2(00^\circ1)$ to $CF_2Cl_2(\nu_4+\nu_7)$ as given by the following pathway.

Pathway V

$$CO_2(00^\circ1) + CF_2Cl_2(0) \longrightarrow CO_2(10^\circ0) + CF_2Cl_2(\nu_4+\nu_7) + 79\ cm^{-1} \quad (4.11a)$$

$$CO_2(00^\circ1) + CF_2Cl_2(0) \longrightarrow CO_2(02^\circ0) + CF_2Cl_2(\nu_4+\nu_7) + 182\ cm^{-1} \quad (4.11b)$$

$$CF_2Cl_2(\nu_4+\nu_7) + CF_2Cl_2(0) \longrightarrow CF_2Cl_2(\nu_4) + CF_2Cl_2(\nu_7) - 10\ cm^{-1} \quad (4.10)$$

To identify the processes responsible for the deactivation of $CO_2(00^\circ1)$, the SSH-Tanczos theory has been used to theoretically estimate the energy transfer probabilities for the processes (4.1), (4.5), (4.6), (4.8) and (4.11). The molecular parameters used in these calculations are presented in Tables 4.8 to 4.10.

The energy transfer probabilities have been estimated at four different temperatures viz 323 K, 363 K, 413 K and 463 K. The results are summarized in Table 4.11. Experimental probabilities are also given in the same table for comparison purpose.

Table 4.8: Breathing Sphere Parameters for CO_2 †

Level	Energy (cm^{-1})	Degeneracy	Breathing Sphere Parameter
$(10^{\circ}0)$	1388	1	3.2436×10^{-2}
$(01^{\circ}0)$	667	2	8.4768×10^{-3}
$(00^{\circ}1)$	2349	1	8.6376×10^{-3}

†Data taken from ref. 60.

Table 4.9: Breathing Sphere Parameters for CF_2Cl_2 *

Level	Energy (cm^{-1})	Degeneracy	Breathing Sphere Parameter
ν_1	1101	1	7.478×10^{-3}
ν_2	261	1	1.038×10^{-2}
ν_3	667	1	5.731×10^{-3}
ν_4	455	1	7.101×10^{-3}
ν_5	318	1	1.411×10^{-3}
ν_6	922	1	4.909×10^{-3}
ν_7	437	1	7.180×10^{-3}
ν_8	1159	1	2.139×10^{-3}
ν_9	446	1	7.152×10^{-3}

* Calculated using normal coordinate analysis

Table 4.10: Molecular Parameters for CO_2 and CF_2Cl_2

Molecule	L-J Potential Depth[b] ε (erg)[a]	Exponential Repulsion parameter (cm^{-1})	Steric Factor[b]
CO_2	2.6230×10^{-14}	5.5×10^{8}	1/3
CF_2Cl_2	3.9483×10^{-14}		2/3

[a] Lennard-Jones potential depth ε are cited from ref. 61.

[b] Steric factors are used following Stretton (ref. 49).

Table 4.11 Energy Transfer Probabilities obtained from SSH-Tanczos Theory

Process	ΔE (cm^{-1})	Probability			
		T = 323 K	T = 363 K	T = 413 K	T = 463 K
4.1	24	2.024×10^{-8}	2.114×10^{-8}	2.239×10^{-8}	2.373×10^{-8}
4.5a	-198	1.689×10^{-8}	2.285×10^{-8}	3.156×10^{-8}	4.163×10^{-8}
4.5b	-95	5.050×10^{-10}	5.885×10^{-10}	6.968×10^{-10}	8.089×10^{-10}
4.6a	-140	3.139×10^{-7}	3.748×10^{-7}	4.555×10^{-7}	5.409×10^{-7}
4.6b	-37	5.096×10^{-9}	5.464×10^{-9}	5.938×10^{-9}	6.423×10^{-9}
4.8a	39	1.322×10^{-6}	1.396×10^{-6}	1.494×10^{-6}	1.598×10^{-6}
4.8b	142	1.071×10^{-9}	1.248×10^{-9}	1.483×10^{-9}	1.731×10^{-9}
4.11a	79	1.961×10^{-8}	2.419×10^{-8}	2.392×10^{-8}	2.641×10^{-8}
4.11b	182	1.336×10^{-11}	1.616×10^{-11}	1.998×10^{-11}	2.413×10^{-11}
Experimental	--	5.87×10^{-3}	5.56×10^{-3}	5.71×10^{-3}	5.73×10^{-3}

It can be observed from Table 4.11 that the calculated probabilities for processes (4.1) and (4.8a) are 3 to 5 orders of magnitude less than the experimental values. However they appear to be almost temperature independent. The probabilities for the processes (4.5a), (4.5b), (4.6a), (4.6b), (4.8b), (4.11a) and (4.11b) are 4 to 8 orders of magnitude lower than the experimental values and they are showing positive temperature dependence. Since the experimentally observed probabilities are almost temperature independent, the processes (4.5a), (4.5b), (4.6a), (4.6b), (4.8b), (4.11a) and (4.11b) may not be responsible for the deactivation of $CO_2(00^\circ1)$. Though the temperature dependence of the probabilities for processes (4.1) and (4.8a) are almost temperature independent, the large discrepancy between the magnitude of the experimental and the theoretical probabilities predicted by SSH-Tanczos theory indicate that the short range forces may not be responsible for the deactivation of $CO_2(00^\circ1)$ in collisions with CF_2Cl_2.

The importance of long range interactions in molecular energy transfer was brought out by Sharma and Brau (SB) and they successfully predicted energy transfer probabilities in the mixtures of CO_2-N_2 and many other systems, where they used multipole interactions. Since the short range interactions were unable to explain the energy transfer probabilities in CO_2-CF_2Cl_2 system, the theoretical calculations have been performed by adopting the Tam's modification of SB theory (SB-Tam theory). The analysis of the experimental results is presented in the following section.

IV.4.2 Interpretation Based on SB-Tam Theory

In this section the energy transfer probabilities are calculated using SB-Tam theory in which the long range multipole interactions are assumed to be responsible for deactivating $CO_2(00^\circ1)$ mode. The processes considered are the same as given in section IV.4.1 and are listed below for convenience.

$$CO_2(00^\circ1) + CF_2Cl_2(0) \longrightarrow CO_2(0) + CF_2Cl_2(2\nu_8) + 24\ cm^{-1} \quad (4.1)$$

$$CO_2(00^\circ1) + CF_2Cl_2(0) \longrightarrow CO_2(10^\circ0) + CF_2Cl_2(\nu_8) - 198\ cm^{-1} \quad (4.5a)$$

$$CO_2(00^\circ1) + CF_2Cl_2(0) \longrightarrow CO_2(02^\circ0) + CF_2Cl_2(\nu_8) - 95\ cm^{-1} \quad (4.5b)$$

$$CO_2(00^\circ1) + CF_2Cl_2(0) \longrightarrow CO_2(10^\circ0) + CF_2Cl_2(\nu_1) - 140\ cm^{-1} \quad (4.6a)$$

$$CO_2(00^\circ1) + CF_2Cl_2(0) \longrightarrow CO_2(02^\circ0) + CF_2Cl_2(\nu_1) - 37\ cm^{-1} \quad (4.6b)$$

$$CO_2(00^\circ1) + CF_2Cl_2(0) \longrightarrow CO_2(02^\circ0) + CF_2Cl_2(\nu_6) + 39\ cm^{-1} \quad (4.8a)$$

$$CO_2(00^\circ1) + CF_2Cl_2(0) \longrightarrow CO_2(02^\circ0) + CF_2Cl_2(\nu_6) + 142\ cm^{-1} \quad (4.8b)$$

$$CO_2(00^\circ1) + CF_2Cl_2(0) \longrightarrow CO_2(10^\circ0) + CF_2Cl_2(\nu_4+\nu_7) + 79\ cm^{-1} \quad (4.11a)$$

$$CO_2(00^\circ1) + CF_2Cl_2(0) \longrightarrow CO_2(02^\circ0) + CF_2Cl_2(\nu_4+\nu_7) + 182\ cm^{-1} \quad (4.11b)$$

The molecular parameters used in the calculation are presented in Tables 4.12, 4.13 and 4.14.

Table 4.12 : Rotational Constants and Hard Sphere Collision Diameters for CO_2 and CF_2Cl_2

Parameters		CO_2	CF_2Cl_2
Rotational Constants	A	--	0.1373 cm^{-1} [b]
	B	0.39 cm^{-1} [a]	0.0879 cm^{-1}
	C	--	0.0744 cm^{-1}
Hard Sphere Collision Diameter [c]		4.0 Å	5.16 Å

[a] Rotational constant B for CO_2 is taken from reference 62.

[b] Rotational constants for CF_2Cl_2 are quoted from reference 63.

[c] Hard sphere diameters are cited from reference 61.

Table 4.13 : Square of Transition Dipole Moment Matrix Elements for CO_2 Molecule [d]

Transition	Square of Transition Dipole Moment Matrix Element (esu^2cm^2)
$(00^\circ1)-(00^\circ0)$	1.0×10^{-37}
$(00^\circ1)-(10^\circ0)$	1.44×10^{-39}
$(00^\circ1)-(02^\circ0)$	1.22×10^{-39}

[d] Data collected from reference 64.

Table 4.14 : Square of Transition Dipole Moment Matrix Elements for CF_2Cl_2 Molecule

Transition	Intensity[e] (cm^2/mole)	Square of Transition Dipole Moment Matrix Element[f] (esu^2cm^2)
ν_1-0	27.2×10^3	1.08×10^{-37}
ν_6-0	33.6×10^3	1.34×10^{-37}
ν_8-0	17.3×10^3	6.90×10^{-38}

[e]Intensity data taken from reference 58.

[f]Intensity data converted into Square of Transition Dipole moment by the method given in ref. 65.

The square of the transition dipole moments of $CF_2Cl_2(2\nu_8)$ and CF_2Cl_2 $(\nu_4+\nu_7)$ are not available in the literature. Hence the energy transfer probabilities involving these levels were calculated assuming them to be equal to 1×10^{-37} esu^2cm^2 and the actual values were obtained from the experimental values as described later in this section. The calculated probabilities for all the process listed above are summarized in Table 4.15.

It can be observed from Table 4.15 that the probabilities for processes (4.5a), (4.5b), (4.6a), and (4.8b) are about two to four orders of magnitude smaller than the experimental values and hence they are not likely to be responsible for the deactivation of $CO_2(00^\circ1)$. The estimated probabilities of the process (4.11b) is two orders of magnitude smaller than those of process (4.11a). Hence the process (4.11b) can be ignored. Of the remaining processes, (4.1), (4.6b), (4.8a), (4.11a), the transition dipole moment matrix elements for the levels involved in the processes (4.6b) and (4.8a) are known for both the molecules but those for the levels $2\nu_8$ and $(\nu_4+\nu_7)$ of CF_2Cl_2 involved in the processes (4.1) and (4.11a) are not available. However, it is reported that the relative intensity of $2\nu_8$ is medium whereas that of $(\nu_4+\nu_7)$ is strong. Assuming that all these processes are contributing to the deactivation of $CO_2(00^\circ1)$, experimental probability P_{exp} can be written as

$$P_{exp} = P_6 + P_8 + A\,P_{11} + B\,P_1 \qquad (4.12)$$

Table 4.15 : Calculated Energy Transfer Probabilities Using SB-Tam Theory.

Process[a]	ΔE (cm^{-1})	Probability			
		T = 323 K	T = 363 K	T = 413 K	T = 463 K
4.1	24	2.723×10^{-1}	2.552×10^{-1}	2.332×10^{-1}	2.144×10^{-1}
4.5a	-198	6.562×10^{-7}	9.038×10^{-7}	1.272×10^{-6}	1.683×10^{-6}
4.5b	-95	3.734×10^{-5}	4.197×10^{-5}	4.783×10^{-5}	5.295×10^{-5}
4.6a	-140	1.040×10^{-5}	1.282×10^{-5}	1.611×10^{-5}	1.933×10^{-5}
4.6b	-37	1.485×10^{-3}	1.541×10^{-3}	1.612×10^{-3}	1.634×10^{-3}
4.8a	39	2.061×10^{-3}	2.153×10^{-3}	2.250×10^{-3}	2.322×10^{-3}
4.8b	142	1.071×10^{-5}	1.322×10^{-5}	1.648×10^{-5}	1.997×10^{-5}
4.11a	79	1.384×10^{-4}	1.501×10^{-4}	1.640×10^{-4}	1.795×10^{-4}
4.11b	182	1.602×10^{-6}	2.135×10^{-6}	2.884×10^{-6}	3.739×10^{-6}
Experimental	--	5.87×10^{-3}	5.56×10^{-3}	5.71×10^{-3}	5.73×10^{-3}

[a] 4.1 etc. denote the processes represented by Eqns. (4.1) etc. in the text.

where P_6, P_8, P_{11} and P_1 denote the probabilities represented by Processes (4.6b), (4.8a), (4.11a) and (4.1), respectively ; A and B are positive constants with which the assumed value of the square of the dipole moment, viz. 1×10^{-37} esu^2cm^2, in calculating P_{11} and P_1 are to be multiplied respectively. A least square fit of the experimental data to Eqn. (4.12) gave A = 3.89±0.46 and B = $(5.04\pm0.30)\times10^{-3}$ where error corresponds to standard deviation. Thus the square of the dipole moment matrix element obtained from this analysis for the levels $(\nu_4+\nu_7)$ and $2\nu_8$ are $(3.89\pm0.46)\times10^{-37}$ esu^2cm^2 and $(5.04\pm0.30)\times10^{-40}$ esu^2cm^2, respectively. These values are consistent with the reported values of relative intensities for $(\nu_4+\nu_7)$ and $2\nu_8$. The temperature dependence of experimental probability is shown in Fig. 4.6. The calculated values of the probability using Eqn. (4.12) and above A and B are also shown in the same figure as a solid curve.

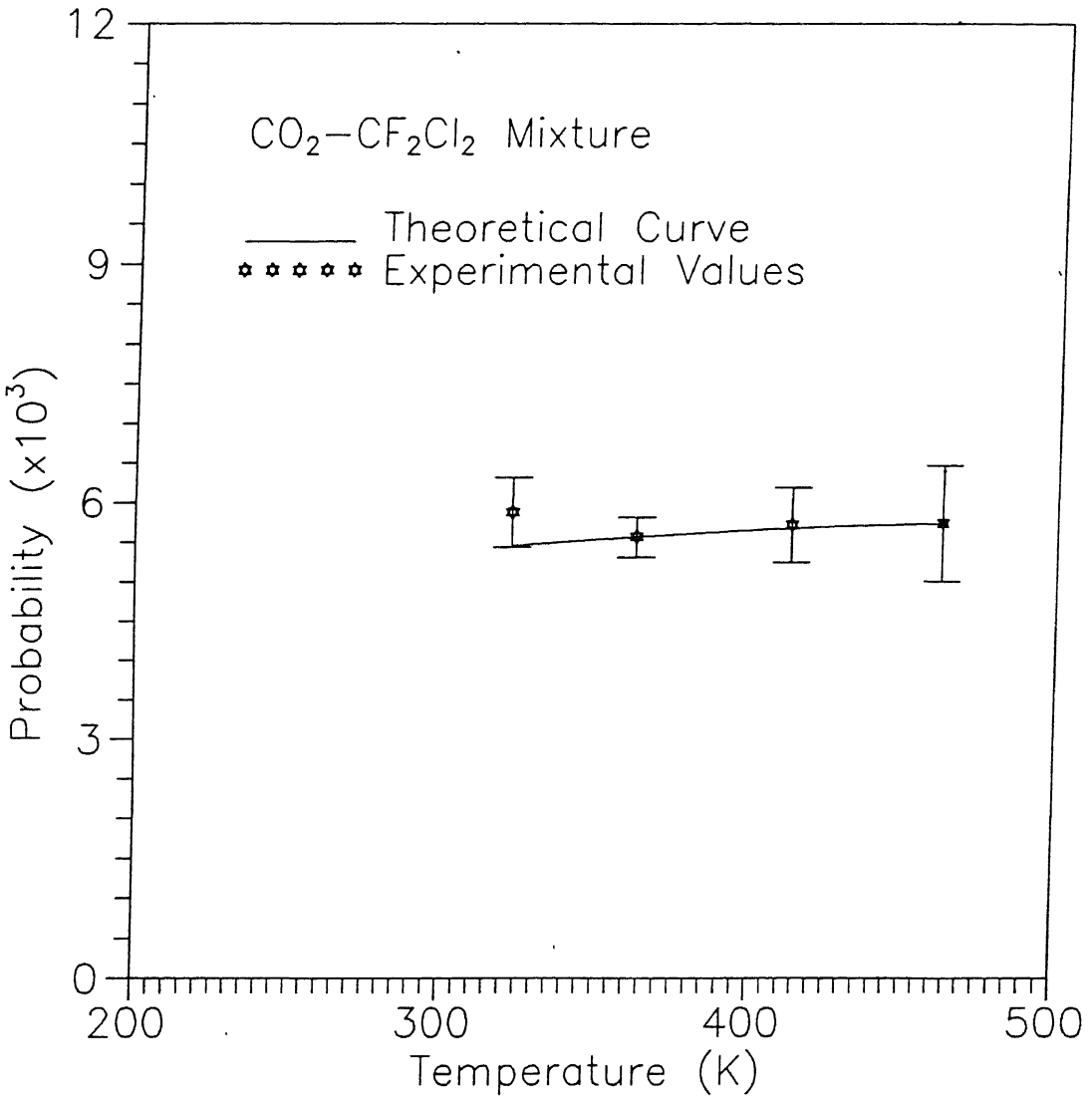

Fig. 4.6 Temperature dependence of energy transfer probability.

CHAPTER V

EXPERIMENTAL RESULTS AND DISCUSSION : CO_2-C_4H_4S SYSTEM

V.1 General Remarks

The deactivation rate of $CO_2(00^\circ1)$ in collisions with C_4H_4S have been studied in the temperature range 323-463 K. The rates were measured at four different temperatures, namely 323 K, 363 K, 413 K and 463 K, for four compositions of CO_2 and C_4H_4S mixtures. The compositions studied were 5.0%, 8.0%, 11.0% and 13.9% C_4H_4S. The maximum percentage of C_4H_4S in the mixture was limited to 13.9% to ensure that the measured relaxation times are at least four to five times greater than the time constants of the detector and the associated electronics. The collisional deactivation rate of $CO_2(00^\circ1)$ was obtained by extrapolating the measured rate to 100% C_4H_4S.

The deactivation rates were found to be large and decreasing with increasing temperature. This indicates that near resonant processes and long range forces are responsible for deactivation of $CO_2(00^\circ1)$ in CO_2-C_4H_4S mixtures. The theoretical calculations of the energy transfer probabilities using the SB-Tam theory were performed and the values were compared with the experimental results. As the transition dipole moment matrix elements of the involved transitions in C_4H_4S are not available in

literature, they were estimated by matching the theoretical and experimental probabilities. The experimental results and analysis are presented below in detail.

V.2 Experimental Results

A typical fluorescence signal at 4.3 μm from $CO_2(00^\circ1)$ level in a CO_2-C_4H_4S mixture (8.0% C_4H_4S, P = 13.04 Torr, T = 323 K) is shown in Fig. 5.1. Fig. 5.2 shows a semilogarithmic plot of intensity of fluorescence signal vs time. It can be observed from this figure that the fluorescence signal exhibits a single exponential decay. A least squares fit of the intensity to the relation $I = I_0\, e^{-t/\tau}$ yielded $\tau^{-1} = (65.79 \pm 7.31)\ ms^{-1}$.

The fluorescence decay was measured at several pressures in the range 4-20 Torr. The dependence of τ^{-1} on the pressure for a 8.0% C_4H_4S mixture at 323 K is shown in Fig 5.3. It can be seen from Fig. 5.3 that the dependence of τ^{-1} on Pressure, P, is linear and a least squares analysis of the data taking into account the errors in the measurement of P as well as τ^{-1} resulted in a value of $(P\tau)^{-1} = (4.84 \pm 0.21)\ Torr^{-1}ms^{-1}$. The experiments were carried out at four different temperatures and results are summarized in the Table 5.1.

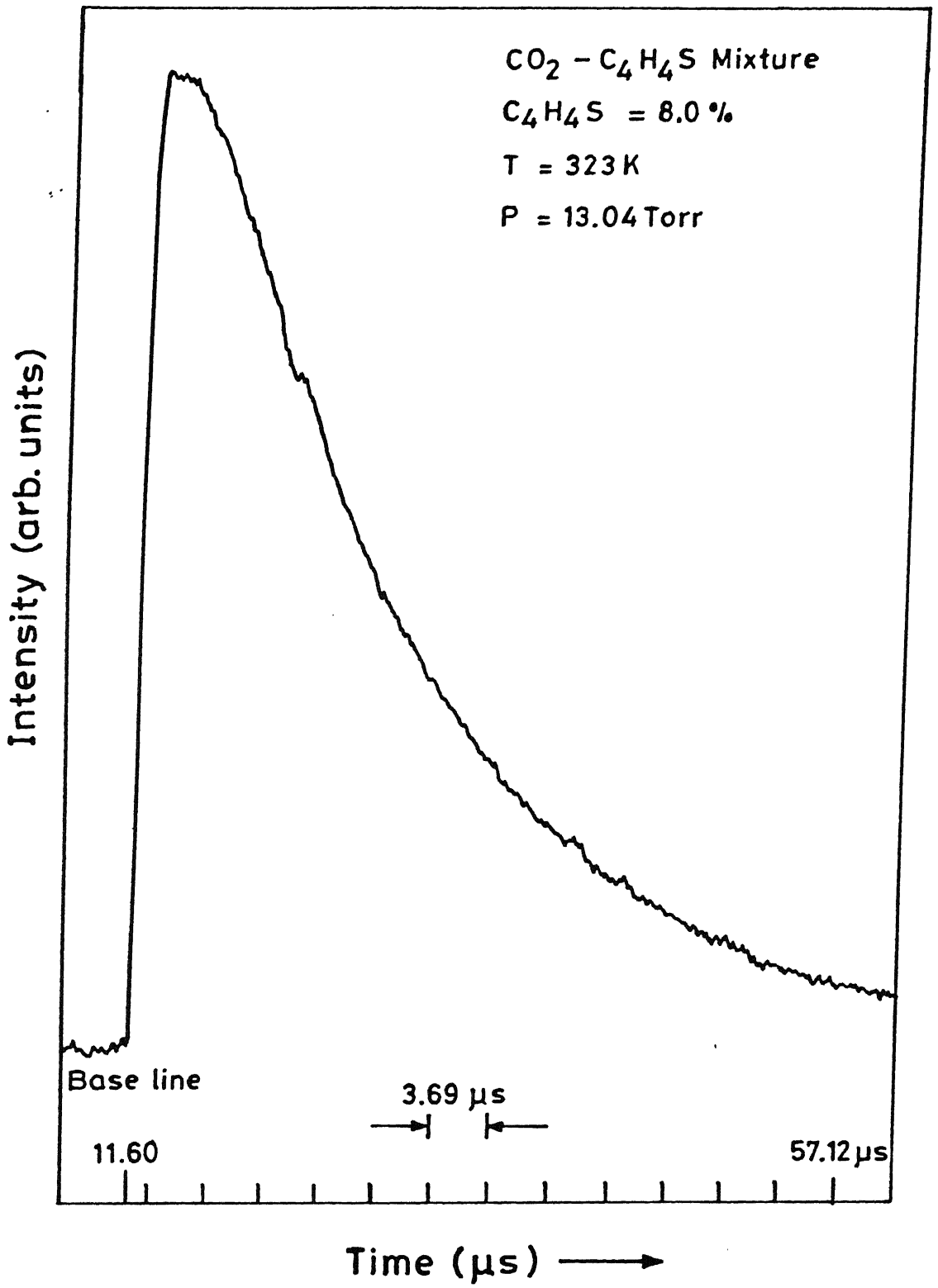

Fig. 5.1 Typical fluorescence signal.

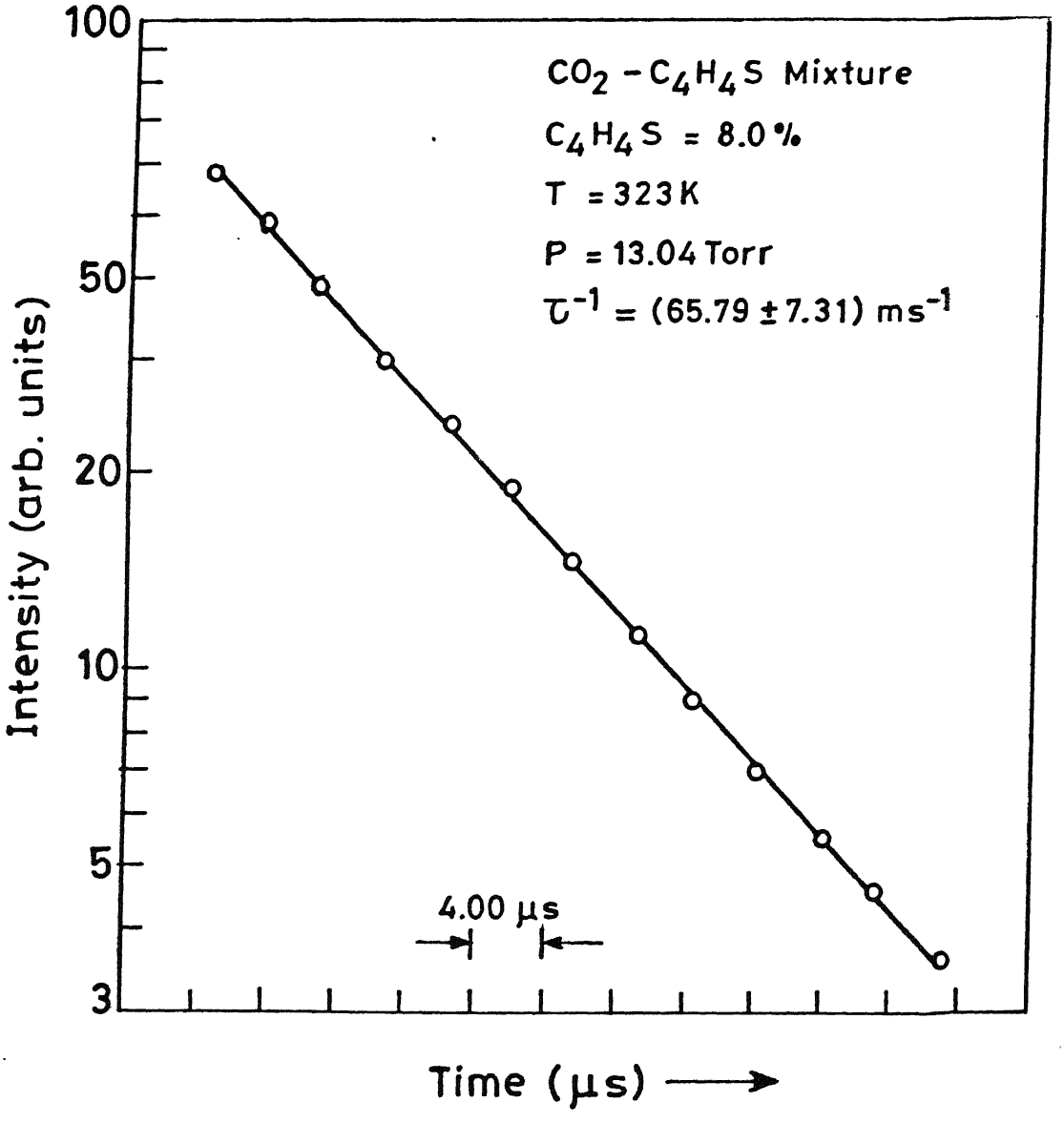

Fig. 5.2 Semilogarithmic plot of fluorescence intensity vs time.

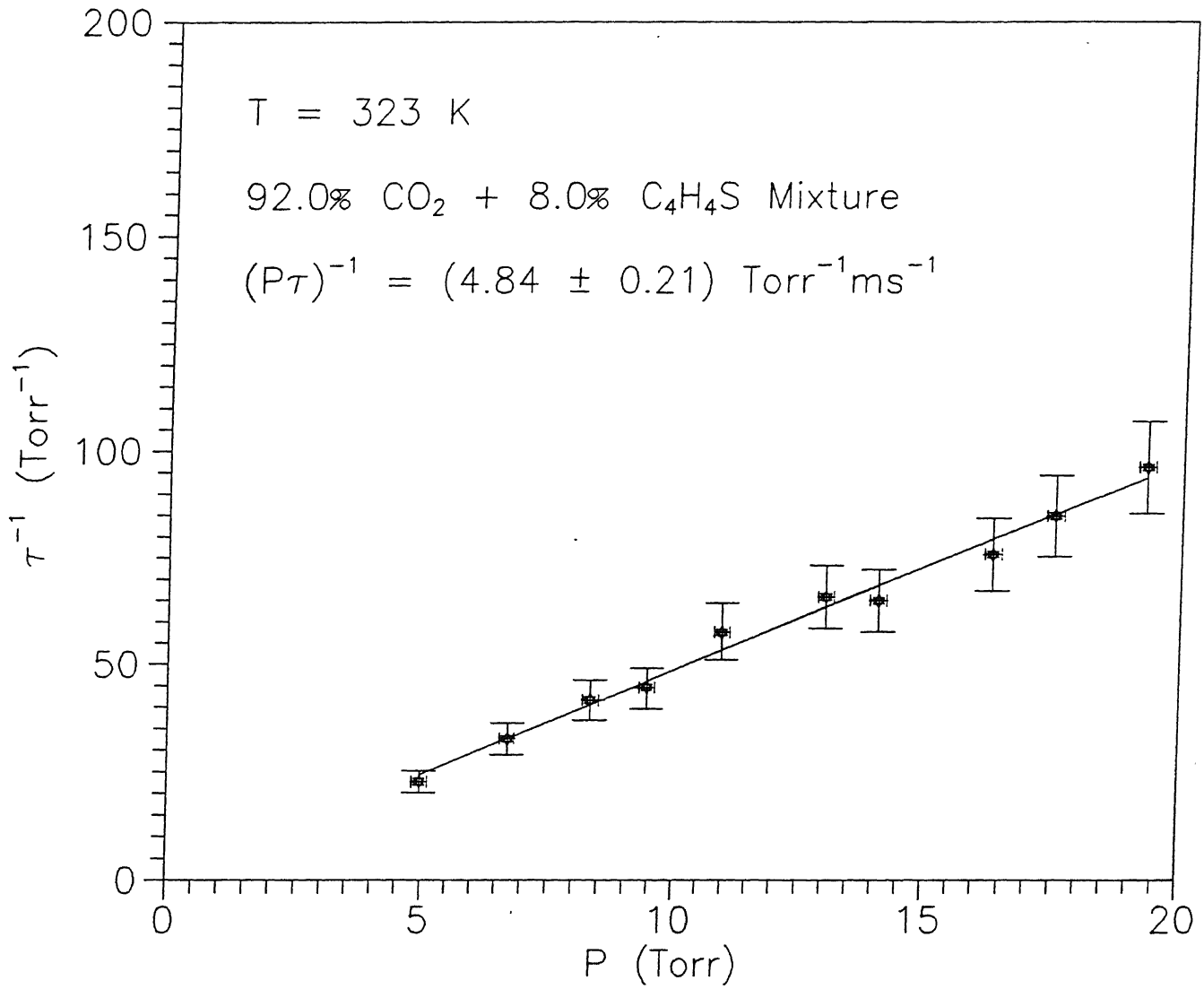

Fig. 5.3 Plot of τ^{-1} vs pressure.

Table 5.1 : Experimental Values of τ^{-1} at Various Pressures and Different Temperatures for a 8.0% C_4H_4S Mixture

T = 323 K		T = 363 K		T = 413 K		T = 463 K	
P (Torr)	τ^{-1} (ms^{-1})	P (Torr)	τ^{-1} (ms^{-1})	P (Torr)	τ^{-1} (ms^{-1})	P (Torr)	τ^{-1} (ms^{-1})
4.96	22.73	4.08	19.84	4.32	14.93	3.92	15.75
6.72	32.68	5.68	24.88	6.16	21.55	5.60	18.66
8.32	41.67	6.96	30.03	7.76	28.25	6.96	28.74
9.44	44.64	9.36	39.68	8.80	37.31	8.72	29.76
10.96	57.47	10.56	47.17	10.16	37.04	10.16	32.36
13.04	65.79	12.48	54.35	11.60	39.06	11.84	38.46
14.08	64.94	14.24	56.82	13.36	49.02	13.28	44.64
16.32	75.76	15.36	67.11	14.08	52.08	15.68	57.47
17.52	84.75	17.84	69.44	15.84	60.24	16.40	55.56
19.28	96.15	19.92	86.21	17.36	66.67	18.40	64.10
				19.28	69.44	19.92	61.73
$(P\tau)^{-1}$ = (4.84 ± 0.21) $Torr^{-1}ms^{-1}$		$(P\tau)^{-1}$ = (4.04 ± 0.20) $Torr^{-1}ms^{-1}$		$(P\tau)^{-1}$ = (3.73 ± 0.18) $Torr^{-1}ms^{-1}$		$(P\tau)^{-1}$ = (3.19 ± 0.20) $Torr^{-1}ms^{-1}$	

In a mixture of CO_2 and C_4H_4S the deactivation of $CO_2(00^\circ1)$ can occur through collision between CO_2 and CO_2 as well as through collisions between CO_2 and C_4H_4S. As the concentration of C_4H_4S in the mixtures increases, the collisions between CO_2 and C_4H_4S increase. This results in increase in the deactivation rate of $CO_2(00^\circ1)$ with the increase of C_4H_4S concentration if C_4H_4S is more efficient than CO_2 in deactivating $CO_2(00^\circ1)$. To determine the effect of composition on the deactivation rate of $CO_2(00^\circ1)$ the relaxation times were measured in four different mixtures of CO_2 and C_4H_4S. A summary of the measured relaxation times at different temperatures and pressures for 5.0%, 11.0% and 13.9% C_4H_4S mixtures are presented in Tables 5.2, 5.3 and 5.4 respectively.

Figures 5.4a, 5.4b, 5.4c and 5.4d show plots of $(P\tau)^{-1}$ versus $X_{C_4H_4S}$ (mole fraction of C_4H_4S) at different temperatures. The linearity of the plots suggest that the deactivation rate of a mixture can be expressed as,

$$(P\tau)^{-1} = (P\tau)^{-1}_{CO_2\text{-}CO_2} (1 - X_M) + (P\tau)^{-1}_{CO_2\text{-}M} X_M$$

or,

$$k = k_{CO_2\text{-}CO_2} (1 - X_M) + k_{CO_2\text{-}M} X_M$$

where M denotes the C_4H_4S molecule and $k_{CO_2\text{-}CO_2}$ and $k_{CO_2\text{-}M}$ represent the rate constants for the deactivation of $CO_2(00^\circ1)$, in collisions with CO_2 molecules only and in collisions with C_4H_4S

Table 5.2 : Experimental Values of τ^{-1} at Various Pressures and Different Temperatures for a 5.0% C_4H_4S Mixture

T = 323 K		T = 363 K		T = 413 K		T = 463 K	
P (Torr)	τ^{-1} (ms^{-1})	P (Torr)	τ^{-1} (ms^{-1})	P (Torr)	τ^{-1} (ms^{-1})	P (Torr)	τ^{-1} (ms^{-1})
4.08	25.06	4.00	12.99	4.32	16.67	5.28	16.67
5.60	36.76	5.04	17.86	5.44	17.39	6.32	16.39
7.84	34.72	7.44	26.88	7.60	23.64	8.08	22.68
9.20	39.68	9.92	32.68	7.92	25.64	9.76	30.03
11.04	52.08	11.44	37.31	9.52	30.30	10.96	30.58
12.48	55.56	12.80	41.67	10.64	34.72	12.72	34.72
14.16	60.98	14.16	46.73	12.24	38.46	13.76	37.04
14.96	66.67	16.00	52.08	13.44	40.32	16.24	47.17
18.32	76.92	16.72	57.47	15.84	45.87	17.52	47.62
18.80	75.76			17.68	56.18	19.20	53.19
$(P\tau)^{-1}$ = (3.63 ± 0.19) $Torr^{-1}ms^{-1}$		$(P\tau)^{-1}$ = (3.28 ± 0.11) $Torr^{-1}ms^{-1}$		$(P\tau)^{-1}$ = (2.90 ± 0.13) $Torr^{-1}ms^{-1}$		$(P\tau)^{-1}$ = (2.71 ± 0.11) $Torr^{-1}ms^{-1}$	

Table 5.3 : Experimental Values of τ^{-1} at Various Pressures and Different Temperatures for a 11.0% C_4H_4S Mixture

T = 323 K		T = 363 K		T = 413 K		T = 463 K	
P (Torr)	τ^{-1} (ms^{-1})	P (Torr)	τ^{-1} (ms^{-1})	P (Torr)	τ^{-1} (ms^{-1})	P (Torr)	τ^{-1} (ms^{-1})
4.16	27.78	3.84	27.78	3.92	27.78	3.84	20.83
6.08	48.54	5.28	32.05	5.44	34.72	6.24	34.72
7.84	61.73	6.48	43.86	7.04	43.86	7.68	43.10
9.68	77.52	8.24	55.56	8.64	47.17	10.08	50.51
10.88	84.75	10.32	70.42	10.08	64.10	10.88	54.35
12.16	80.65	12.80	87.72	12.32	70.42	12.24	64.94
13.76	108.70	13.68	89.29	14.40	81.97	14.24	73.53
15.28	119.00	15.76	105.30	15.68	92.59	16.40	83.33
16.96	131.60	17.44	120.50	17.28	94.34	17.52	87.72
19.84	138.90	18.88	128.20	19.28	109.90	18.56	95.24
$(P\tau)^{-1}$ = (7.15 ± 0.47) $Torr^{-1}ms^{-1}$		$(P\tau)^{-1}$ = (6.85 ± 0.14) $Torr^{-1}ms^{-1}$		$(P\tau)^{-1}$ = (5.34 ± 0.20) $Torr^{-1}ms^{-1}$		$(P\tau)^{-1}$ = (4.90 ± 0.12) $Torr^{-1}ms^{-1}$	

Table 5.4 : Experimental Values of τ^{-1} at Various Pressures and Different Temperatures for a 13.9% C_4H_4S Mixture

T = 323 K		T = 363 K		T = 413 K		T = 463 K	
P (Torr)	τ^{-1} (ms^{-1})	P (Torr)	τ^{-1} (ms^{-1})	P (Torr)	τ^{-1} (ms^{-1})	P (Torr)	τ^{-1} (ms^{-1})
4.32	41.67	4.16	37.88	5.84	47.17	4.56	33.78
5.76	62.50	6.24	58.82	7.36	56.82	6.56	45.87
7.44	74.63	7.44	71.43	9.04	80.65	8.48	62.50
9.36	99.01	9.36	84.75	12.88	104.20	9.44	65.79
11.28	119.00	10.64	98.04	14.48	116.30	10.88	80.65
12.80	125.00	11.84	108.70	16.16	135.10	12.64	89.29
15.92	149.30	13.44	125.00	17.36	140.80	14.08	98.04
19.92	196.10	16.32	151.50	19.44	158.70	15.68	108.70
						18.96	135.10
$(P\tau)^{-1}$ = (9.37 ± 0.38) $Torr^{-1}ms^{-1}$		$(P\tau)^{-1}$ = (9.23 ± 0.15) $Torr^{-1}ms^{-1}$		$(P\tau)^{-1}$ = (8.12 ± 0.27) $Torr^{-1}ms^{-1}$		$(P\tau)^{-1}$ = (6.95 ± 0.17) $Torr^{-1}ms^{-1}$	

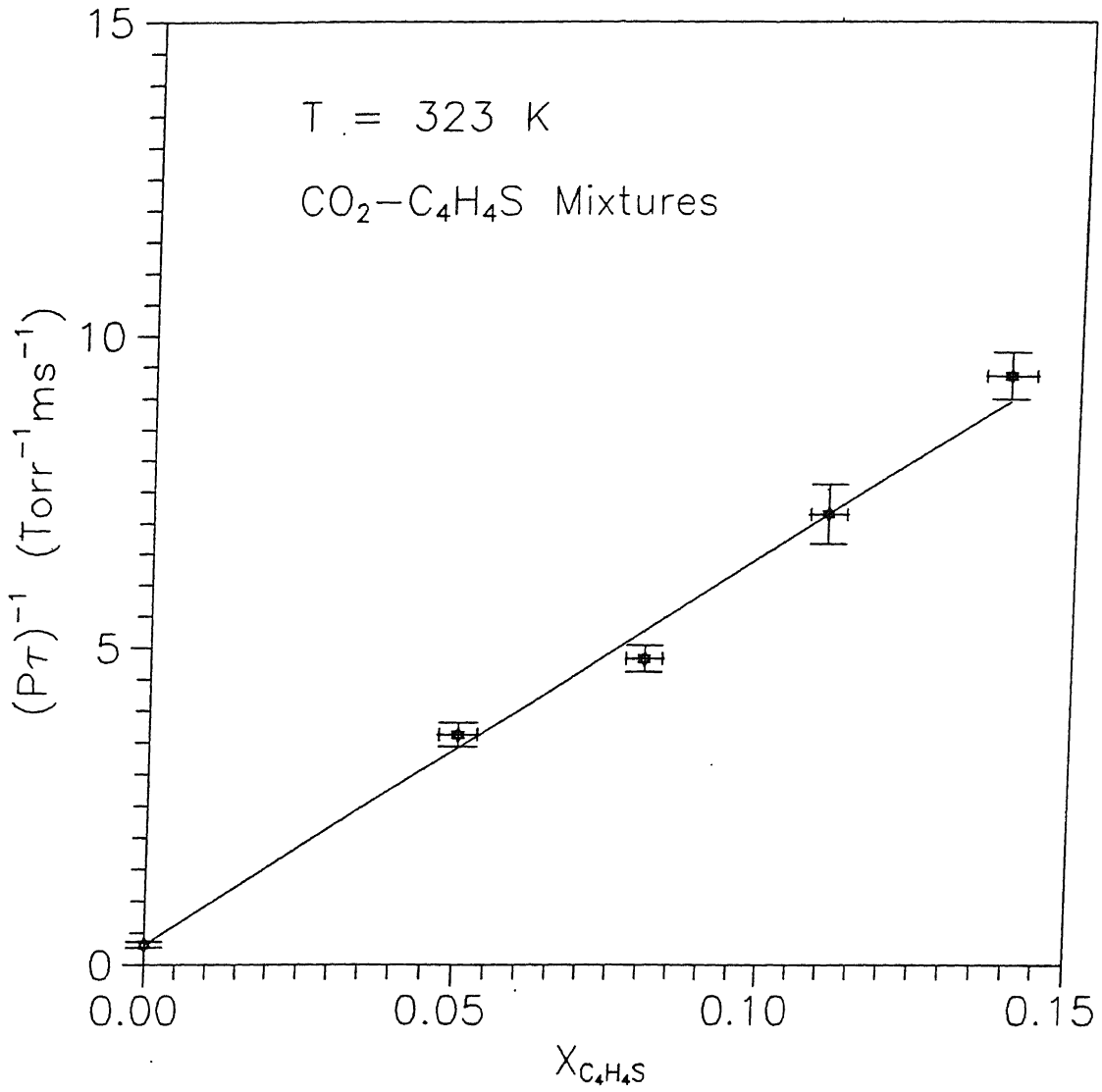

Fig. 5.4a Composition dependence of $(P\tau)^{-1}$ at 323 K.

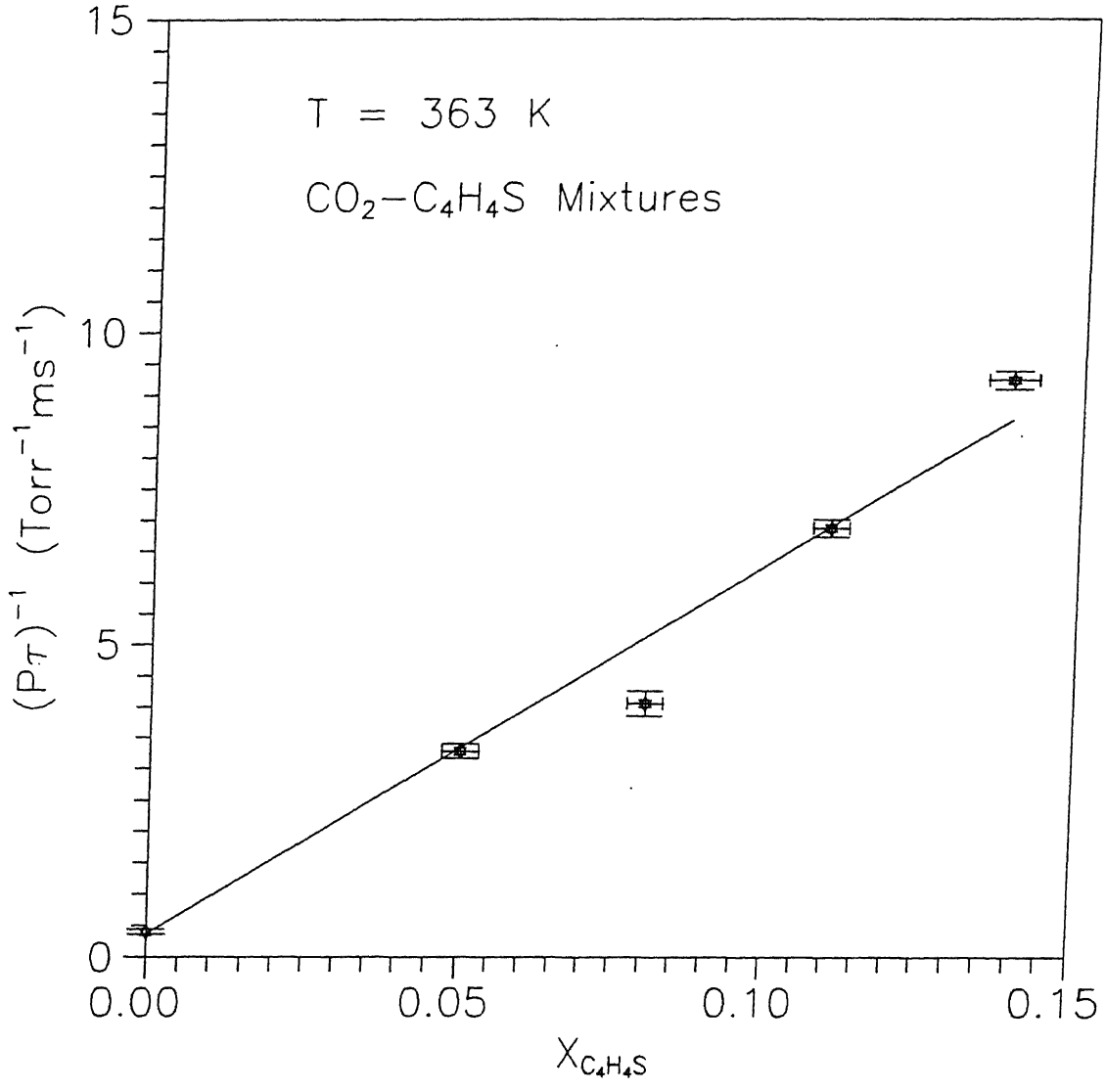

Fig. 5.4b Composition dependence of $(P\tau)^{-1}$ at 363 K.

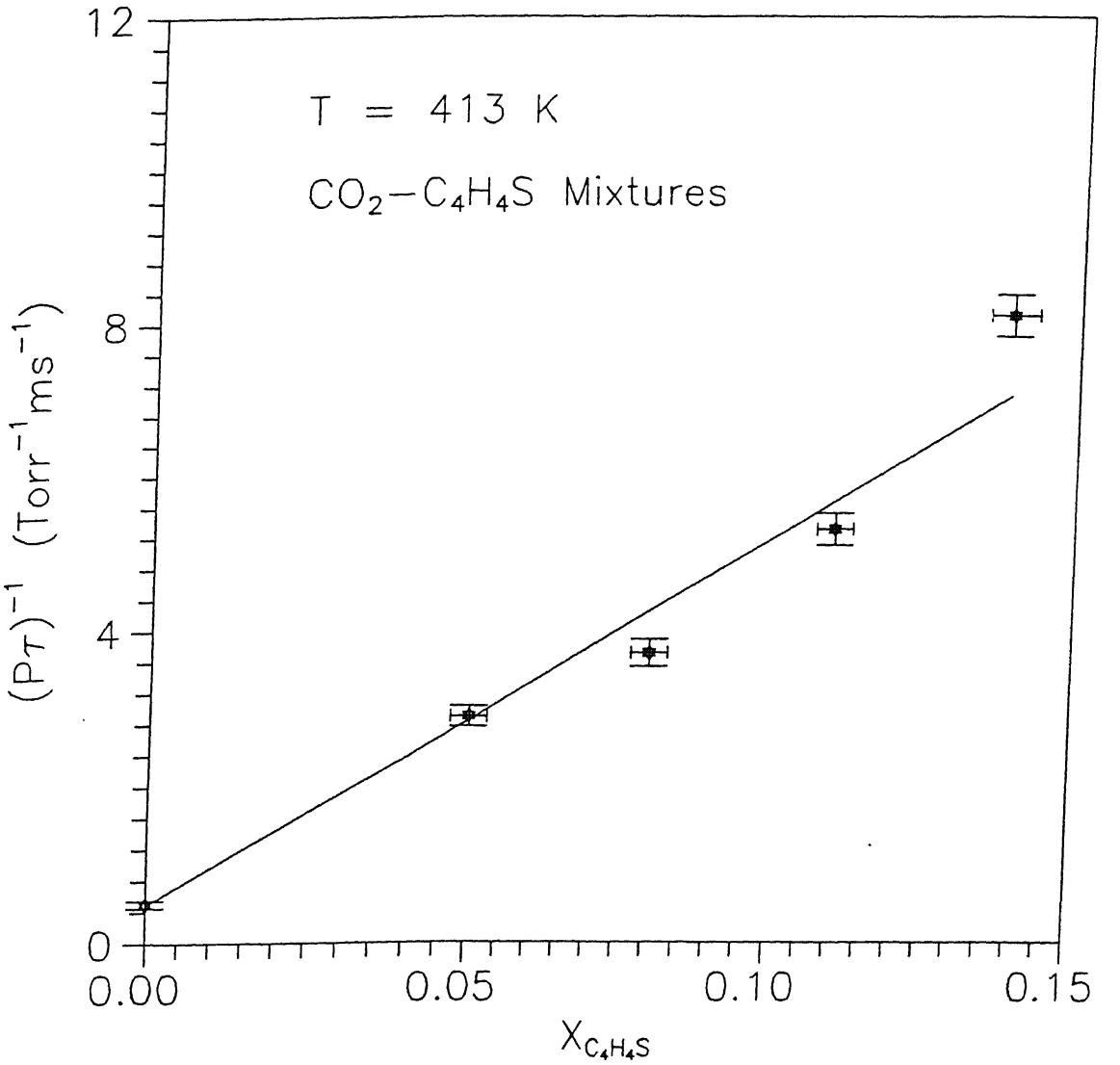

Fig. 5.4c Composition dependence of $(P\tau)^{-1}$ at 413 K.

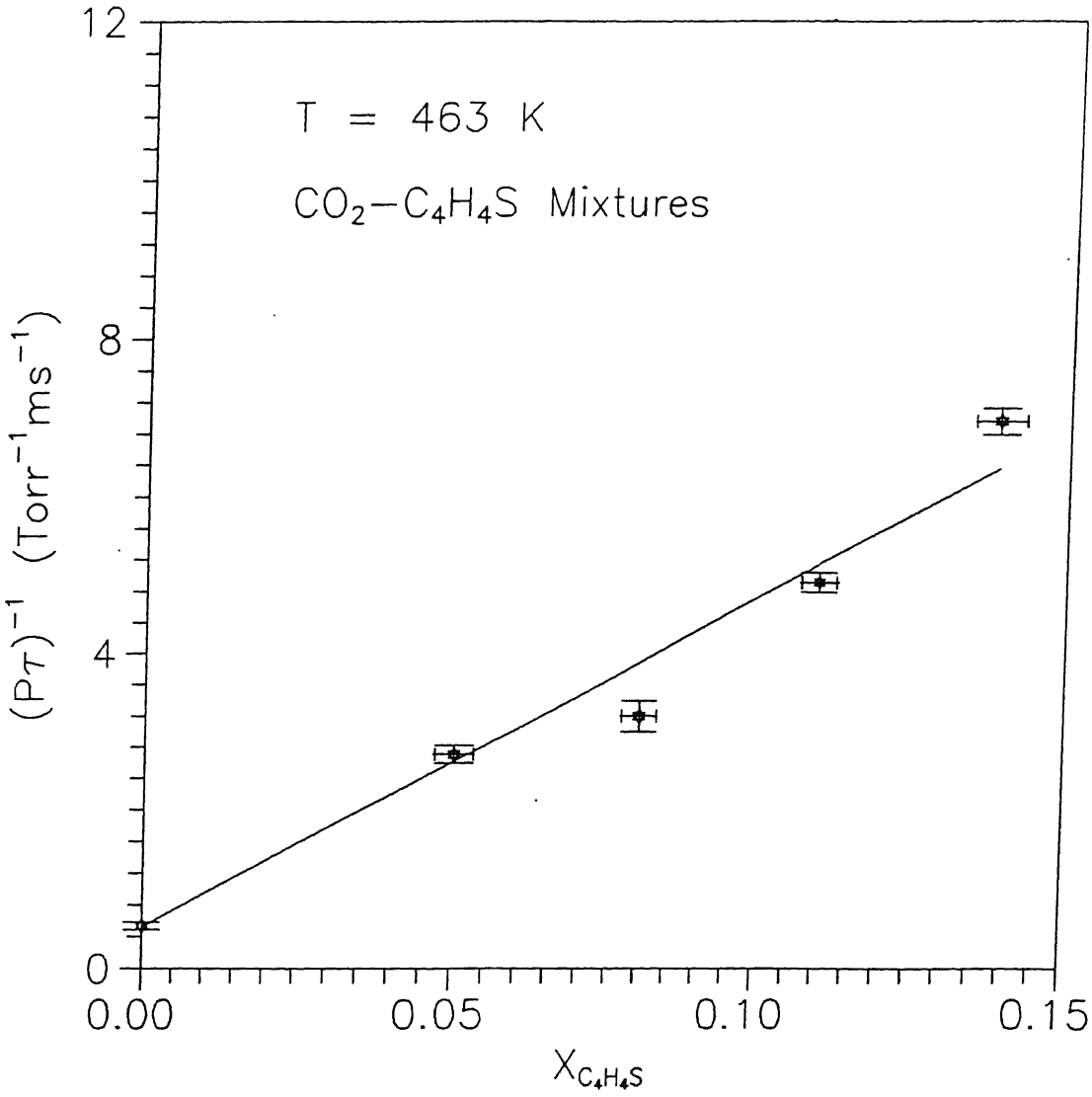

Fig. 5.4d Composition dependence of $(P\tau)^{-1}$ at 463 K.

only, respectively. Therefore the rate constants $k_{CO_2-C_4H_4S}$ can be obtained by extrapolating the $(P\tau)^{-1}$ value to $X_{C_4H_4S} = 1$.

Similar analysis has been carried out with experimental data at other temperatures also and the data are summarized in the Table 5.5. The experimental rate constants have been converted into energy transfer probabilities using Eqn. (2.8) discussed in Chapter II. The results are given in Table 5.6.

V.3 Interpretation of Experimental Results

C_4H_4S molecule has 22 fundamental modes of vibration, out of which only 14 have been reported to be IR active[66]. Three of the fundamental modes lie far above 2349 cm^{-1}. A partial energy level diagram of C_4H_4S and CO_2 is shown in Figure 5.5 in which the fundamental modes of C_4H_4S which are far away from 2349 cm^{-1} are not included as these levels are not likely to participate in the deactivation of $CO_2(00^\circ1)$. It can be observed from Fig. 5.5 that no level of C_4H_4S is close to $CO_2(00^\circ1)$. However, two fundamental modes ν_6 (1083 cm^{-1}) and ν_7 (1036 cm^{-1}) are close to the energy difference 1064 cm^{-1} corresponding to $(00^\circ1\text{-}02^\circ0)$ in CO_2.

In light of the criteria discussed in Section IV.3 for selecting the possible energy transfer processes, the following processes are expected to be responsible in deactivating $CO_2(00^\circ1)$ level.

Table 5.5 : Composition Dependence of $(P\tau^{-1})$ at Different Temperatures

$X_{C_4H_4S}$	$(P\tau^{-1})$ $(Torr^{-1}ms^{-1})$			
	T = 323 K	T = 363 K	T = 413 K	T = 463 K
0	0.32	0.40	0.50	0.54
0.050	3.63	3.28	2.91	2.71
0.080	4.84	4.04	3.73	3.19
0.110	7.15	6.85	5.34	4.90
0.139	9.37	9.23	8.12	6.95

Table 5.6 : Rate constants and Probabilities for Energy transfer from CO_2 $(00^{\circ}1)$ to C_4H_4S

T(K)	$k_{CO_2-C_4H_4S}$ $(Torr^{-1}ms^{-1})$	Probability$(\times 10^3)$
323	62.50±2.41	4.97±0.19
363	59.47±3.62	5.02±0.31
413	47.90±3.66	4.31±0.33
463	42.41±2.84	4.04±0.27

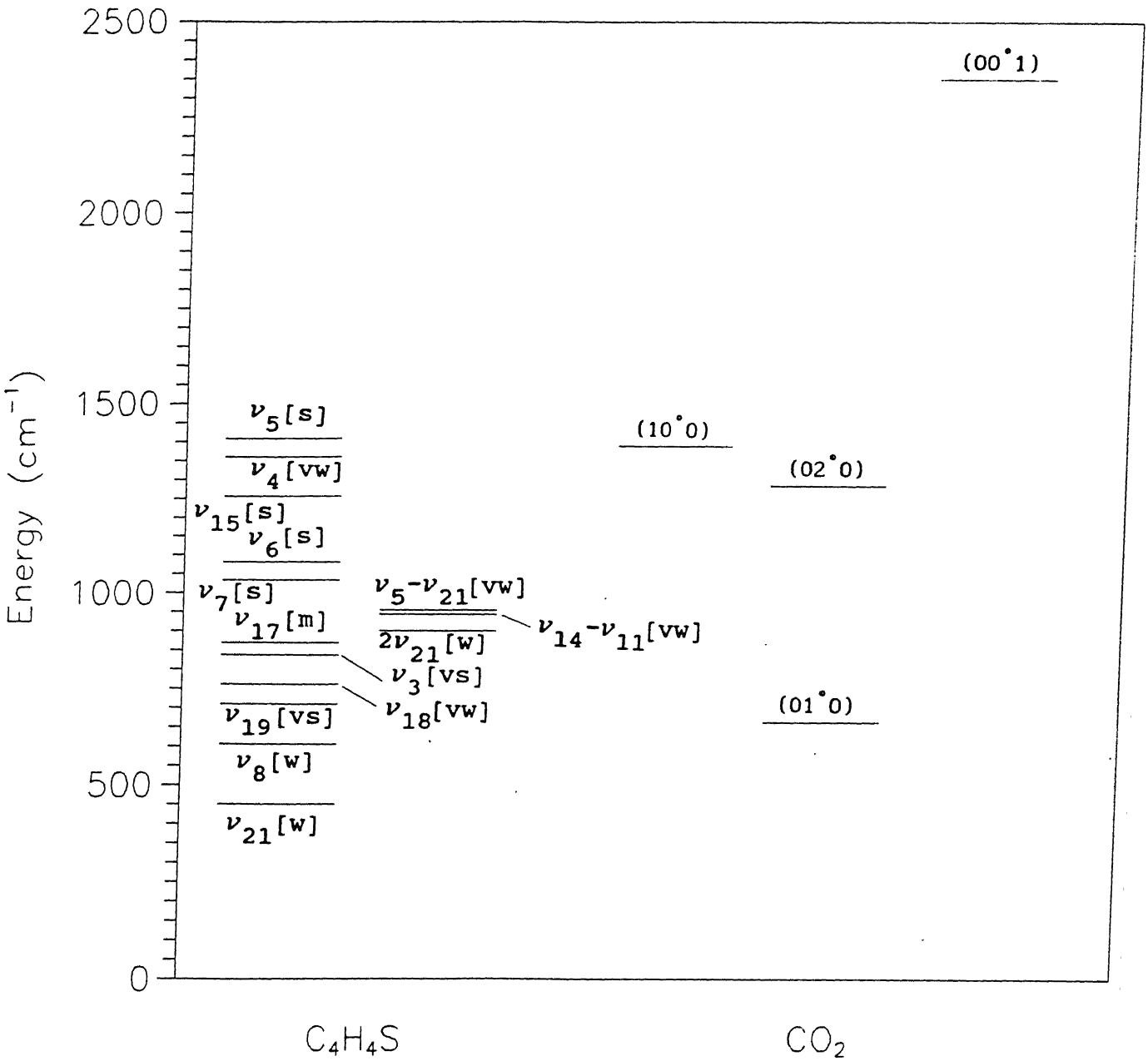

Fig. 5.5 Partial energy level diagram for C_4H_4S and CO_2.

$$CO_2(00^\circ1) + C_4H_4S(0) \longrightarrow CO_2(10^\circ0) + C_4H_4S\ (\nu_6) - 122\ cm^{-1} \quad (5.1)$$

$$CO_2(00^\circ1) + C_4H_4S(0) \longrightarrow CO_2(10^\circ0) + C_4H_4S\ (\nu_7) - 75\ cm^{-1} \quad (5.2)$$

$$CO_2(00^\circ1) + C_4H_4S(0) \longrightarrow CO_2(02^\circ0) + C_4H_4S\ (\nu_6) - 19\ cm^{-1} \quad (5.3)$$

$$CO_2(00^\circ1) + C_4H_4S(0) \longrightarrow CO_2(02^\circ0) + C_4H_4S\ (\nu_7) + 28\ cm^{-1} \quad (5.4)$$

The probabilities for all the above V-V energy exchange processes can be estimated with the help of SB-Tam theory. The square of the transition dipole moments of the involved transitions for CO_2 are known. But the transition dipole moments for the transitions involved in C_4H_4S are not available. If the absolute intensities of the bands are known the dipole moments can be estimated. These are also not available except that ν_6 and ν_7 bands in C_4H_4S are reported to be strong. The various molecular parameters of CO_2 and C_4H_4S used in predicting the energy transfer probabilities using SB-Tam theory are presented in Table 5.7.

Since the transition dipole moments for C_4H_4S are not available in the literature, the energy transfer probabilities have been calculated with an assumed value of 1×10^{-37} esu^2cm^2. By matching the theoretical probabilities with the experimental values, the actual transition dipole moment for C_4H_4S was

Table 5.7 : Molecular parameters for CO_2 and C_4H_4S

Parameters		CO_2	C_4H_4S
Rotational Constants	A	-	0.268 cm^{-1} [b]
	B	0.39 cm^{-1} [a]	0.181 cm^{-1}
	C	-	0.108 cm^{-1}
Hard sphere collision diameter		4.0 Å [c]	4.652 Å

[a] The rotational constant B for CO_2 is taken from ref. 62

[b] The rotational constants for C_4H_4S are taken from ref. 67

[c] The hard sphere collision diameter for CO_2 is taken from ref. 61

calculated. The rotational level population in C_4H_4S was estimated assuming the molecule to be a prolate symmetric top. This assumption is justified in view of the fact that the rotational constants B and C are almost equal. The hard sphere collision diameter for C_4H_4S was estimated from the Van der Waal's b parameter, which is equal to 0.127 lit/mole[68] using the relation[69],

$$b = 4N_A \left[\frac{4}{3} \pi \left(\frac{\sigma}{2} \right)^3 \right]$$

where N_A is Avogadro number and σ is hard sphere diameter.

The SB-Tam theory was used to obtain the energy transfer probabilities for the processes (5.1) to (5.4) at various temperatures. The calculated probabilities are presented in Table 5.8. To facilitate comparison the experimental probabilities are also listed in the same table.

It can be observed from Table 5.8 that the experimental probabilities are of the order of 10^{-3} and show a negative temperature dependence. The calculated probabilities for the processes (5.1) and (5.2) are of the order of 10^{-5} and 10^{-4} and exhibit a positive temperature dependence. In view of this the processes (5.1) and (5.2) are not likely to be responsible for deactivation of $CO_2(00^o1)$. But the probabilities for the

Table 5.8 : Calculated Energy Transfer Probabilities at Different Temperatures

Process	ΔE (cm^{-1})	Probability			
		T = 323 K	T = 363 K	T = 413 K	T = 463 K
5.1*	-122	3.981×10^{-5}	4.607×10^{-5}	5.415×10^{-5}	6.155×10^{-5}
5.2	-75	2.567×10^{-4}	2.753×10^{-4}	3.059×10^{-4}	3.373×10^{-4}
5.3	-19	3.807×10^{-3}	3.474×10^{-3}	3.096×10^{-3}	2.799×10^{-3}
5.4	28	3.407×10^{-3}	3.166×10^{-3}	2.871×10^{-3}	2.629×10^{-3}
Experimental	---	4.97×10^{-3}	5.02×10^{-3}	4.31×10^{-3}	4.04×10^{-3}

* 5.1 etc. denote the probability for the processes represented by Eqns. (5.1) etc. in the text.

Processes (5.3) and (5.4) are of the order 10^{-3} and have negative temperature dependence. Hence these processes are likely to deactivate $CO_2(00^\circ1)$.

Since the energy levels ν_6 and ν_7 are very close to each other (the difference being only 47 cm^{-1}), it is very difficult to exactly identify whether process (5.3) or (5.4) is responsible for the deactivation of $CO_2(00^\circ1)$. Hence it is reasonable to assume that these two levels contribute equally to the energy transfer probability, the energy transfer probability for each of these levels being the average value of the two probabilities for the processes (5.3) and (5.4). These average values of the probabilities were matched with the experimental values to obtain the transition dipole moment as indicated below.

$$P_{exp} = A\,P_3 + B\,P_4 \tag{5.5}$$

where P_3 and P_4 denote the probabilities represented by the processes (5.3) and (5.4) respectively, and A and B are multiplicative constants. In view of the assumption

$$P_3 = P_4 = \frac{(P_3 + P_4)}{2} \tag{5.6}$$

$$P_{exp} = (A + B)\,\frac{(P_3 + P_4)}{2} \tag{5.7}$$

The calculated value of (A + B) gave the sum of the transition dipole moments for the involved transitions as $(1.44\pm0.03) \times 10^{-37}$ esu^2cm^2. The temperature dependence of the experimental probabilities are shown in Fig. 5.6. The calculated values of probability using the estimated values of (A + B) are shown as a solid curve in the same figure.

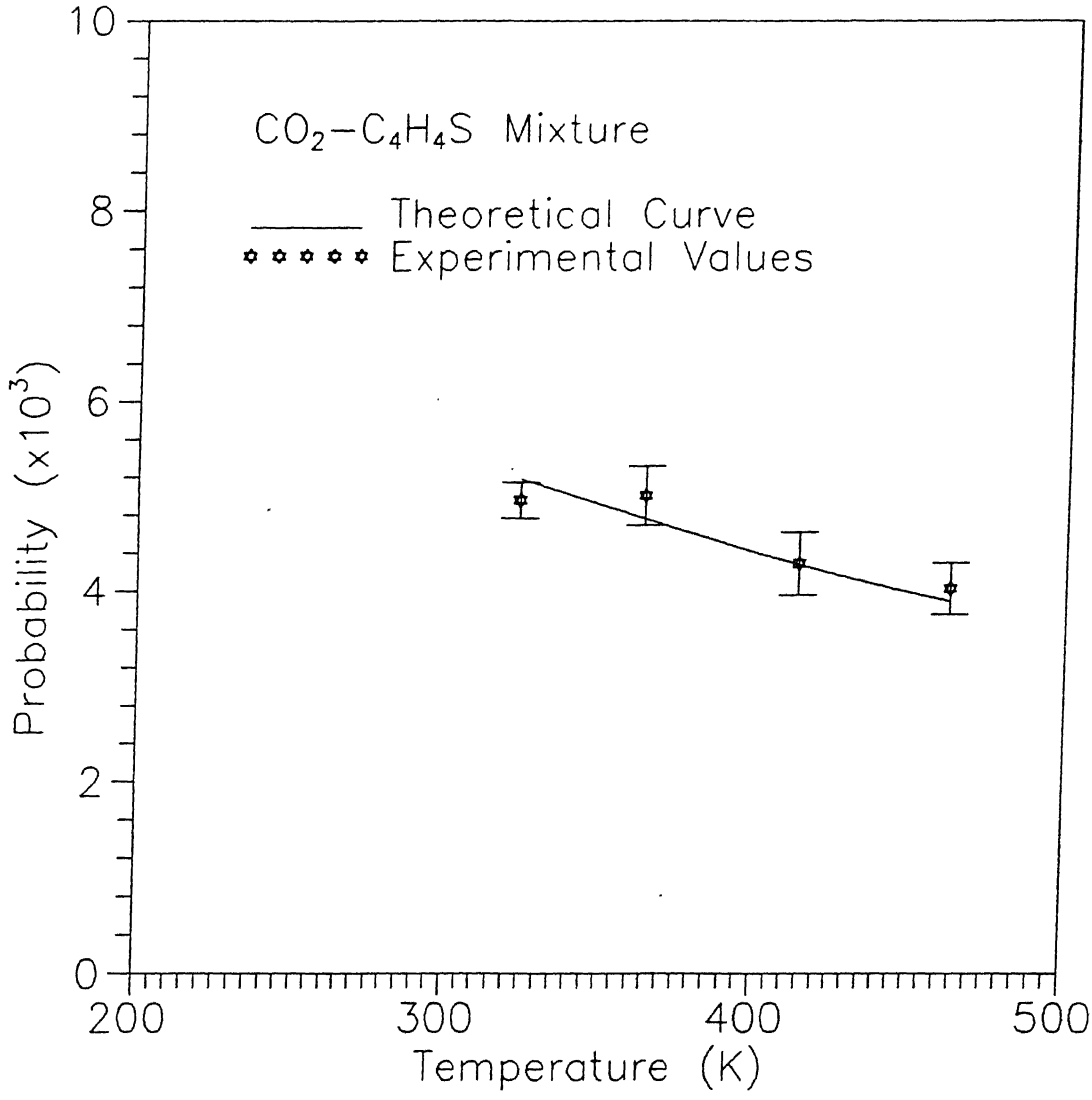

Fig. 5.6 Temperature dependence of energy transfer probability.

CHAPTER VI

EXPERIMENTAL RESULTS AND DISCUSSIONS : CO_2-$(CD_3)_2CO$ SYSTEM

VI.1 GENERAL REMARKS

The deactivation rates of CO_2 ($00^\circ1$) in mixtures of CO_2 and Acetone-d_6 [$(CD_3)_2CO$] were studied by monitoring the time history of fluorescence from $CO_2(00^\circ1)$ level at 4.3 μm. These rates were studied for different mixture compositions namely 3.0%, 5.1%, 8.0%, 11.0% and 13.8% of $(CD_3)_2CO$ at different temperatures, 323 K, 363 K, 413 K, and 463 K. The maximum percentage of $(CD_3)_2CO$ was limited by the time constant of the detector and associated electronics as discussed earlier. The deactivation rates of $CO_2(00^\circ1)$ in collisions with $(CD_3)_2CO$ were obtained by extrapolating their measured rates to 100% $(CD_3)_2CO$.

The observed deactivation rates indicate that near resonant processes are responsible for deactivating $CO_2(00^\circ1)$. These rates decreased with increasing temperature, which suggests that long range forces are responsible in the deactivating process. Therefore SB-Tam theory was used to calculate the energy transfer probabilities, which were compared with the experimental values. The experimental results and analysis are given below in detail.

VI.2 Experimental Results

A typical fluorescence signal at 4.3μm from $CO_2(00^\circ1)$ level in a 3.0% $(CD_3)_2CO$ mixture at T = 323 K and P = 9.84 Torr is

presented in Fig. 6.1. A semilogarithmic plot of intensity of the fluorescence signal versus time is shown in Fig. 6.2. A least squares fit of the data to a straight line gave τ^{-1} = (38.46±4.27) ms^{-1}, where error corresponds to standard deviation.

The fluorescence decay time was measured at several pressures in the range 4-20 Torr. A typical plot of P versus τ^{-1} at 323 K for a 3.0% $(CD_3)_2CO$ mixture is shown in Fig. 6.3. The dependence of τ^{-1} on P was found to be linear. A least squares analysis of this data considering error in both P and τ^{-1} yielded $(P\tau)^{-1}$ = (3.73±0.09) $Torr^{-1}ms^{-1}$. The values of $(P\tau)^{-1}$ were obtained following the above procedure for all the four temperatures and different compositions and the results are presented in Tables 6.1 through 6.5.

Figures 6.4a, 6.4b, 6.4c and 6.4d show plots of $(P\tau)^{-1}$ vs mole fraction of $(CD_3)_2CO$, at 323 K, 363 K, 413 K and 463 K. Since the dependence of $(P\tau)^{-1}$ on $X_{(CD_3)_2CO}$ is linear the deactivation rate of the mixture can be written as

$$(P\tau)^{-1} = (P\tau)^{-1}_{CO_2-CO_2} (1-X_M) + (P\tau)^{-1}_{CO_2-M} X_M$$

or $$k = k_{CO_2-CO_2} (1-X_M) + k_{CO_2-M} X_M$$

where M denotes the $(CD_3)_2CO$ molecule; $k_{CO_2-CO_2}$ and k_{CO_2-M} represent the rate constants for the deactivation of $CO_2(00^\circ1)$, in collisions with CO_2 molecules only and in collisions with $(CD_3)_2CO$ molecules only, respectively.

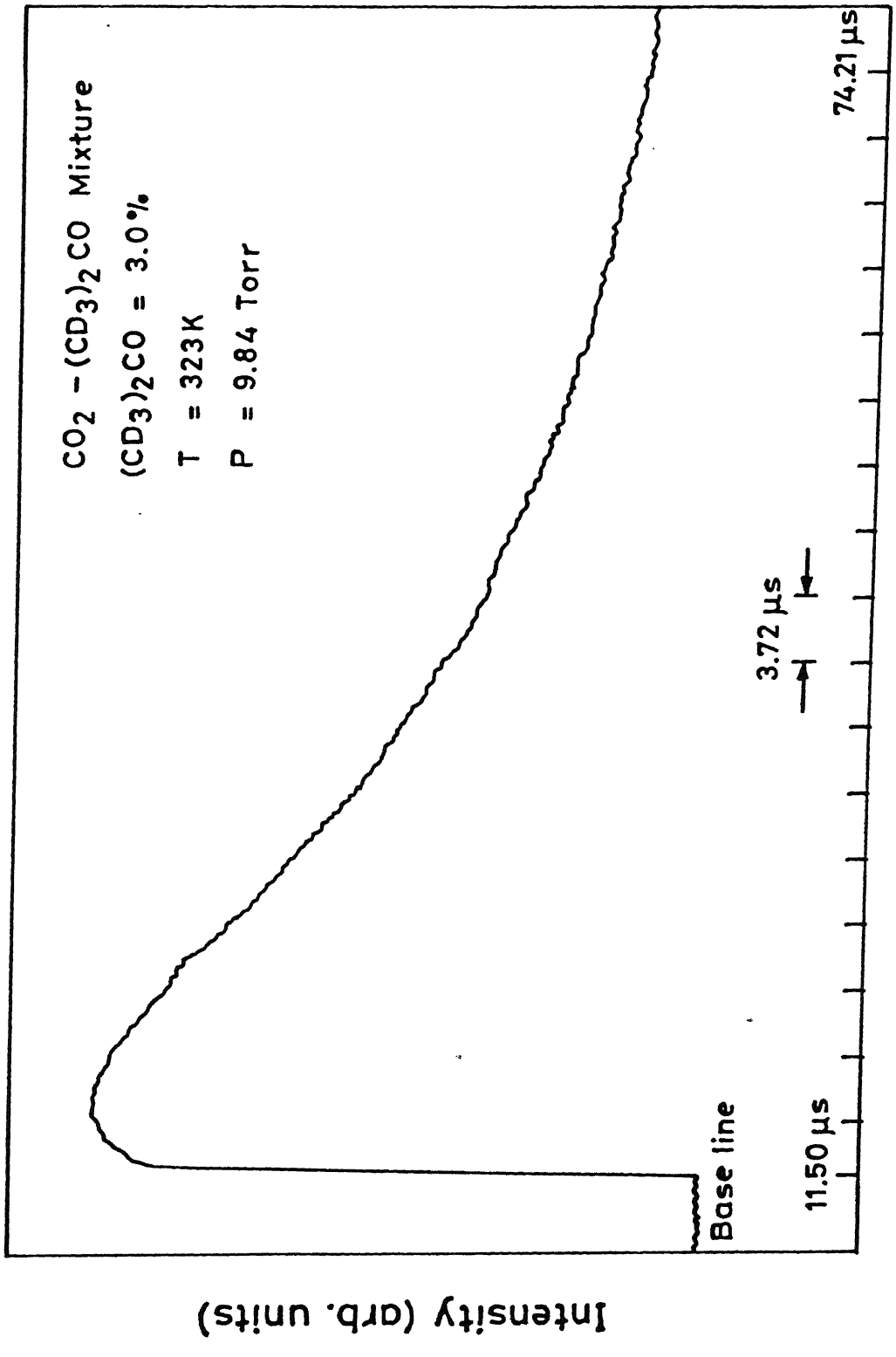

Fig. 6.1 Typical fluorescence signal.

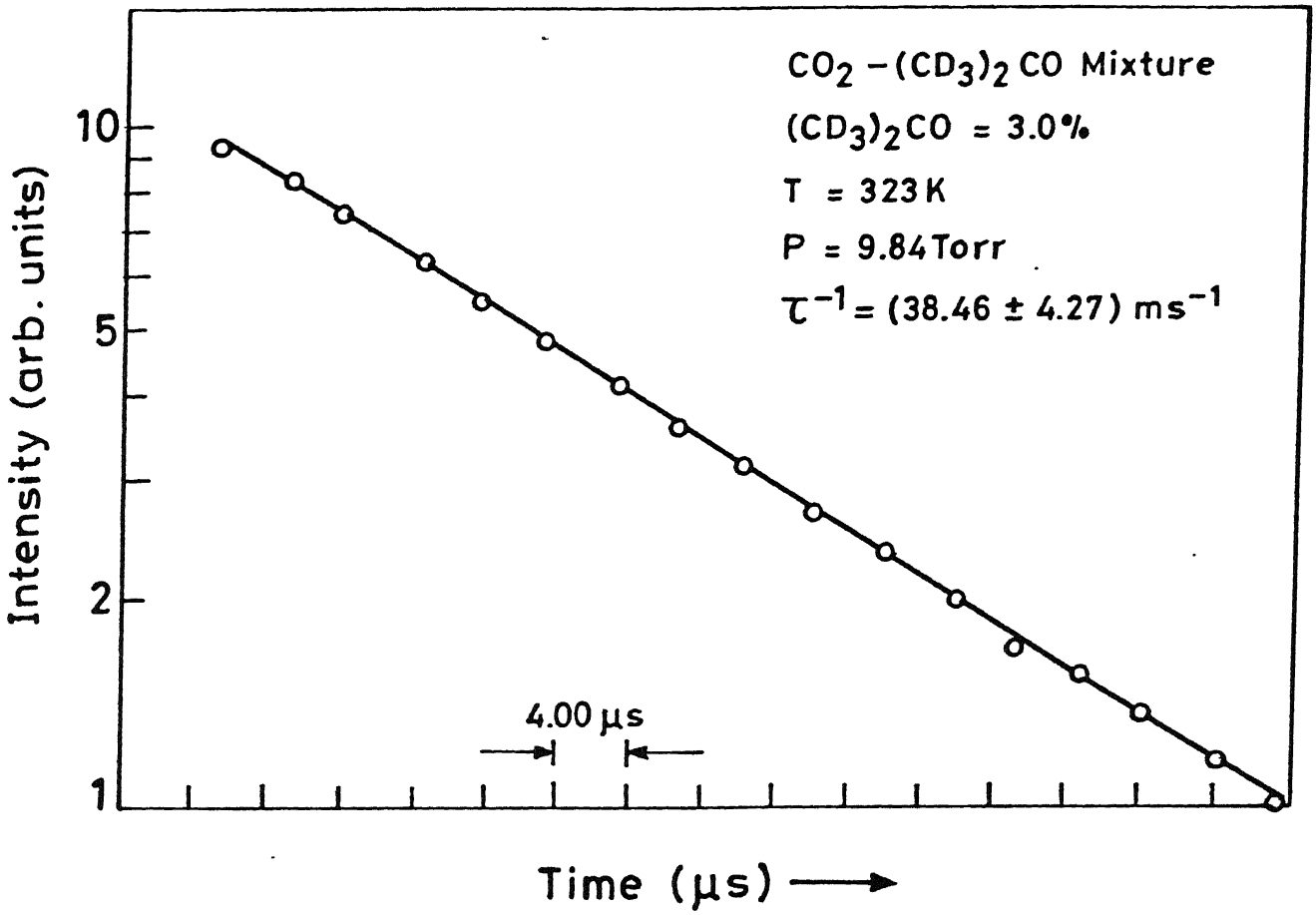

Fig. 6.2 Semilogarithmic plot of fluorescence intensity vs time.

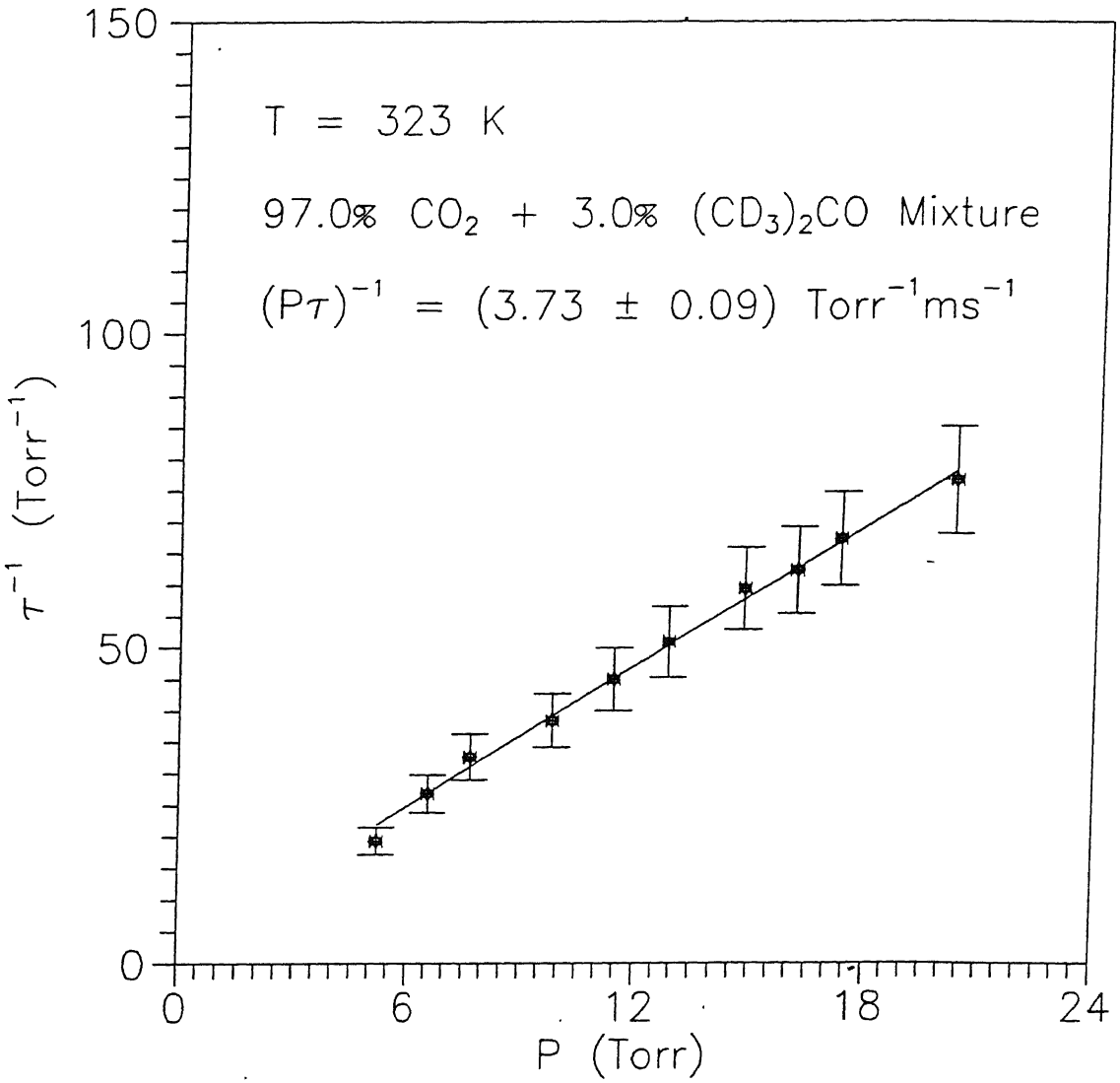

Fig. 6.3 Plot of τ^{-1} vs pressure.

Table 6.1 : Experimental Values of τ^{-1} at Various Pressures and Different Temperatures for a 3.0% $(CD_3)_2CO$ Mixture

T = 323 K		T = 363 K		T = 413 K		T = 463 K	
P (Torr)	τ^{-1} (ms^{-1})	P (Torr)	τ^{-1} (ms^{-1})	P (Torr)	τ^{-1} (ms^{-1})	P (Torr)	τ^{-1} (ms^{-1})
5.20	19.38	4.72	14.49	4.24	12.17	4.08	10.55
6.56	26.88	5.92	27.55	5.68	19.53	5.68	14.39
7.68	32.68	6.24	26.67	6.88	21.55	7.28	22.32
9.84	38.46	7.20	25.25	8.72	27.10	9.52	24.51
11.44	45.05	8.96	27.17	10.96	31.45	10.32	27.10
12.88	51.02	9.60	35.09	12.32	35.09	12.00	31.45
14.80	59.52	10.88	36.76	14.32	40.00	13.36	35.71
16.16	62.50	12.00	46.30	16.08	53.19	15.12	37.88
17.28	67.57	12.96	43.10	17.44	53.19	16.80	52.63
20.32	76.92	13.76	50.00	19.12	55.56	18.00	51.55
		15.28	54.35				
		15.60	56.50				
		16.32	61.73				
		18.16	62.50				
		18.56	60.24				
		20.32	68.49				
$(P\tau)^{-1}=(3.73\pm 0.09)Torr^{-1}ms^{-1}$		$(P\tau)^{-1}=(3.27\pm 0.18)Torr^{-1}ms^{-1}$		$(P\tau)^{-1}=(2.97\pm 0.19)Torr^{-1}ms^{-1}$		$(P\tau)^{-1}=(3.05\pm 0.25)Torr^{-1}ms^{-1}$	

Table 6.2 : Experimental Values of τ^{-1} at Various Pressures and Different Temperatures for a 5.1% $(CD_3)_2CO$ Mixture

T = 323 K		T = 363 K		T = 413 K		T = 463 K	
P (Torr)	τ^{-1} (ms^{-1})	P (Torr)	τ^{-1} (ms^{-1})	P (Torr)	τ^{-1} (ms^{-1})	P (Torr)	τ^{-1} (ms^{-1})
5.04	29.76	4.72	26.88	4.88	25.25	4.64	22.22
6.48	43.10	5.84	30.86	6.32	25.45	5.36	23.64
6.96	34.25	7.36	37.59	8.00	31.45	6.72	25.06
7.28	31.25	9.12	39.68	9.84	34.25	7.52	27.55
8.40	56.50	9.92	53.19	10.32	50.00	9.60	35.21
8.64	45.45	11.68	68.49	12.40	60.98	11.36	39.68
9.44	53.76	13.60	62.50	13.20	54.95	12.72	44.25
10.80	64.94	15.68	76.92	15.52	58.14	13.92	52.08
10.88	71.94	17.20	80.65	16.48	56.82	15.92	59.52
12.72	72.99			19.04	79.37	17.12	61.73
13.84	70.42						
14.32	94.34						
15.68	72.46						
16.56	73.53						
16.80	79.37						
18.40	111.10						
$(P\tau)^{-1}=(5.00\pm 0.66)Torr^{-1}ms^{-1}$		$(P\tau)^{-1}=(4.54\pm 0.46)Torr^{-1}ms^{-1}$		$(P\tau)^{-1}=(3.74\pm 0.51)Torr^{-1}ms^{-1}$		$(P\tau)^{-1}=(3.41\pm 0.16)Torr^{-1}ms^{-1}$	

Table 6.3 : Experimental Values of τ^{-1} at Various Pressures and Different Temperatures for a 8.0% $(CD_3)_2CO$ Mixture

T = 323 K		T = 363 K		T = 413 K		T = 463 K	
P (Torr)	τ^{-1} (ms^{-1})	P (Torr)	τ^{-1} (ms^{-1})	P (Torr)	τ^{-1} (ms^{-1})	P (Torr)	τ^{-1} (ms^{-1})
4.32	46.30	4.32	40.32	3.92	39.37	4.88	39.37
5.76	48.54	5.44	46.30	5.04	42.74	6.72	41.32
7.44	71.43	7.92	58.82	7.20	51.55	8.16	50.51
8.16	65.79	8.56	66.67	9.36	58.82	9.92	55.56
9.36	84.75	10.64	79.37	12.16	108.70	11.44	62.50
9.92	78.13	12.40	102.00	12.24	86.21	11.68	67.57
12.32	94.34	14.40	119.00	15.12	104.20	13.76	70.42
12.80	113.60	16.00	126.60	15.36	104.20	14.80	98.04
13.92	117.60	19.28	138.90	17.28	114.90	16.32	101.00
18.48	142.90	19.76	140.80	18.08	114.90	17.44	112.40
$(P\tau)^{-1}=(7.28\pm 0.50)Torr^{-1}ms^{-1}$		$(P\tau)^{-1}=(6.95\pm 0.40)Torr^{-1}ms^{-1}$		$(P\tau)^{-1}=(5.96\pm 0.69)Torr^{-1}ms^{-1}$		$(P\tau)^{-1}=(6.34\pm 0.64)Torr^{-1}ms^{-1}$	

Table 6.4 : Experimental Values of τ^{-1} at Various Pressures and Different Temperatures for a 11.0% $(CD_3)_2CO$ Mixture

T = 323 K		T = 363 K		T = 413 K		T = 463 K	
P (Torr)	τ^{-1} (ms^{-1})	P (Torr)	τ^{-1} (ms^{-1})	P (Torr)	τ^{-1} (ms^{-1})	P (Torr)	τ^{-1} (ms^{-1})
4.72	64.10	4.40	51.02	4.72	48.54	4.32	44.64
5.28	64.94	5.68	66.23	6.32	54.95	5.52	47.17
6.40	70.92	6.48	65.79	8.40	73.53	6.80	51.55
8.32	101.01	6.80	72.46	9.84	83.33	7.28	60.98
9.84	111.11	8.72	85.47	11.28	128.20	8.40	62.50
12.24	129.87	10.48	108.69	11.92	107.52	10.00	69.44
13.84	156.25	11.28	131.57	13.20	128.20	11.60	81.97
15.28	147.05	12.24	135.13	13.60	138.88	13.52	94.34
17.52	136.98	14.64	158.73	15.04	126.58	14.80	111.11
18.16	169.49	14.64	151.51	15.60	131.57	15.68	112.35
$(P\tau)^{-1}=(7.41\pm 0.92)Torr^{-1}ms^{-1}$		$(P\tau)^{-1}=(10.73\pm 0.59)Torr^{-1}ms^{-1}$		$(P\tau)^{-1}=(8.92\pm 1.30)Torr^{-1}ms^{-1}$		$(P\tau)^{-1}=(6.40\pm 0.36)Torr^{-1}ms^{-1}$	

Table 6.5 : Experimental Values of τ^{-1} at Various Pressures and T = 323 K for a 13.8% $(CD_3)_2CO$ Mixture

P (Torr)	τ^{-1} (ms^{-1})
3.36	62.89
4.48	74.07
6.32	90.09
8.00	129.87
8.64	140.84
10.00	140.84
11.84	192.30
12.08	192.30
13.36	185.18
15.76	204.08
$(P\tau)^{-1}$ = 12.61±1.27 $Torr^{-1}ms^{-1}$	

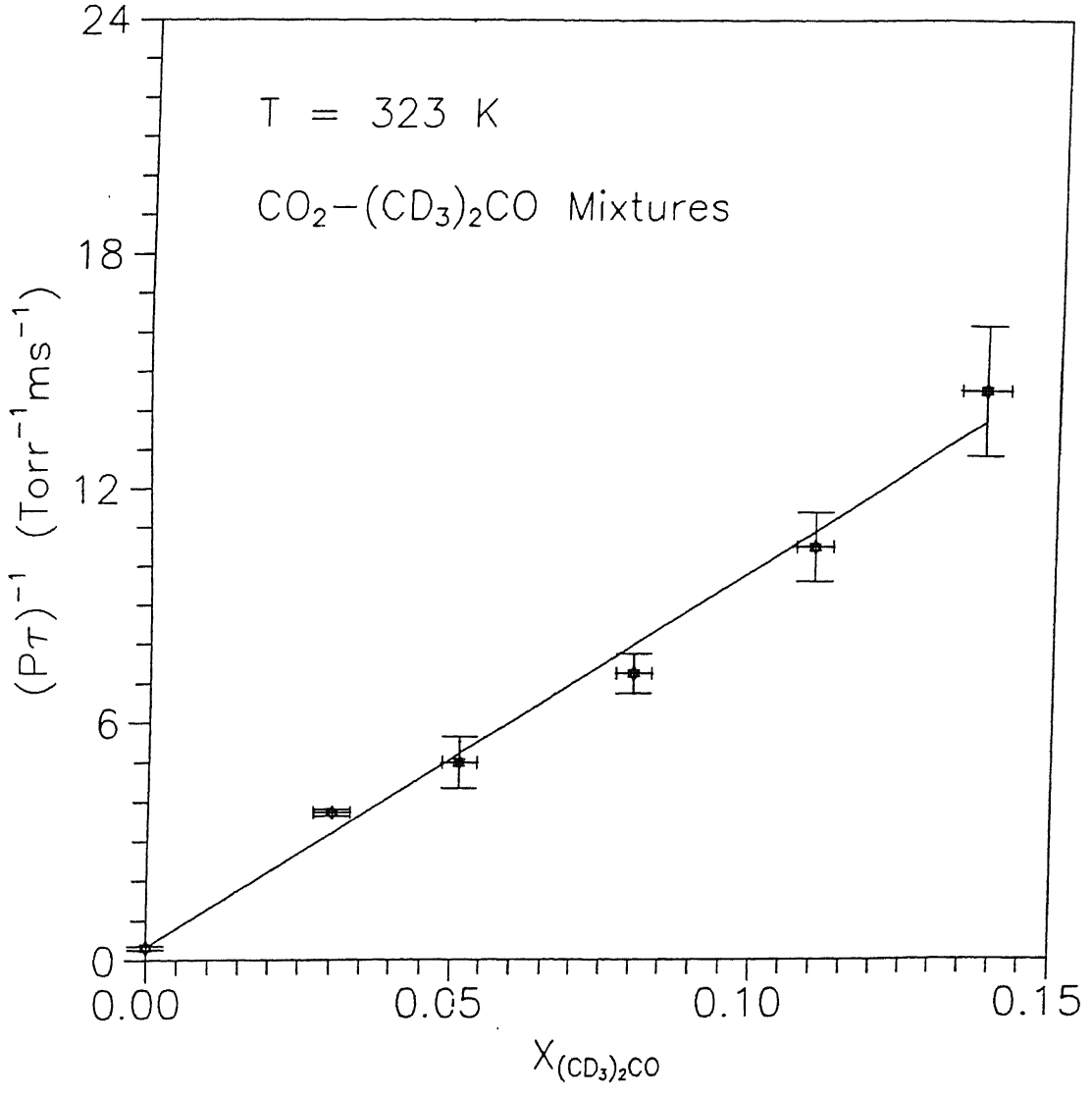

Fig. 6.4a Composition dependence of $(P\tau)^{-1}$ at 323 K.

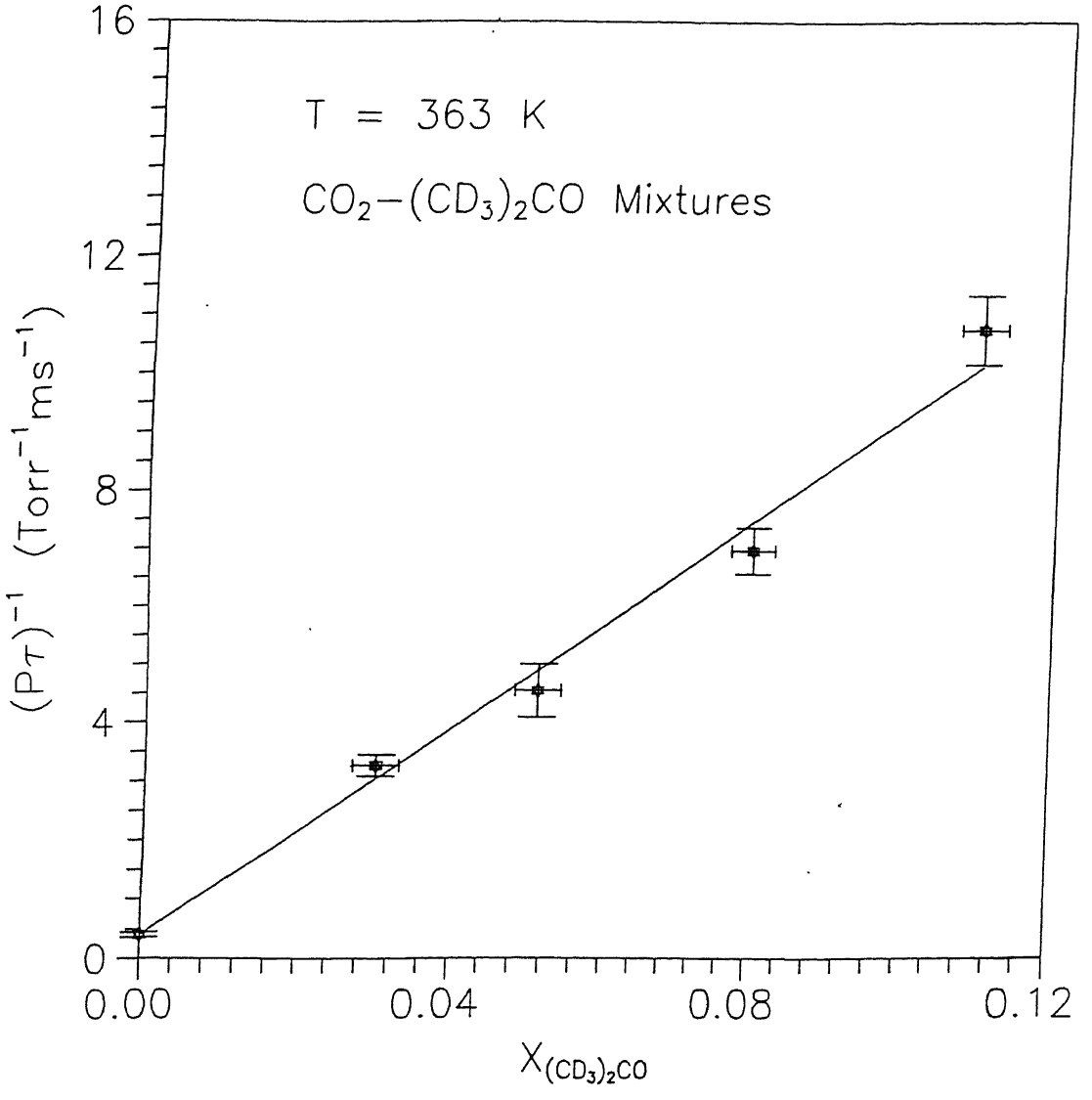

Fig. 6.4b Composition dependence of $(P\tau)^{-1}$ at 363 K.

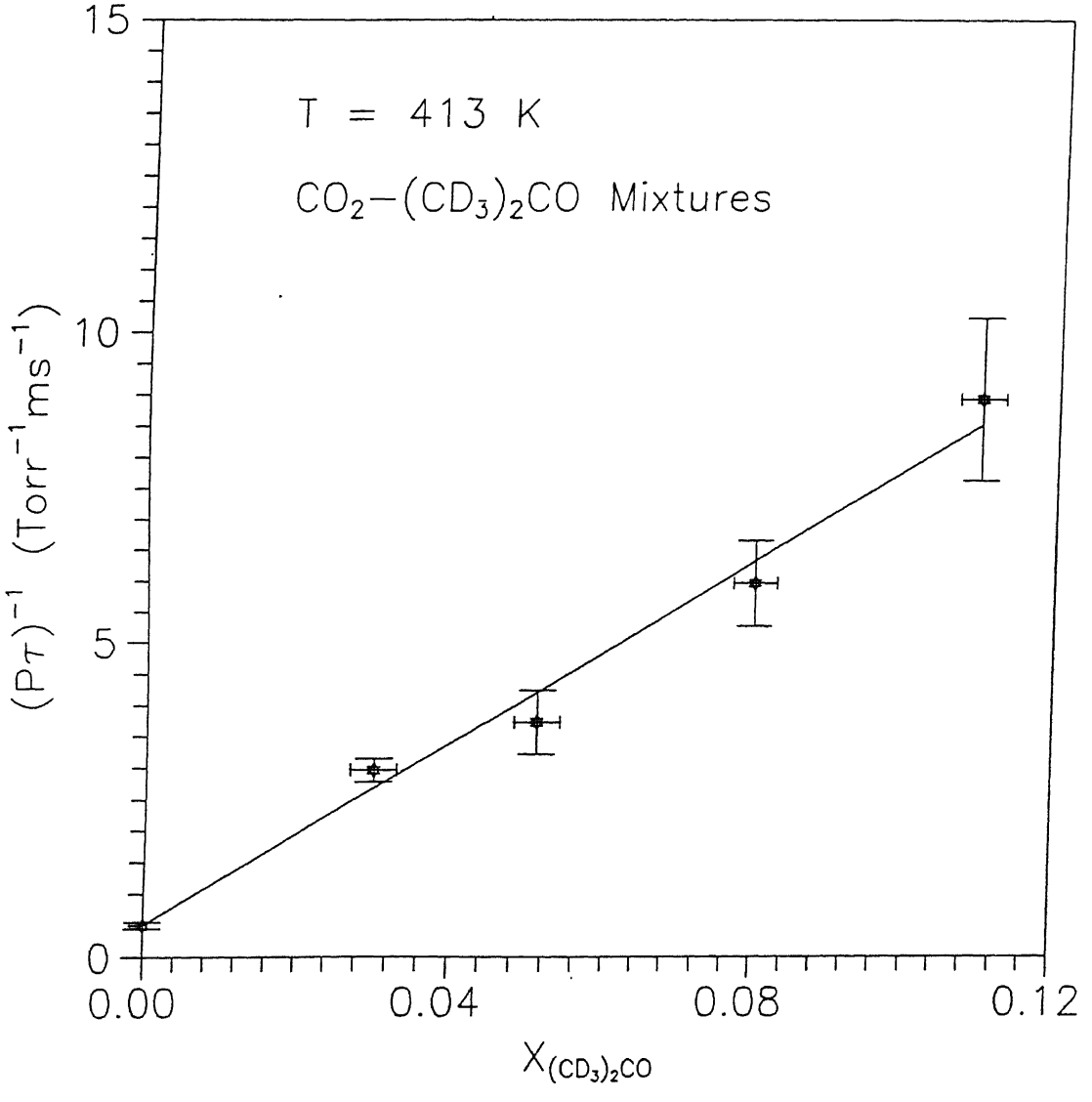

Fig. 6.4c Composition dependence of $(P\tau)^{-1}$ at 413 K.

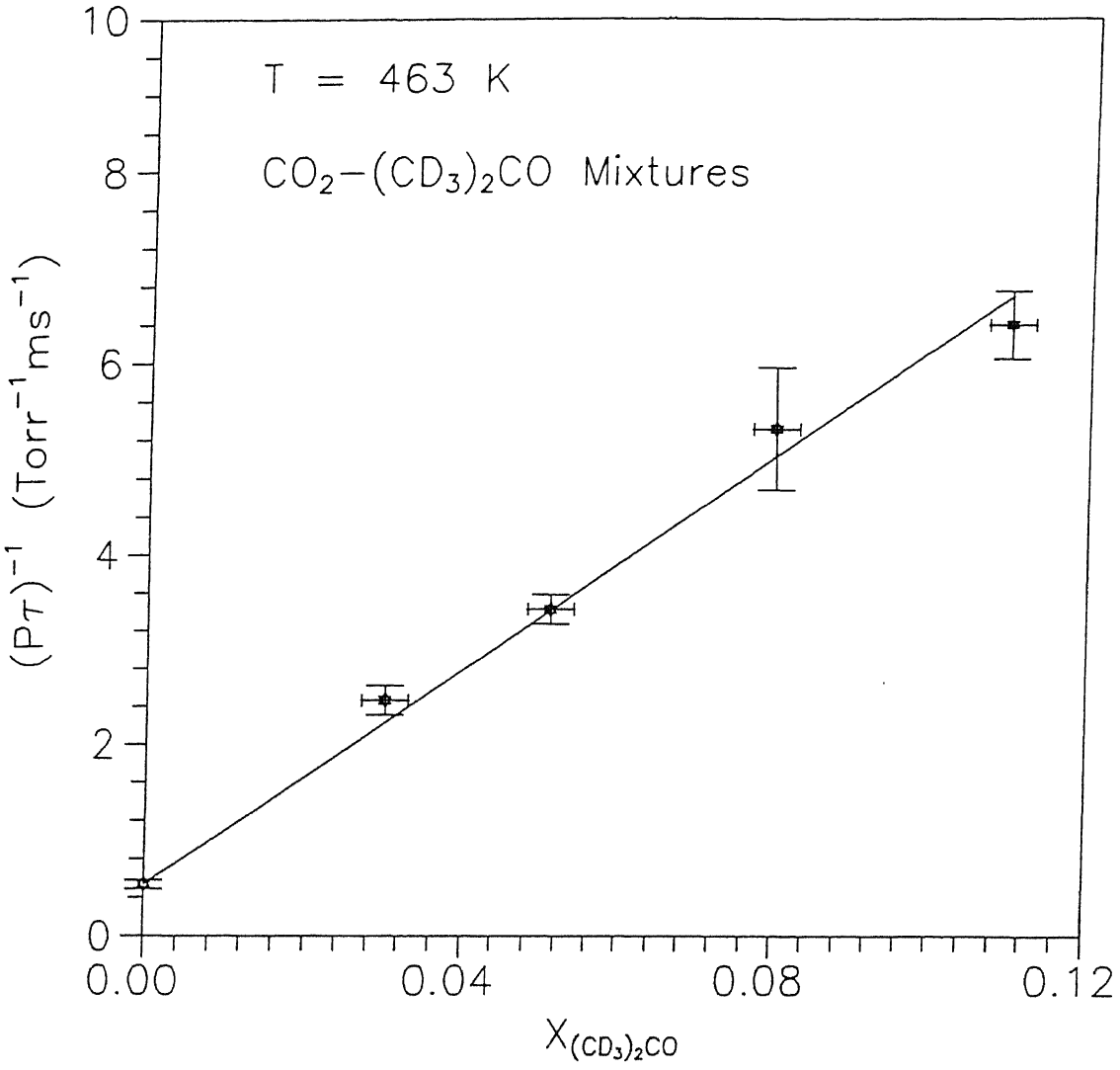

Fig. 6.4d Composition dependence of $(P\tau)^{-1}$ at 463 K.

The value of k_{CO_2-M} was obtained by extrapolating the $(P\tau)^{-1}$ data to $X_M = 1$. A least squares analysis of the data to a straight line fit, considering errors in both the variables was performed to obtain the value of $k_{CO_2-(CD_3)_2CO}$ at all the four temperatures studied and the data are presented in Table 6.6.

The experimental rate constants were converted into energy transfer probabilities using the Eqn. (2.8). The results are summarized in Table 6.7.

VI.3 Interpretation

Acetone-d_6 [$(CD_3)_2CO$], molecule has 25 fundamental modes of vibration, out of which only 14 are reported[70] to be IR active. A partial energy level diagram of $(CD_3)_2CO$ and CO_2 is shown in Fig. 6.5. It can be observed from Fig. 6.5 that two fundamental levels ν_{13}(2263.5 cm^{-1}) and ν_{20}(2226.5 cm^{-1}) of $(CD_3)_2CO$ are close to $CO_2(00^\circ1)$ level. In addition to these, four fundamental modes ν_4(1080 cm^{-1}), ν_{16}(1035 cm^{-1}), ν_{17}(1054 cm^{-1}) and ν_{21}(1050 cm^{-1}); two combination bands $\nu_{17}+\nu_{19}$(1160 cm^{-1}) and $\nu_6+\nu_{24}$(960 cm^{-1}) have energies which are in the neighborhood of 1064 cm^{-1} or 961 cm^{-1} corresponding to the transitions ($00^\circ1$-$02^\circ0$) and ($00^\circ1$-$10^\circ0$), in CO_2, respectively.

Table 6.6 : Composition Dependence of $(P\tau)^{-1}$ at Different Temperatures

$X_{(CD_3)_2CO}$	$(P\tau)^{-1}$ $(Torr^{-1}ms^{-1})$			
	T = 323 K	T = 363 K	T = 413 K	T = 463 K
0	0.32	0.40	0 50	0.54
0.030	3.73	3.27	2.97	2.46
0.051	5.00	4.54	3.74	3.41
0.080	7.28	6.95	5.96	5.31
0.110	10.52	10.73	8.92	6.40
0.138	14.50			

Table 6.7 : Rate Constants and Probabilities For Energy Transfer From $CO_2(00^\circ1)$ to $(CD_3)_2CO$.

T (K)	$k_{CO_2-(CD_3)_2CO}$ $(Torr^{-1}ms^{-1})$	Probability $(\times10^3)$
323	96.57±5.53	6.76±0.39
363	88.57±3.73	6.57±0.28
413	73.27±4.34	5.80±0.34
463	56.47±2.09	4.73±0.18

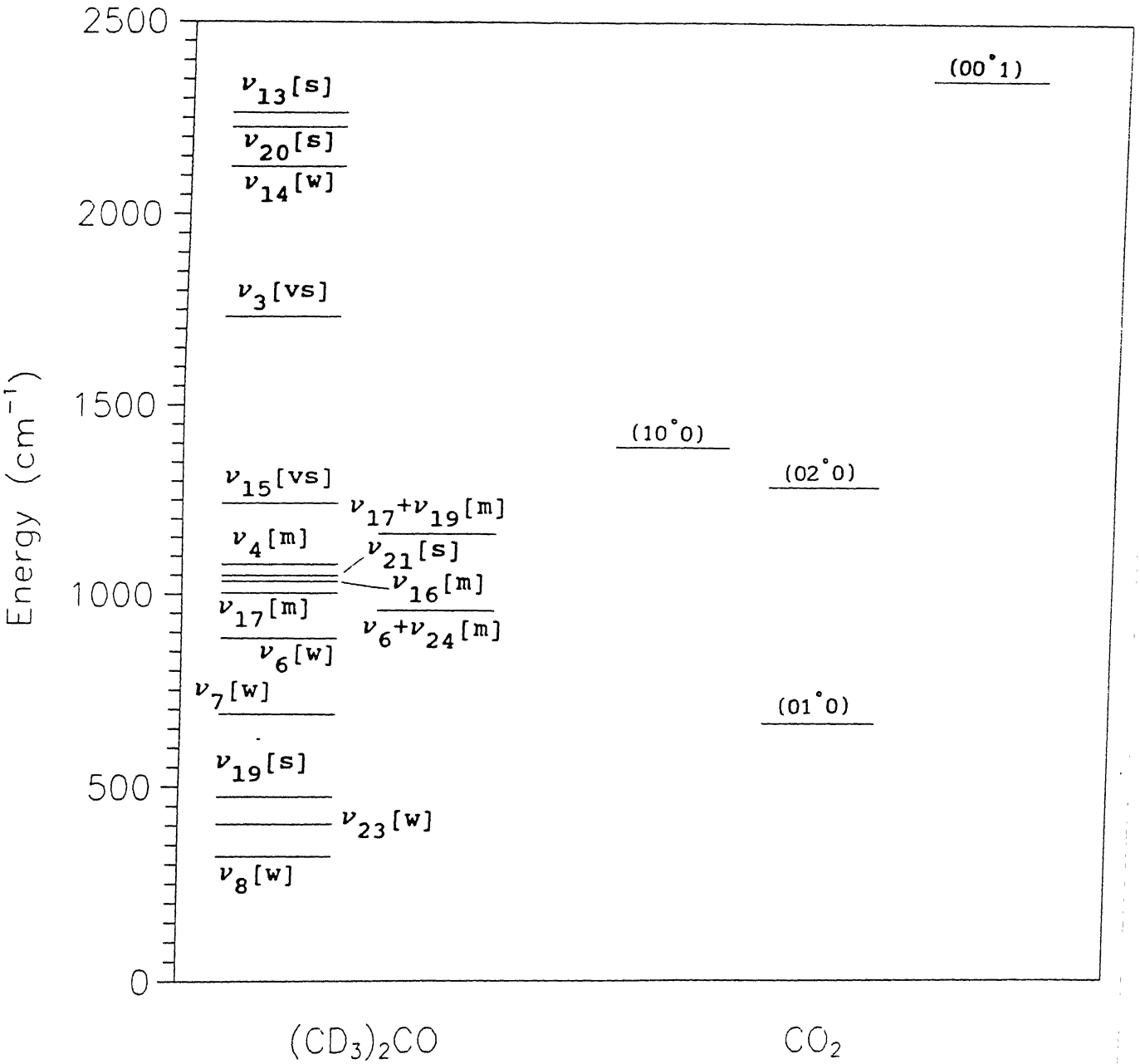

Fig. 6.5 Partial energy level diagram for $(CD_3)_2CO$ and CO_2.

Taking into account the above facts and the criteria discussed in Section IV.3 for selecting the possible energy transfer processes, the following processes were considered to be responsible for the deactivation of $CO_2(00^\circ1)$ level

$$CO_2(00^\circ1) + (CD_3)_2CO(0) \rightarrow CO_2(0) + (CD_3)_2CO(\nu_{13}) + 85.5\ cm^{-1} \quad (6.1)$$

$$CO_2(00^\circ1) + (CD_3)_2CO(0) \rightarrow CO_2(0) + (CD_3)_2CO(\nu_{20}) + 122.5\ cm^{-1} \quad (6.2)$$

$$CO_2(00^\circ1) + (CD_3)_2CO(0) \rightarrow CO_2(02^\circ0) + (CD_3)_2CO(\nu_4) - 16\ cm^{-1} \quad (6.3)$$

$$CO_2(00^\circ1) + (CD_3)_2CO(0) \rightarrow CO_2(02^\circ0) + (CD_3)_2CO(\nu_{21}) + 14\ cm^{-1} \quad (6.4)$$

$$CO_2(00^\circ1) + (CD_3)_2CO(0) \rightarrow CO_2(02^\circ0) + (CD_3)_2CO(\nu_{16}) + 29\ cm^{-1} \quad (6.5)$$

$$CO_2(00^\circ1) + (CD_3)_2CO(0) \rightarrow CO_2(10^\circ0) + (CD_3)_2CO(\nu_{17}) - 43\ cm^{-1} \quad (6.6)$$

$$CO_2(00^\circ1) + (CD_3)_2CO(0) \rightarrow CO_2(02^\circ0) + (CD_3)_2CO(\nu_{17}) + 60\ cm^{-1} \quad (6.7)$$

$$CO_2(00^\circ1) + (CD_3)_2CO(0) \rightarrow CO_2(10^\circ0) + (CD_3)_2CO(\nu_6+\nu_{24}) + 1\ cm^{-1} \quad (6.8)$$

$$CO_2(00^\circ1) + (CD_3)_2CO(0) \rightarrow CO_2(02^\circ0) + (CD_3)_2CO(\nu_{17}+\nu_{19}) - 96\ cm^{-1} \quad (6.9)$$

The probability of energy transfer for the V-V exchange processes (6.1) to (6.9) can be calculated using SB-Tam theory.

The transition dipole moment matrix elements or absolute intensities for the levels involved in $(CD_3)_2CO$ molecule are not available. Only relative intensities of the above bands are known. It was reported[70] that ν_{13}, ν_{20}, ν_{21}, levels are strong while ν_4, ν_{16}, ν_{17}, $\nu_6+\nu_{24}$ and $\nu_{17}+\nu_{19}$, are medium.

The molecular parameters used in the calculation of energy transfer probabilities are presented in Table 6.8.

Since the values of transition dipole moment matrix elements for $(CD_3)_2CO$ are not available in the literature, the probabilities for energy transfer were calculated with an assumed values of 1 X 10^{-37} esu^2cm^2 for $(CD_3)_2CO$. The probabilities are directly proportional to the squares of the transition dipole moment matrix elements. Therefore a comparison of the theoretical and experimental probabilities yields the dipole moments of the involved transitions in $(CD_3)_2CO$. Since the rotational constants A and B are approximately same, the $(CD_3)_2CO$ molecule, is treated as an oblate symmetric top in the calculation of rotational population.

The calculated probabilities of energy transfer using SB-Tam theory for the above processes at various temperatures are presented in Table 6.9. The experimental values are also given in the same table for comparison purpose.

Table 6.8 : Molecular Parameters for CO_2 and $(CD_3)_2CO$

Parameter		CO_2	$(CD_3)_2CO$
Rotational Constants	A	---	0.56 cm^{-1} [b]
	B	0.39 cm^{-1} [a]	0.47 cm^{-1}
	C	---	0.27 cm^{-1}
Hard Sphere Collision Diameter [c]		4.0 Å	5.669 Å

[a] Value taken from ref. 62

[b] Collected from ref. 70

[c] Cited from ref. 61

Table 6.9 : Calculated Energy Transfer Probabilities at Different Temperatures.

Process	ΔE (cm^{-1})	Probability			
		T = 323 K	T = 363 K	T = 413 K	T = 463 K
6.1[a]	85.5	8.276×10^{-3}	9.210×10^{-3}	1.086×10^{-2}	1.319×10^{-2}
6.2	122.5	1.703×10^{-3}	1.991×10^{-3}	2.377×10^{-3}	2.785×10^{-3}
6.3	-16	1.833×10^{-3}	1.677×10^{-3}	1.506×10^{-3}	1.367×10^{-3}
6.4	14	2.020×10^{-3}	1.834×10^{-3}	1.627×10^{-3}	1.469×10^{-3}
6.5	29	1.643×10^{-3}	1.480×10^{-3}	1.312×10^{-3}	1.190×10^{-3}
6.6	-43	1.308×10^{-3}	1.270×10^{-3}	1.199×10^{-3}	1.121×10^{-3}
6.7	60	4.980×10^{-4}	5.505×10^{-4}	6.181×10^{-4}	6.639×10^{-4}
6.8	1	2.847×10^{-3}	2.556×10^{-3}	2.221×10^{-3}	1.969×10^{-3}
6.9	-96	5.504×10^{-5}	6.187×10^{-5}	7.244×10^{-5}	8.368×10^{-5}
Experimental	--	6.76×10^{-3}	6.57×10^{-3}	5.80×10^{-3}	4.73×10^{-3}

[a] 6.1 etc. denote the processes represented by Eqns. (6.1) etc. in the text.

It can be observed from Table 6.9 that the calculated probabilities for processes (6.1), (6.2), (6.7), and (6.9) are increasing with temperature. The experimentally observed energy transfer probabilities have a negative temperature dependence. In view of this disagreement regarding the temperature dependence, these processes are not likely to be responsible for the deactivation of $CO_2(00^\circ1)$. The processes (6.3), (6.4), (6.5), (6.6) and (6.8) show a negative temperature dependence. Hence they may be responsible for the deactivation of $CO_2(00^\circ1)$. It may be noted that the calculated probabilities for all these processes are approximately equal and that the $(CD_3)_2CO$ levels involved in these processes are very close to each other. It is therefore difficult to identify a particular process from this set which may be responsible for the deactivation of $CO_2(00^\circ1)$.

It is more likely that all these processes are equally responsible in deactivating $CO_2(00^\circ1)$. In that case P_{exp} is given by

$$P_{exp} = A_1 P_3 + A_2 P_4 + A_3 P_5 + A_4 P_6 + A_5 P_8 \qquad (6.10)$$

where P_3, P_4, P_5, P_6 and P_8 denote the calculated probabilities for the processes (6.3), (6.4), (6.5) (6.6) and (6.8), respectively and $A_1 \ldots A_5$ are multiplicative constants associated with the square of the transition dipole moments . It is not possible to evaluate all these constants from the present data.

Though the absolute intensities are not known, relative intensities of the various observed IR bands have been reported[70].

Therefore, one extreme case is considered in which the levels which have smaller values of transition dipole moments are ignored. Since ν_{21} is the only level having strong intensity whereas the other levels in the set are of medium intensity it is reasonable to ignore the levels with medium intensity and consider the ν_{21} level only to obtain an approximate value of the transition dipole moment. Therefore P_{exp} may be written as

$$P_{exp} = A\ P_4$$

Using the least squares fit, the dipole moment of ν_{21} is obtained as $(3.43\pm0.07) \times 10^{-37} esu^2 cm^2$. The temperature dependence of experimental probabilities and the theoretical plot for this model are shown in Fig. 6.6.

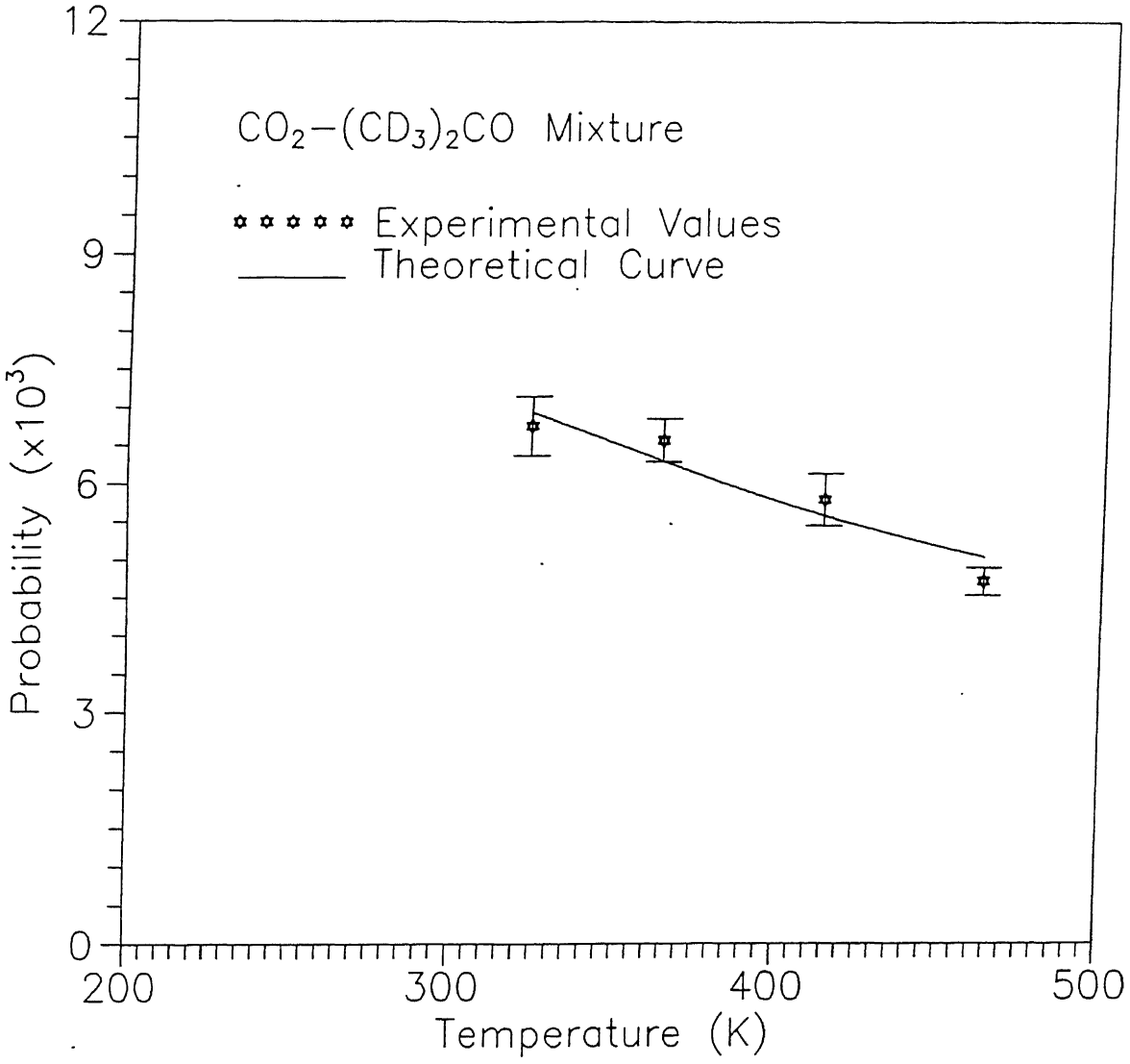

Fig. 6.6 Temperature dependence of energy transfer probability.

CHAPTER VII

CONCLUSION

The overall rates for the transfer of energy from $CO_2(00^\circ1)$ to CF_2Cl_2, C_4H_4S and $(CD_3)_3CO$ were measured at four different temperatures in the range 323-463 K. The probability of energy transfer for CO_2-CF_2Cl_2 mixtures was found to be independent of temperature, whereas the probability for CO_2-C_4H_4S and CO_2-$(CD_3)_2CO$ mixtures showed a negative temperature dependence. SSH-Tanczos theory and SB-Tam theory were used to calculate the probabilities of energy transfer in CO_2-CF_2Cl_2 system. The former theory could not explain the experimental data either quantitatively or their temperature dependence. But SB-Tam theory explained both the aspects satisfactorily. Squares of the transition dipole moments for the combination band $\nu_4+\nu_7$ and the overtone $2\nu_8$ in CF_2Cl_2 , which were not available, were calculated by matching the experimental and theoretical estimated probabilities. They are in qualitative agreement with the reported relative intensities of these levels. SB-Tam theory was used to analyze experimental data of CO_2-C_4H_4S and CO_2-$(CD_3)_2CO$ systems. The sum of the squares of the transition dipole moments for the levels ν_6 and ν_7 of C_4H_4S and the square of the transition dipole moment for ν_{21} level of $(CD_3)_2CO$ were also obtained.

Further Scope of Work

In the present work the fluorescence emitted from $CO_2(00^\circ1)$ level was monitored. No attempt was made to measure the rise and fall times of individual levels of the collision partners of CO_2. These type of measurements will help in identifying the exact energy transfer mechanism.

Extending the work over higher temperatures will help to understand the nature of intermolecular potential better and the transition dipole moments can be obtained more accurately.

The existing theories take into account either repulsive part or attractive part of the intermolecular potential. Since the intermolecular potential consists of both these parts, a theory in which both repulsive and attractive parts are incorporated would be more suitable.

REFERENCES

1. C. K. N. Patel, *Phys. Rev. Lett.* **12**, 588 (1964); *ibid* **13**, 617 (1964).
2. C. K. N. Patel, W. H. Faust and R. A. McFarlance, *Bull Amer. Phys. Soc.* **9**, 500 (1964).
3. C. K. N. Patel, P. K. Tein and J. H. McFee, *Appl. Phys. Lett.* **7**, 274 (1965).
4. G. Moeller and J. D. Rigden, *Appl. Phys. Lett.* 7, 274 (1965).
5. E. T. Gerry, *IEEE Spectrum* **7**, 51 (1970).
6. O. P. Judd, *Appl. Phys. Lett.* **22**, 95 (1973).
7. N. V. Karlov, *Appl. Optics* **13**, 310 (1974).
8. J. C. Stephenson and S. M. Freud, *J. Chem. Phys.* **65**, 1893 (1976).
9. J. M. Preses, R. E. Weston, Jr. and G. W. Flynn, *Chem. Phys. Lett.* **46**, 69 (1977).
10. I. P. Herman, R. P. Mariella, Jr. and A. Javan, *J. Chem. Phys.* **65**, 3796 (1976); *J. Chem. Phys.*, **68**, 1070 (1978).
11. T. L. Cottrell and J. C. McCoubrey, *Molecular Energy Transfer in Gases*, Butterworth, London, (1961).
12. G. M. Burnett and A. M. North, Eds., *Transfer and Storage of Energy by Molecules, Vol. 2, Vibrational Energy*, Wiely Intersciene, London (1969).
13. J. N. Bradley, *Shock Waves in Chemistry and Physics*, Methuen, London (1962).

14. A. G. Gaydon and I. R. Hurle, *The Shock Tube in High-Temperature Chemical Physics*, Reinhold, New York (1963).

15. K. F. Herzfeld and T. A . Litovitz, *Absorption and Dispersion of Ultrasonic Waves*, Academic Press, London (1959).

16. Y. Sato, S. Tsuchiya and K. Kuratani, *J. Chem. Phys.* **50,** 1911 (1969).

17. D. J. Seery, *J. Chem. Phys.* **63**, 3115 (1975).

18. J. H. Kiefer and R. W. Lutz, *Phys. Fluids* **8**, 1393 (1965).

19. V. V. N. Kishore, S. V. Babu and V. Subba Rao, *Chem. Phys.* **46**, 297 (1980).

20. L. O. Hocker, M. A. Kovacs, C. K. Rhodes, G. W. Flynn and A. Javan, *Phys. Rev. Lett.* **17**, 233 (1966).

21. C. B. Moore, R. E. Wood, B. B. Hu and J. T. Yardley, *J. Chem. Phys.* **46**, 4222 (1967).

22. J. T. Yardley and C. B. Moore, *J. Chem. Phys.* **45**, 1066 (1966); *ibid* **49**, 1111 (1968).

23. L. Landau and E. Teller, *Z. Phys. Sowjetunion* **10**, 34 (1936).

24. R. N. Schwartz, Z. I. Slawsky and K. F. Herzfeld, *J. Chem. Phys.* **20**, 1591 (1952).

25. W. A. Rosser, Jr., A. D. Wood and E. T. Gerry, *J. Chem. Phys.* **50,** 4996 (1969).

26. R. D. Sharma and C. A. Brau, *Phys. Rev. Lett.* **19**, 1273 (1967).

27. R. D. Sharma and C. A. Brau, *J. Chem. Phys.* **50**, 924 (1969).

28. J. C. Stephenson, R. E. Wood and C. B. Moore, *J. Chem. Phys.* **52**, 2333 (1970).

29. J. T. Yardley, *Introduction to Molecular Energy Transfer*, Academic Press, New York (1980).

30. W. A. Rosser, Jr., A. D. Wood and E. T. Gerry, *J. Chem. Phys.* **50**, 4996 (1969).

31. M. N. Mikhailova and P. V. Slobodskaya, *Opt. Spectros.* **22**, 14 (1967).

32. M. A. Kovacs, D. R. Rao and A. Javan, *J. Chem. Phys.* **48**, 3339 (1968).

33. *F. I.* Tanczos, *J. Chem. Phys.* **25**, 439 (1956).

34. D. Rapp, *J. Chem. Phys.* **43**, 316 (1956).

35. B. H. Mahan, *J. Chem. Phys.* **46**, 98 (1967).

36. J. C. Stephenson, R. E. Wood and C. B. Moore, *J. Chem. Phys.* **48**, 4790 (1968).

37. I. Burak, Y. Noter, A. M. Ronn and A. Szoke, *J. Chem. Phys.* **58**, 306 (1972).

38. R. D. Sharma, H. L. Cheen and A. Szoke, *J. Chem. Phys.* **58**, 3519 (1973).

39. W. Q. Jeffers and J. D. Kelly, *J. Chem. Phys.* **55**, 4433 (1971).

40. R. D. Sharma, *Phy. Rev.* **177**, 102 (1969).

41. B. M. Hoplons, H. L. Chen and R. D. Sharma, *J. Chem. Phys.* **59**, 5758 (1973).

42. W. A. Rosser Jr., R. D. Sharma, and E. T. Gery, *J. Chem. Phys.* **54**, 1196 (1971).

43. D. Frenkel, J. I. Steinfeld, R. D. Sharma and L. Pousen, *Chem. Phys. Lett.* **28**, 485 (1974).

44. R. D. Sharma, *J. Chem. Phys.* **50**, 919 (1969).

45. R. D. Sharma and C. W. Kern, *J. Chem. Phys.* **55**, 1171 (1971).

46. I. W. M. Smith and C. Morley, *Trans. Faraday Soc.* **67**, 2575 (1971).

47. C. Zener, *Phys. Rev.* **37**, 556 (1931).

48. R. N. Schwartz and K. F. Herzfeld, *J. Chem. Phys.* **22**, 767 (1954).

49. J. L. Stretton, *Trans. Faraday Soc.* **61**, 1053 (1965).

50. W. G. Tam, *Can. J. Phys.* **50**, 2691 (1972).

51. C. G. Gray and J. Van Kranendonk, *Can. J. Phys.* **44**, 2411 (1966).

52. M. Abramowitz and I. A. Stegun, *Handbook of Mathematical Functions*, (NBS Applied Mathematics Series, Vol. 55, p. 1001 (1964).

53. W. G. Tam, *Chem. Phys. Letts.* **15**, 113 (1972).

54. M. Abramonitz and I. A. Stegun, *Handbook of Mathematical Functions*, NBS Applied Mathematics Series, Vol. 55, p. 231 (1964).

55. J. T. Houghton, *Proc. Phys. Soc. Lond.* **91**, 697 (1974).

56. B. C. Reed, *Am. J. Phys.* **57**, 642 (1989).

57. E. K. Plyler and W. S. Dnedict, *J. Res. Nat. Bur. Stan.* **47**, 2245 (1951).

58. J. Morcillo, L. J. Zamorans and J. M. V. Heredia, *Spectrochim. Acta* **22**, 1969 (1966).

59. R. S. Karve, S. K. Sarkar, K. V. S. Rama Rao and J. P. Mittal, *Spectrochim Acta* **43A**, 165 (1987).

60. J. T. Yardley and C. B. Moore, *J. Chem. Phys.* **46**, 4491 (1967).

61. J. O. Hirschfelder, C. F. Curtiss and R. B. Bird, *Molecular Theory of Gases and Liquids*, Wiley, New York (1954).

62. G. Herzberg, *Infrared and Raman Spectra of Polyatomic Molecules*, Van Nostrand Reinhold Co., New York (1945).

63. H. Takeo and C. Matsumura, *Bull. Chem. Soc. Jap.* **50**, 636 (1977).

64. S. R. Drayson and C. Young, *J. Quant. Spect. Rad. Trans.* **7**, 993 (1967).

65. K. S. Seshadri and R. N. Jones, *Spectrochim. Acta* **19**, 1013 (1963).

66. M. Rico, J.M. Orza and J. Morcillo, *Spectrochim. Acta*, **21**, 689 (1965).

67. G. Herzberg, *Electronic Spectra of Polyatomic Molecules*, Van Nostrand Reinhold Co., New York (1966).

68. *Handbook of Chemistry and Physics*, CRC Press, Florida, 67th edition (1986-87).

69. G. M. Barrow, *Physical Chemistry*, McGraw Hill, New York (1988).

70. G. Delleplane and J. Overend, *Spectrochim. Acta* **22**, 593 (1966).

71. Wilson, Decius and Cross, *Molecular Vibrations*, McGraw-Hill, London, (1955).

APPENDIX A

CALCULATION OF BREATHING SPHERE PARAMETERS USING NORMAL COORDINATE ANALYSIS

The cartesian displacements are derived from normal coordinate analysis of the molecular vibration[71]. One of the products of this analysis is a transformation matrix L, which is the link between internal coordinates R and the normal coordinates Q. The relations between these two sets of coordinates is given by

$$R = LQ \tag{A.1}$$

The cartesian displacements X are related to the changes in internal coordinates by the matrix B, as

$$R = Bx \tag{A.2}$$

The squares of the cartesian displacements are given by

$$x^2 = Q'L^{-1}H(L')^{-1}Q \tag{A.3}$$

where the matrix H is defined as

$$H = BM^{-2}B' \tag{A.4}$$

M being a diagonal matrix of the atomic masses. Comparison of Eqn. (3.4.11) with the definition of Wilson's G matrix

$$G = BM^{-1}B' \tag{A.5}$$

shows that the elements H are easily obtained from G. For unit change of the n^{th} normal coordinate only, the sum of the squares of the cartesian displacements of all the atoms is given by

$$\sum_{i=1}^{3N} x_i = \left[L^{-1}H(L')^{-1}\right]_{nn} \tag{A.6}$$

where N is the number of atoms in the molecule. In order to obtain the average displacement of the surface atoms, or $\langle A_n^2 \rangle$, the moments of various types of atom in the molecule need to be calculated separately. This is done by including only the required (surface) atomic masses in the diagonal matrix when H is computed according to Eqn. (A.4)

$$\langle A_n^2 \rangle = \frac{1}{N_s}\left[L^{-1}H(L')^{-1}\right]_{nn} \tag{A.7}$$

where N_s is the number of surface atoms.

APPENDIX B

DETAILS OF EVALUATION OF THE INTEGRALS IN EQN. (3.54)

The integrals in Eqn.(3.54) of the text, are of the type

$$S_n = \int_0^\infty e^{-2\omega b/v} v^n e^{-\alpha v^2} dv \qquad (B.1)$$

Substituting $x = \omega b\sqrt{\alpha}$ and $u = \sqrt{\alpha}\, v$ yields the integrals in the form

$$S_n = \alpha^{-(n+1)/2} \int_0^\infty e^{-[(2x/u)+u^2]} u^n du \qquad (B.2)$$

Defining

$$f_n(2x) = \int_0^\infty e^{-[(2x/u)+u^2]}\, u^n\, du \qquad (B.3)$$

We have

$$\int_0^\infty v\, G_\ell(\omega b/v)\, e^{-\alpha v^2} dv = (1/\alpha)\, [A_\ell\, f_1(2x) + B_\ell\, x\, f_0(2x) + C_\ell\, x^2\, f_{-1}(2x) + D_\ell\, x^3\, f_{-2}(2x) + E_\ell\, x^4\, f_{-3}(2x)]$$

$$= (1/\alpha)\, I_\ell(b, \omega, T) \qquad (B.4)$$

Eqn. (B.4) when substituted in Eqn.(3.54) will result in Eqn. (3.55). The same integrals are involved in evaluating $\langle v^{-2} J_\ell^2(\omega d/v) \rangle_v$ which results in the following formula

$$\langle v^{-2} J_\ell^2(\omega d/v)\rangle_v = 2\alpha\,[a_\ell f_1(x/2) + b_\ell x\, f_0(x/2) + c_\ell x^2 f_{-1}(x/2) + d_\ell\, x^3\, f_{-2}(x/2)\,]$$
$$= 2\alpha I_\ell(0,\omega,T) \qquad \text{(B.5)}$$

Here $x=\omega d\sqrt{\alpha}$. This leads to Eqn.(3.59) of the text. The following values were used in evaluating $I_2(d,\omega,T)$ and $I_2(0,\omega,T)$for dipole-dipole interaction (ℓ=2).

A_2=0.3333	B_2=0.6717	C_2=0.7980	D_2=1.0428	E_2=0.0006
a_2=0.25	b_2=0.0977	c_2=0.0208	d_2=0.0022	

The function $f_1(y)$ is calculated using the polynomial approximation given in ref. 52 of the text,

$$2\, f_1(y) = \sum_{k=0}^{\infty} (a_k \ln y + b_k)\, y^k \qquad \text{(B.6)}$$

The following relations hold good for the integrals $f_n(y)$

$$f_{n-1}(y) = -\frac{d}{dy} f_n(y) \qquad \text{(B.7)}$$

$$2f_n(y) = (n-1)f_{n-2}(y) + yf_{n-3}(y) \qquad \text{(B.8)}$$

The constants a_k and b_k are given by

$$a_k = \frac{-2a_{k-2}}{k(k-1)(k-2)} \quad ; \quad b_k = \frac{-2b_{k-2} - (3k^2-6k+2)a_k}{k(K-1)(k-2)}$$

$$a_o = a_1 = 0 \quad ; \quad b_0 = 1$$

$$a_2 = -b_0 \quad ; \quad b_1 = -\sqrt{\pi},\ b_2 = 3(1-\gamma)/2$$

where, γ is the Euler constant having a value 0.5772. $f_1(y)$ is a monotonically decreasing function of y and its maximum value is 0.5 when y=0.

An examination of the values of $f_1(y)$ as a function of y reveals that Eqn.(B.6) holds good for $y \leq 3$. For $y>3$ the following asymptotic approximation given in ref. 52 of the text is used.

$$f_n(y) = \sqrt{\pi/3}\ 3^{-n/2} v^{n/2} e^{-v} (a_0 + a_1/v + a_2/v^2 + \ldots + a/v^k + \ldots) \qquad (B.9)$$

where, $v = 3(y/2)^{2/3}$. The constants a_k of Eqn.(B.9) are calculated using the following relations.

$$a_0 = 1 \quad ; \quad a_1 = (3n^2 + 3n - 1)/12$$

$$12(k+2)a_{k+2} = -(12k^2+36k-3n^2-3n+25)a_{k+1}$$

$$+1/2(n-2k)(2k+3-n)(2k+3+2n)a_k \qquad (k=0,1,2\ldots)$$

The other functions f_0, f_{-1}, f_{-2} etc. are calculated using the relations given by Eqns. (B.7) and (B.8).

APPENDIX C

DETAILS OF EVALUATION OF INTEGRALS IN EQN. (3.70)

The first term in Eqn. (3.70) for dipole-dipole interaction (ℓ=2) is

$$\int_d^\infty e^{-2\omega b/v}(A_2/b^3)\,db \tag{C.1}$$

Making the substitution $y = 2\omega b/v$ results in

$$A_2(2\omega/v)^2\int_{2\omega d/v}^\infty (1/y^3)e^{-y}\,dy \tag{C.2}$$

which can be integrated by parts to give

$$\tfrac{1}{2}(1/d^2)A_2e^{-2\omega d/v} - A_2(\omega/dv)e^{-2\omega d/v} + 2A_2(\omega^2/v^2)E_1(2\omega d/v) \tag{C.3}$$

The second term $\int_d^\infty e^{-2\omega b/v}B_2(\omega b/v)(1/b^3)db$ reduces to

$$2B_2(\omega/v)^2\int_{2\omega d/v}^\infty (1/y^2)e^{-y}dy = B_2(\omega/dv)e^{-2\omega d/v} - 2B_2(\omega/v)^2E_1(2\omega d/v) \tag{C.4}$$

The third term is

$$\int_d^\infty e^{-2\omega b/v}C_2(\omega b/v)^2(1/b^3)db = C_2(\omega/v)^2\int_{2\omega d/v}^\infty (1/y)e^{-y}dy$$

$$= C_2(\omega/v)^2E_1(2\omega d/v) \tag{C.5}$$

The fourth term

$$\int_d^\infty e^{-2\omega b/v} D_2(\omega b/v)^3 (1/b^3) db = \frac{1}{2} D_2(\omega/v)^2 e^{-2\omega d/v} \qquad (C.6)$$

and the last term

$$\int_d^\infty e^{-2\omega b/v} E_2(\omega b/v)^4 (1/b^3) db = \frac{1}{4} E_2(\omega/v)^2 \int_{2\omega d/v}^\infty y e^{-y} dy$$

$$= \frac{1}{2} E_2(\omega/v)^3 d e^{-2\omega d/v} + \frac{1}{4} E_2(\omega/v)^2 e^{-2\omega d/v} \qquad (C.7)$$

Adding up the Eqns. (C.1) to (C.7) will give the following expression

$$\begin{aligned} F_2(\omega d/v) = {} & \frac{1}{2} A_2 (1/d^2) e^{-2\omega d/v} + (B_2 - A_2)(\omega/dv) e^{-2\omega d/v} \\ & + \frac{1}{4}(2D_2 + E_2)(\omega/v)^2 e^{-2\omega d/v} + \frac{1}{2} E_2 (\omega/v)^3 d e^{-2\omega d/v} \\ & + (2A_2 - 2B_2 + C_2)(\omega/v)^2 E_1(2\omega d/v) \end{aligned} \qquad (C.8)$$

The evaluation of $\langle v^{-2} F_2(\omega d/v) \rangle$ is simply the integration of Eqn. (C.8) over the velocity v which involves the same integrals as evaluated in Appendix B except for the last term of Eqn. (C.8). The final result is given in Eqn. (3.76).

PHY-1995-D-SIR-LAS